

## Copyright Warning & Restrictions

The copyright law of the United States (Title 17, United States Code) governs the making of photocopies or other reproductions of copyrighted material.

Under certain conditions specified in the law, libraries and archives are authorized to furnish a photocopy or other reproduction. One of these specified conditions is that the photocopy or reproduction is not to be “used for any purpose other than private study, scholarship, or research.” If a user makes a request for, or later uses, a photocopy or reproduction for purposes in excess of “fair use” that user may be liable for copyright infringement,

This institution reserves the right to refuse to accept a copying order if, in its judgment, fulfillment of the order would involve violation of copyright law.

**Please Note: The author retains the copyright while the New Jersey Institute of Technology reserves the right to distribute this thesis or dissertation**

Printing note: If you do not wish to print this page, then select “Pages from: first page # to: last page #” on the print dialog screen

The Van Houten library has removed some of the personal information and all signatures from the approval page and biographical sketches of theses and dissertations in order to protect the identity of NJIT graduates and faculty.

## ABSTRACT

### **RAPID TOOLING BY INTEGRATION OF SOLID FREEFORM FABRICATION AND ELECTRODEPOSITION**

by  
**Bo Yang**

Rapid tooling (RT) techniques based on solid freeform fabrication (SFF) are being studied worldwide to speed up the design-production cycle and thus keep manufacturers at a competitive edge. This dissertation presents a novel rapid tooling process that integrates SFF with electrodeposition to produce molds, dies, and electrical discharge machining (EDM) electrodes rapidly, accurately and cost effectively. Experimental investigation, thermomechanical modeling and analysis, as well as case studies reveal that integration of electroforming with solid freeform fabrication is a viable way for metal tool making.

The major research tasks and results of this dissertation study are as follows:

- Rapid electroforming tooling (RET) process development and understanding. 3D CAD model design, metalization, electroforming, separation and backing are studied through experimental and analytical work. Methods of implementation based on the factors of tooling time, cost, and tooling accuracy are developed.
- Identification of inaccuracy factors in RET process and methods for improving tooling accuracy. The accuracy of the formed mold cavity or EDM electrode depends upon the material and geometry of the RP part, the properties of the electroformed metal, and process parameters. The thermal stress induced by the burnout process that

removes the SFF part from the electroform is one of the major inaccuracy sources. Another one is the deformation generated by solidification of the molten metal that is used to back the electroform to form a solid mold cavity or an EDM electrode.

- FEM based thermomechanical modeling and analysis of the thermal stress during the SFF part burnout process has been performed. The model is implemented in ANSYS software. It is found that a stepped thermal load for the pattern burnout generates much smaller thermal stress than a ramped thermal load.
- The thermal stress is largely reduced when an SFF part is designed as a hollow or shelled structure, or when the electroform thickness is increased. The wall thickness of SFF part is determined by two criteria. The wall thickness must be thin enough to guarantee that the thermal stresses are smaller than the yield strength of the electroformed metal. On the other hand, the wall thickness must also be large enough to resist the electroforming stress during the electroforming process. The electroform thickness is related to tooling time, cost and tool strength.
- Strain gage based thermal stress measurements demonstrate that the results obtained from the experiment accurately match the results obtained from the FEM-based thermomechanical analysis model. Thus the model can be used to predict the thermal stress induced during the burnout process.
- The established thermomechanical model and FEM based numerical simulation provide an effective method that determines the geometry of the SFF part and the electroform thickness for minimizing the manufacturing time and cost while satisfying the tooling accuracy requirement.

**RAPID TOOLING BY INTEGRATION OF SOLID FREEFORM  
FABRICATION AND ELECTRODEPOSITION**

**by  
Bo Yang**

**A Dissertation  
Submitted to the Faculty of  
New Jersey Institute of Technology  
in Partial Fulfillment of the Requirements for the Degree of  
Doctor of Philosophy in Mechanical Engineering**

**Department of Mechanical Engineering**

**May 2000**

Copyright © 2000 by Bo Yang  
ALL RIGHTS RESERVED

**APPROVAL PAGE**

**RAPID TOOLING BY INTEGRATION OF SOLID FREEFORM  
FABRICATION AND ELECTRODEPOSITION**

**Bo Yang**

---

Dr. Ming C. Leu, Dissertation Advisor Date  
New Jersey State Sponsored Chair in Manufacturing/Productivity  
Professor of Mechanical Engineering, NJIT

---

Dr. Zhiming Ji, Committee Member Date  
Associate Professor of Mechanical Engineering, NJIT

---

Dr. Denis Blackmore, Committee Member Date  
Professor of Mathematics, NJIT

---

Dr. Reggie J. Caudill, Committee Member Date  
Professor of Industrial and Manufacturing Engineering, NJIT

---

Dr. Ernest S. Geskin, Committee Member Date  
Professor of Mechanical Engineering, NJIT

## BIOGRAPHICAL SKETCH

**Author:** Bo Yang  
**Degree:** Doctor of Philosophy  
**Date:** May 2000

### **Undergraduate and Graduate Education:**

- Doctor of Philosophy in Mechanical Engineering, New Jersey Institute of Technology, Newark, NJ, USA, 2000
- Master of Science in Mechanical Engineering, Harbin Institute of Technology, Harbin, P.R.China, 1994
- Department of Mechanical Engineering, Nanjing Institute of Technology, Nanjing, P.R.China, 1988

**Major:** Mechanical Engineering

### **Publications:**

Ming C. Leu and Bo Yang. 2000. "Application of Finite Element Analysis for Prediction of Thermal Stress in Rapid Tooling," to appear in Handbook on Layered Manufacturing & Rapid Prototyping: Technologies, Fundamentals and Applications, edited by M. C. Leu, to be published by Academic Press Inc.

Bo Yang and Ming C. Leu. 2000. "EDM Tooling by Electrodeposition of Rapid Prototyping masters," International Journal of Agile Manufacturing, Vol.1/2000.

Bo Yang and Ming C. Leu. 2000. "Rapid Electroforming Tooling," invited paper for Material Research Society Spring 2000 Meeting.

Bo Yang and Ming C. Leu. 1999. "Rapid Production of Engineering Tools and Hollow Bodies by Integration of Electroforming and Solid Freeform Fabrication," Filed with the United States Patent and Trademark Office for a patent application.



- Bo Yang and Ming C. Leu. 1999. "Rapid Tooling by Integrating Electroforming and Solid Freeform Fabrication Techniques," Proceedings of Tenth Solid Freeform Fabrication Symposium, Austin, Texas, August 8-11.
- Bo Yang and Ming C. Leu. 1999. "Integration of Rapid Prototyping and Electroforming for Tooling Application," the Annals of the CIRP, Vol.48/1.
- Ming C. Leu, Bo Yang and Wenlong Yao. 1998. "A Feasibility Study of EDM Tooling Using Metalized Stereolithography Models," Technical Papers of NAMRI/SME, MR90-180.
- Bo Yang, Ming C. Leu and Wei Zhang. 1998. "Rapid Tooling of Dies and Molds Through Rapid Fabrication of EDM Electrodes," Proceedings of North American Stereolithography User Group Conference and Annual Meeting, San Antonio, Texas, March 1-5.
- Bo Yang, Ming C. Leu and Ji Zhou. 1998. "Error Analysis for Four-axis Side Milling of Undevelopable Ruled Surface," IFAC Journal of Control Engineering Practice, Vol. 6:4.
- Bo Yang, Miaoan Ouyang, and Ji Zhou. 1995. "5-axis NC Machining & Auto-programming System for Turbo Wheel." Proceedings of International Conference on Intelligent Manufacturing (ICIM'95), Wuhan, PR China, June 14-17.
- Bo Yang, Xiangli Han and Zhejun Yuan. 1995. "Simulation of Machining Process for Multi-axis NC Verification," Proceedings of ICIM'95. Wuhan, China, June 14-17.
- Xiangli Han, Bo Yang and Zhejun Yuan. "A Study on Method of Post-processing of 5-axis CNC Machining Tool," Journal of Modular Machine Tool & Automatic Manufacturing Technology (in Chinese), Vol.3.
- Miaoan Ouyang, Bo Yang and Ji Zhou. 1995. "An Intelligent Conceptual System for Modular Design of Machine Tools," Proceedings of International Conference on Engineering Design, Praha, Czech, Aug. 22-24.
- Bo Yang, Minhua Wu and Ji Zhou. 1994. "Analysis and Computation of Tolerance Resulted From 4-axis NC Machining Impeller," Journal of Modular Machine Tool & Automatic Manufacturing Technology (in Chinese), Vol.12.
- Bo Yang. 1994. "A Study on Surface Modeling and Multi-Axis NC Machining & Auto-Programming System for Turbine Impellers," Master Thesis, Mechanical Engineering. Harbin Institute of Technology, March.

This dissertation is dedicated to my beloved family.

## ACKNOWLEDGMENT

I would like to express my appreciation and deepest gratitude to Dr. Ming C. Leu, who not only served as my research supervisor, providing valuable and countless guidance, resources, insight, and intuition, but also constantly gave me encouragement, reassurance, and research assistantship throughout this research. His broad knowledge, pleasant personality and working attitude will benefit me forever.

I am very grateful to Drs. Zhiming Ji, D. Blackmore, Reggie J. Caudill, and E. R. Geskin for their fruitful suggestions and discussions on this dissertation and actively serving as members of the committee. Many of my fellow researchers, Yanchun Luo, Wei Zhang, etc. in the Rapid Intelligent Manufacturing and Prototyping Laboratory are deserving of recognition for their support.

This research is partially supported by the New Jersey Commission on Science and Technology via the Multi-lifecycle Engineering Research Center (MERC) at New Jersey Institute of Technology. Dr. Caudill is the Executive Director of MERC.

Specially, I thank my wife Hongying Qian and my daughter Chiana Yang for their patience, comfort, and support. I also dedicate my thanks to my parents and the members of family for their support throughout my life.

# TABLE OF CONTENTS

<b>Chapter</b>	<b>Page</b>
1 INTRODUCTION.....	1
2 LITERATURE SURVEY.....	7
2.1 OVERVIEW OF RAPID PROTOTYPING PROCESSES .....	7
2.1.1 Working Principles of Rapid Prototyping Processes .....	8
2.1.2 Comparison of Performance Characteristics of Rapid Prototyping Processes .....	11
2.2 Stereolithography Apparatus .....	17
2.2.1 Photocurable Resin and Photo Polymerization.....	19
2.2.2 Laser Exposure.....	20
2.3 Rapid Tooling Research and Development .....	24
2.3.1 Direct Rapid Tooling.....	24
2.3.2. Indirect Rapid Tooling .....	25
2.4 Accuracy Comparison among Current Rapid Tooling Techniques.....	30
3 RESEARCH OBJECTIVES, ISSUES AND APPROACHES.....	32
3.1 Tooling Approaches.....	32
3.1.1 Electroplating Tooling.....	32
3.1.2 Electroforming Tooling.....	33
3.2 Research Objectives, Issues and Approaches .....	36
3.3 Research and Development Tasks .....	38
4 ELECTROPLATING TOOLING FOR EDM ELECTRODES.....	41
4.1 EDM Principles and Its Tooling Background.....	41

**TABLE OF CONTENTS**  
**(Continued)**

<b>Chapter</b>	<b>Page</b>
4.2 The Experiment.....	45
4.2.1. EDM Machining Parameters.....	45
4.2.2 Preparation of Stereolithography Electrodes.....	48
4.2.3 Performance Attributes .....	48
4.2.4 The Experimental Steps .....	49
4.3 Experimental Results .....	50
4.3.1 Roughing.....	50
4.3.2 Semi-Roughing .....	51
4.3.3 Finishing.....	53
4.4 Discussion of Workpiece Damage and Plating Thickness .....	55
4.4.1 Workpiece Damage.....	55
4.4.2 Damage Monitoring .....	56
4.4.3 Plating Thickness .....	58
4.5 Closure .....	59
5 RAPID ELECTROFORMING TOOLING.....	61
5.1 Introduction of Electroforming Tooling .....	61
5.1.1 Electroforming and Rapid Electroforming Tooling.....	61
5.1.2 Advantages and Disadvantages of Rapid Electroforming Tooling.....	63
5.1.3 Introduction of Electroless Plating.....	65
5.2 Rapid Electroforming Tooling of EDM Electrodes.....	66
5.2.1 Tooling Process .....	66

**TABLE OF CONTENTS**  
**(Continued)**

<b>Chapter</b>	<b>Page</b>
5.2.2 Performance Testing .....	68
5.2.3 Case Study.....	69
5.2.4 Electroforming Thickness .....	72
5.3 Rapid Electroforming Tooling of Molds .....	74
5.3.1 Tooling Process .....	74
5.3.2 Case Studies .....	76
5.4 Tooling Accuracy.....	78
5.5 Environmental Performance of the Rapid Electroforming Tooling.....	82
5.6 Discussion of Tooling Time and Cost-effectiveness.....	88
5.7 Closure .....	89
6 THERMOMECHANICAL MODELING AND ANALYSIS.....	91
6.1 Properties of Tooling Materials .....	91
6.1.1 Properties of Seterolithography Resin.....	92
6.1.2 Properties of Electroformed Copper .....	96
6.1.3 Properties of Electroformed Nickel.....	97
6.2 Failure Criteria.....	99
6.3 Analytical Calculation of Thermal Stresses.....	101
6.4 Thermomechanical Modeling of the Burnout Process.....	105
6.4.1 Thermal Modeling of the Burnout Process .....	106
6.4.2 Structure Modeling of the Burnout Process .....	108

**TABLE OF CONTENTS**  
**(Continued)**

<b>Chapter</b>	<b>Page</b>
6.5 FEM Based Numerical Simulation .....	110
6.5.1 General .....	110
6.5.2 FEM Based Simulation .....	113
6.5.3 Convergence Study .....	116
6.6 Simulation Results and Discussion.....	118
6.6.1 Thermal Stress Simulation for a Two-Dimensional Case.....	118
6.6.2 Thermal Stress Simulation for an EDM Electrode.....	123
6.6.3 Thermal Stress Simulation for a Mold .....	129
6.6.4 Discussion of Non-uniform Electroform Thickness .....	134
6.7 Experiment Verification.....	135
6.7.1 Sample Preparation .....	135
6.7.2 Experimental Environment .....	137
6.7.3 Experimental Results.....	139
6.8 Process Implementation and Optimization Model.....	141
6.9 Closure .....	144
7 CONCLUSION AND FUTURE WORK.....	145
7.1 Major Contributions.....	145
7.2 Future Work .....	148
APPENDIX A DISCUSSION OF BOUNDARY CONDITIONS FOR THE THERMOMECHANICAL MODEL.....	150
REFERENCES.....	153

## LIST OF TABLES

<b>Table</b>		<b>Page</b>
2.1	Comparison of some Rapid Prototyping processes.....	14
2.2	Accuracy based comparison among rapid metal tooling processes.....	31
4.1	The EDM machining parameters.....	46
4.2	Default process parameters for the selected E settings.....	47
4.3	EDM process performance attributes.....	49
5.1	Performance data of electroformed ( $E_1$ ) and electroplated ( $E_2$ ) electrodes vs. regular solid copper electrode ( $E_3$ ) using E 403 Setting.....	70
5.2	Performance data of electroformed ( $E_1$ ) and electroplated ( $E_2$ ) electrodes vs. regular solid copper electrode ( $E_3$ ) using E 342 setting.....	70
5.3	Performance data of electroformed ( $E_1$ ) and electroplated ( $E_2$ ) electrodes vs. regular solid copper electrode ( $E_3$ ) using E 293 setting.....	71
5.4	Dimensional data of SL parts vs. those of electroformed copper shell (unit: mm).....	72
5.5	Dimensional data of SL parts versus electroformed mold cavities (unit:mm)....	78
5.6	Comparison of machining with SFF processes.....	83
5.7	Environmental performance of RT process .....	87
6.1	Mechanical properties of SL 5170 at 20°C (UV Post Cured 60 minutes).....	92
6.2	Thermal properties of SL 5170 (UV Post Cured 60 minutes).....	93
6.3	Typical mechanical properties of SL 5210 at 20°C.....	94
6.4	Thermal properties of SL 5210.....	95
6.5	Mechanical and thermal properties of electroformed copper at 20 °C.....	96
6.6	Mechanical and thermal properties of sulfate electroformed copper vs. temperature.....	97



**LIST OF TABLES**  
**(Continued)**

<b>Table</b>	<b>Page</b>
6.7 Mechanical and thermal properties of electroformed nickel at 20 °C.....	98
6.8 Mechanical and thermal properties of sulfamate electroformed nickel vs. temperature.....	98
6.9 Convergence of thermal stress with different element type, size and models....	117
6.10 Electroforming deformation (ED) for different sets of parameters <b>A</b> and <b>t</b> .....	120
6.11 Comparison of build time and material cost for different SL parts.....	121
6.12 Comparison of build time and material cost for different SL parts.....	128
6.13 Samples for experimental verification.....	137

## LIST OF FIGURES

<b>Figure</b>		<b>Page</b>
2.1	Some of the current Rapid Prototyping processes.....	8
2.2	Working principles of Rapid Prototyping Technologies .....	10
2.3	The Stereolithography Apparatus system.....	18
2.4	Fabrication sequence of SLA prototype.....	18
2.5	Photopolymerization process: initiation, propagation, and termination.....	19
2.6	Laser exposure of a line.....	23
2.7	Laser exposure of a layer.....	23
2.8	UV based silicone molding process.....	25
2.9	The 3D Keltool processes (Jacobs, 1996b).....	26
2.10	Total production time and cost vs. number of parts.....	28
2.11	Spray metal tooling.....	29
3.1	Electroplating tooling using RP pattern.....	32
3.2	The tooling process being investigated.....	35
4.1	A Basic EDM Machine.....	42
4.2	Gap voltage and current waveforms of EDM pulses and definition of A, B, R and U.....	46
4.3	Material removal rate of copper-coated SL electrode vs. regular copper electrode using E 403 setting .....	51
4.4	Surface finish of copper-coated SL electrode vs. regular copper electrode using E 403 setting.....	51
4.5	Tool end wear of copper-plated SL electrode vs. regular copper electrode using E 342 setting.....	52

**LIST OF FIGURES**  
**(Continued)**

<b>Figure</b>	<b>Page</b>
4.6 Tool wear ratio of copper-coated SL electrode vs. regular copper electrode using E 342 setting.....	52
4.7 Material removal rate of copper-coated SL electrode vs. regular copper electrode using E 342 setting.....	52
4.8 Surface finish of copper-coated SL electrode vs. regular copper electrode using E 342 setting.....	53
4.9 Tool end wear of copper-coated SL electrode vs. regular electrode using E 293 setting.....	53
4.10 Tool wear ratio of copper-coated SL electrode vs. regular copper electrode using E 293 setting.....	54
4.11 Material removal rate of copper-coated SL electrode vs. regular copper electrode using E 293 setting.....	54
4.12 Surface finish of copper-coated SL electrode vs. regular copper electrode using E 293 setting.....	55
4.13 The tested workpieces and the SL electrode.....	56
4.14 Machining parameters displayed on-line in the machining control page.....	57
4.15 $R_i$ , $U_i$ and $B_i$ versus time under E 342 setting when the SL electrode is used...	58
4.16 $I_S$ , $M_O$ and $G_L$ vs. time under E 342 setting when the SL electrode is used.....	58
5.1 EDM tooling process using SL master and electroforming.....	66
5.2 Electroformed electrode and EDM generated workpiece.....	71
5.3 Critical thickness investigation.....	73
5.4 Typical setup of nickel electroforming.....	74
5.5 Mold tooling process using RP master and electroforming.....	75

**LIST OF FIGURES**  
**(Continued)**

<b>Figure</b>	<b>Page</b>
5.6 Nickel electroformed molds with fine features.....	76
5.7 Dimensions measured.....	78
5.8 Indirect tooling processes.....	84
5.9 Lifecycle environmental performance model of indirect RT process.....	78
6.1 Young's modulus and coefficient of thermal expansion of SL 5170 vs. temperatures.....	93
6.2 Young's modulus and coefficient of thermal expansion of SL 5210 vs. temperatures.....	95
6.3 Pressure generated at the interface of the SL master and the nickel shell due to heating of the model.....	100
6.4 Pressures and thermal stresses vs. electroforming thickness.....	103
6.5 Partially yielded nickel shell under internal pressure.....	104
6.6 Two scenarios of thermal loads.....	108
6.7 Thermal stress analysis model.....	111
6.8 ANSYS-based thermal stress simulation model.....	112
6.9 Comparison of meshes and thermal stresses for two and three dimensional models.....	115
6.10 Two dimensional case: nickel electroformed SL cylinder.....	117
6.11 Temperature distribution for the two dimensional models with different SL parts and electroform thickness.....	118
6.12 Two dimensional simulation of thermal stresses with different SL parts and electroform thickness.....	121

**LIST OF FIGURES**  
**(Continued)**

<b>Figure</b>	<b>Page</b>
6.13	Maximum thermal stress vs. electroform thickness for burnout process.....122
6.14	Maximum thermal stress vs. time during burnout process.....122
6.15	Meshed models for EDM electrodes.....123
6.16	Heat transfer simulation for solid and shelled SL parts with 2 mm thick of copper electroform.....124
6.17	Thermal stress simulation for solid and shelled SL parts with 2 mm thick of copper electroform.....125
6.18	Maximum thermal stresses vs. burning time under stepped thermal load for EDM electrodes.....128
6.19	Maximum thermal stresses vs. burning time under ramped thermal load for EDM electrodes.....128
6.20	Meshed models for molds with 2 mm thick of nickel electroform.....129
6.21	Heat transfer simulation for solid and hollowed SL part with 2 mm thick of nickel electroform for mold tooling.....130
6.22	First principal stress simulation for solid and hollowed SL parts with 2 mm thick of nickel electroform.....131
6.23	Thermal stress generated for nickel electroform vs. burning time for stepped thermal load for mold.....133
6.24	Thermal stress generated for nickel electroform Vs. burning time for ramped thermal load for mold.....133
6.25	Strange gage on a nickel electroform with solid SL part.....135
6.26	Strange gage on a nickel electroform with hollow SL part.....136
6.27	Thermal Stress measuring Environment.....138
6.28	Wired samples in the furnace.....138

**LIST OF FIGURES**  
**(Continued)**

<b>Figure</b>	<b>Page</b>
6.29 Analytical first principal stress vs. measured first principal stress for 1 mm nickel plated on solid SL part.....	139
6.30 Analytical first principal stress vs. measured first principal stress for 2 mm nickel plated on solid SL part.....	139
6.31 Analytical thermal stress vs. measured thermal stress for 4 mm nickel plated on solid SL master.....	140
6.32 Analytical thermal stress vs. measured thermal stress for 1 mm nickel plated on hollowed SL master.....	140
6.33 Analytical thermal stress vs. measured thermal stress for 2 mm nickel plated on hollowed SL master.....	141
6.34 Analytical thermal stress vs. measured thermal stress for 4 mm nickel plated on hollowed SL master.....	141
6.35 Implementation and optimization model for determining the SFF part structure and electroforming thickness.....	143

# CHAPTER 1

## INTRODUCTION

Tool manufacturing represents a significant area of production technology since it influences the feasibility and economics of producing a large number of discrete components. Tools referred to in this dissertation include molds, dies and EDM electrodes which are used in manufacturing industries to make other products. Modern tool manufacturing includes all aspects of manufacturing: part design, tool design, process modeling, prototype production, and control of dimensional and surface quality by use of mechanical, electrical, and electrochemical machining methods. In most countries the tool industry consists mainly of small companies, typically with fewer than 100 employees[Destefani, 1993]. In the U.S., for example, approximately 15,000 die shops represent an annual sale of about \$20 billion. The user of dies and molds increasingly expect that: a) Manufacturing costs and lead times are reduced, b) dimensional accuracy and overall quality are increased, c) dies and molds allow the production of short prototype series quickly for testing and evaluation purposes, and d) design changes can be easily accommodated. As a result of these requirements, tool makers are forced to increase communication with their customers, improve the training level of their employees, and utilize modern manufacturing technologies such as process modeling, high-speed and unmanned machining, automated polishing and CAD/CAM [Kruth and Kesteloot, 1989].

Presently, there exist two general categories of methods for tool making. One is machining, which includes, for example, milling, lathe cutting, drilling, grinding, flame

cutting, and electrical discharge machining. The common feature of tool making in this category is material removal. All machining methods begin with a workpiece in which the shape of tool is achieved by either manually or automatically controlling the cutting path relative to the workpiece to remove material until the desired shape of tool has been reached. The second category for making tools utilizes rapid prototyping (RP), also known as solid freeform fabrication (SFF), which emerged in the mid 1980's as a viable way of making parts. The common feature of rapid prototyping is that material is added in a layer-by-layer fashion by controlling the build paths for the layers. In rapid prototyping, the CAD data of a three-dimensional object is sliced into multiple two-dimensional layers. With the supporting technologies of laser, material, and numerical control (NC), two-dimensional layers of small thickness can be made and bonded layer by layer sequentially. Different materials and ways of building and binding these layers constitute different RP processes. Laser Stereolithography (SL), Laminated Object Manufacturing (LOM), Fused Deposition Modeling (FDM), Selective Laser Sintering (SLS), Sanders Prototyping and Three-dimensional Printing (3DP) are some of the commercially available processes [Leu and Zhang, 1998a; Beaman, et al., 1997; Kochan, 1993]. The implementation of RP technology has substantially cut the product development time and improved the product quality for manufacturers in many industries. Thanks to the further research and development in the supporting technologies, such as new materials, novel processes, and higher performance laser systems, RP has seen continuous improvement in part/tooling accuracy, productivity, part size, functionality, and mechanical properties.



Rapid tooling (RT) is defined here as the process of directly or indirectly employing RP technologies to fabricate dies, molds, EDM electrodes, etc. [Leu, et al, 1998b; Yang and Leu, 1999]. The main advantage of rapid tooling is shortening the design-production cycle. The direct RT method uses an RP process to directly build tools, such as building mold inserts using stereolithography (SL), making cores or cavities by printing a binder onto a metal powder (i.e. 3DP), or selectively sintering and binding metal powders (i.e. SLS). Post processing such as sintering, infiltration, etc. may be needed. The indirect RT method involves secondary steps usually with conventional tooling methods. For example, investment casting [Dickens, 1998a], silicon RTV (room temperature vulcanizing), etc. can be used with RP to produce testable prototypes or final parts, and metal spraying, metal electroplating, etc. can be used with RP to form a metal coated core or cavity or an EDM electrode [Dickens, 1998b]. Rapid tooling finds its niche by overcoming the weaknesses of conventional tool making such as long lead times, inability to incorporate design changes, early commitment to financial resources in the product development cycle, and inability to provide early products for testing and customer evaluation.

Electroforming, invented by M.H. Jacobi of the Academy of Science of St. Peterburg, Russia in 1838 [Spiro, 1968], enables the fabrication of simple and complicated components by means of electroplating of metal onto a master that is subsequently separated from the deposit (called the electroform). The fine difference of electroforming with electroplating is that electrodeposited metal on an electroplated product is an integral part of the product, but electroforming is the use of electroplating technology to fabricate a separate, freestanding entity composed entirely of

electrodeposited metal. So electroplating is more of a surface finishing technique but electroforming is a manufacturing technology. Electroforming was mainly used to copy antique masterpieces in the last century. Currently, it is widely used in the electronics, aerospace, automotive, and instrumentation industries for a variety of processes. Electroformed parts most commonly are made of copper, nickel, iron, silver, cobalt or some kind of alloy. Electroforming can be used to make molds and dies which can not be readily made by machining or other mechanical processes [Degarmo, 1984, Dibari, 1996, Lu, 1991]. Making of masters for electroforming is conventionally done by machining or molding. After the master is made, metal is electrodeposited upon the metalized master. Upon reaching the desired thickness, the metal-covered master is removed from the solution. The master is then removed to form a metal shell. The shell is then backed with other materials to form a mold cavity or an EDM electrode. A nickel or nickel-cobalt alloy electroformed master can be used for a prototyping tool or a production tool, and a copper electroformed master can be used as an EDM electrode. Metals deposited by electroforming have distinct properties [Safranek, 1986]. Dimensional deviation can be as low as 0.01%, and surface finish of  $0.05 \mu\text{m}$  or better can be obtained quite readily if the master is adequately smooth. Factors against wide application of electroforming include difficulty in the making of electroforming master, uneven deposition of metal onto the master, and difficulty in the master removal [Spiro, 1968; Yang and Leu, 1999; Yang and Leu, 2000].

The emergence of the SFF technology has brought about new opportunities for electroforming in rapid tooling. Electroforming masters can be built by RP machines and then electroformed to accurately copy the shape of the master. The integration of RP and

electroforming can produce complex metal cavities and inserts required in dies and molds. Because the outside surfaces of electroformed shells are very rough and uneven, only the inside surface (working surface), which contacts the master surface, of the electroformed shell is used as the cavity for molding. Unlike other metal powder sinter processes, electroforming can produce cores, cavities and EDM electrodes with excellent working surface finish, dimensional and geometric accuracy, as well as material properties. Integration of SFF with electroforming meets the challenge of making products and components that are difficult or impossible to make using any other conventional machining techniques. Electroforming can make thin walled hollow bodies of intricate shapes and accurate inner dimensions, such as waveguide tubes, wind tunnels and venturi nozzles with varying sections, etc.

This doctoral dissertation study is aimed at developing a novel rapid tooling process by integrating SFF with electroforming to produce metal dies, molds, and EDM electrodes quickly, accurately and cost-effectively. The study includes process development and understanding, process modeling and FEM-based analysis, as well as experimental investigation and verification. Chapter 2 reviews state-of-the-art rapid prototyping and rapid tooling processes in terms of their applications, advantages and limitations. Chapter 3 describes the tooling process, statements of the problems, research objectives and research tasks. Chapter 4 introduces a feasibility study of electroplating tooling for EDM electrode fabrication. The experimental investigation of electroforming tooling process for making molds, dies, EDM electrodes and hollow bodies is presented in Chapter 5. Chapter 6 presents the thermomechanical modeling and analysis for the thermal stress induced in the burnout process that removes the RP part from the

electroform. Chapter 7 provides considerations and general rules for design RP parts for electroforming tooling, and implementation of the tooling process. Final conclusions are summarized in Chapter 8.

## CHAPTER 2

### LITERATURE SURVEY

This chapter reviews the recent progress in the research and development of Rapid Prototyping and Tooling technologies. The processes of Rapid Prototyping (RP), also called Solid Freeform Fabrication or Layered Manufacturing, are categorized according to the form of material preparation prior to fabrication of parts. Although RP has brought in a new revolution in manufacturing processes of materials by using layer-by-layer material additive processing techniques, its crown has gradually shifted to rapid tooling/manufacturing, i.e. not just prototypes but functional products. The currently available rapid tooling technologies are briefly discussed in terms of their applications, advantages and limitations. The purpose of this chapter is provide background information for this dissertation.

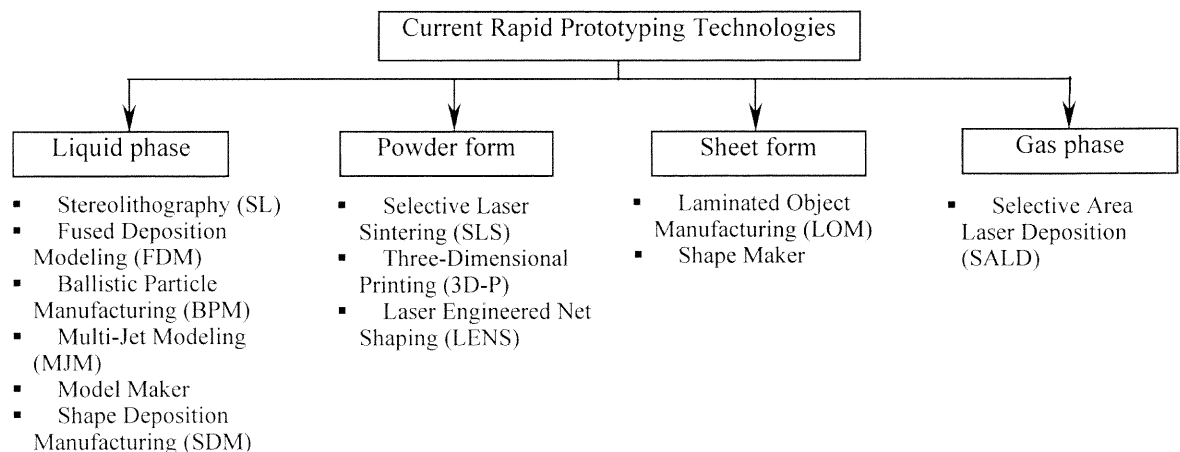
#### **2.1 Overview of Rapid Prototyping Processes**

In the middle to late 1980s, several Rapid Prototyping (RP) technologies were invented. They are capable of converting a three-dimensional CAD model directly into a solid physical model. Taking advantage of computer hardware and software technologies, the CAD data of a three-dimensional object is sliced into multiple two-dimensional layers. With the supporting technologies of laser, material, and numerical control (NC), two-dimensional layers can be made and bonded to the previous layers one by one sequentially. Different materials and ways of building and binding these layers constitute

different RP processes. Stereolithography (SL), Laminated Object Manufacturing (LOM), Fused Deposition Modeling (FDM) [Jacobs, 1996], Selective Laser Sintering (SLS) [Bourell, et al, 1994], and Three-dimensional Printing (3DP) [Sachs, 1997] are some of the commercialized processes.

### 2.1.1 Working Principles of Rapid Prototyping Processes

The existing RP processes can be classified in many ways, such as the form of material preparation, method of material fabrication, source of energy, etc. The classification shown in Fig. 2.1 is done according to the form of material preparation used in the building process [Beman, et al., 1997; Kruth, et al., 1998]. The current RP processes are classified into four categories: liquid, powder, sheet, and gas based. The processes categorized in Fig. 2.1 are illustrated in Fig. 2.2.



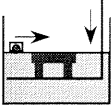
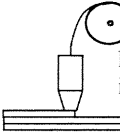
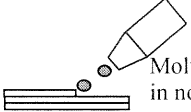
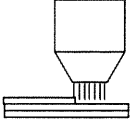

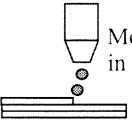
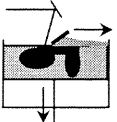
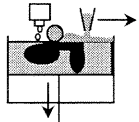
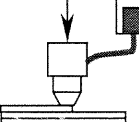
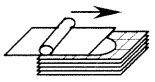
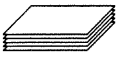
**Figure 2.1** Some of the current Rapid Prototyping processes

### ***A. Liquid Phase Based Processes***

In liquid phase processes, the material used for fabricating the parts is in the liquid phase, such as the photo curable resin used in stereolithography (SL) and the fused polymer or metal used in many depositing processes. All the materials used in the liquid phase processes are subject to phase change during part building. In fact, the phase change is the way through which the part is made. Phase change may be caused by photo exposure or by environmental cooling. In SL, the liquid resin is cured by a focused UV laser beam; in other liquid-phase processes, such as FDM, MJM, BPM, and SDM, the phase change is all caused by environmental cooling [Beaman, et al., 1997]. However, they still differ from each other in the way liquid material is deposited as well as other aspects. For example, in FDM, the fused wax or ABS is extruded out of a nozzle by feeding of a filament. In MJM, the molten plastic is ejected from a 96-element print head in a drop-on-demand manner. In SDM, the molten metal is also ejected from a nozzle. However, when solidified, the new layer is machined by a 5-axis milling machine, making the layer more accurate for both layer thickness and edge angle. The Laboratory for Solid Freeform Fabrication of Advanced Ceramics at Rutgers University has developed Fused Deposition of Ceramics (FDC) to make functional components of Ceramic materials [Dai, et al., 1997; Rangarajan, et al., 1997]

### ***B. Powder Based Processes***

Currently, there are three approaches using the building material in the powdered form: SLS, 3DP, and LENS. In SLS, a layer of powder is deposited in a bed, leveled, and then selectively sintered by a focused high power laser beam. In 3DP, the binding of powder for each layer is achieved by printing some binder based on ink-jet printing technology. In LENS, the powder is fed through a nozzle onto the substrate or a previous layer where it is melted by a high-power laser beam and then deposited [Beaman, et al., 1997].

Process	Material preparation	Layer creation technique	Phase Change during layer creation
<b>Stereolithography (SL)</b>	Liquid resin in a vat 	Laser scanning	Photo-polymerization
<b>Fused Deposition Modeling (FDM)</b>	 Filament melted in nozzle	Continuous extrusion and deposition	Solidification by cooling
<b>Ballistic Particle Manufacturing (BPM)</b>	 Molten plastic in nozzle	Drop-on-demand injection	Solidification by cooling
<b>Multi-Jet Modeling (MJM)</b>	 Molten plastic in nozzle	Drop-on-demand printing (96 elements)	Solidification by cooling
<b>Model Maker</b>	 Molten plastic in nozzle	Drop-on-demand deposition followed by cutting	Solidification by cooling
<b>Shape Deposition Modeling (SDM)</b>	 Molten metal in nozzle	Drop-on-demand deposition followed by milling and peening	Solidification by cooling
<b>Selective Laser Sintering (SLS)</b>	 Powder in bed	Laser scanning	Sintering
<b>Three-Dimensional Printing (3D-P)</b>	 Powder in bed	Drop-on-demand binder printing	No phase change
<b>Laser Engineered Net Shaping (LENS)</b>	 Powder delivered through nozzle	Continuous laser casting and deposition	Solidification by cooling
<b>Laminated Object Manufacturing (LOM)</b>	 Feeding and binding of sheets with adhesives	laser cutting	No phase change
<b>Shape Maker</b>	 Manual binding of sheets	Cutting by heated wire	No phase change

**Figure 2. 2** Working principles of Rapid Prototyping processes



### ***C. Sheet Based Processes***

LOM and Shape Maker are sheet material based processes. They differ from each other in the ways of making each layer and binding the generated layers. In LOM, the sheet material is cut by a focused high-power laser beam to create the contour of each layer. Adjacent layers are automatically glued together by heating the backing adhesives. In the Shape Maker process, the contour of each layer is cut by a heated wire and the angled edge of the contour reflects the wire orientation. Layers are then registered and bonded manually in a process that allows the construction of a prototype at a rate of approximately one vertical foot per hour [Lee, et al., 1997].

### ***D. Gas Phase Based Processes***

Rather than using solid or liquid feedstock, an approach using gas-phase precursors is SALD [Lee, et al., 1995]. This technique is a generalization of laser chemical vapor deposition and has been developed at the University of Connecticut, the University of Texas at Austin, and Rensselaer Polytechnic Institute [Maxwell, et al., 1993]. This approach results in formation of solid parts from gas-phase materials such as carbon bearing gases,  $\text{CH}_4$  and  $\text{C}_2\text{H}_2$ .

## **2.1.2 Comparison of Performance Characteristics of Rapid Prototyping Processes**

Each RP process has advantages and restrictions in terms of accuracy, material diversity, part size, build speed, and cost. None of the current RP processes excels over others in all aspects. For example, although SL is limited in material diversity, it makes parts with very good accuracy and surface finish, and is widely used for conceptual visualization,

form and fit analysis, and secondary tooling creation. The following is a comparison of the various RP processes. Table 2.1 summarizes the comparison of some RP processes [Leu and Zhang, 1998].

#### *A. Accuracy*

The accuracy of a built part with RP technology is determined by many factors. Some of the usual factors include: machine scanning/leveling/sweeping accuracy, material shrinkage during phase change, post-processing, energy, and material addition control. It is clear that the energy of laser beam in laser-based processes is much easier to control than the temperature of flow material in some heat-based depositing processes [Kochan, 1993]. So generally, the accuracy of parts made by heat related processes (such as FDM) is lower than by pure laser related processes (such as SL). However, some heat-related processes may have techniques to eliminate the inaccuracy caused by heat. For example, in the Model Maker II manufactured by Sanders Prototypes, the molten material is printed onto the previous layer or substrate and the temperature change will cause material shrinkage. However, since the material is printed in very small drops and that each printed layer is further milled by a slab cutter, the part accuracy is greatly improved. SDM is also a heat-related process. The deposited metal is subject to substantial shrinkage and thermal stress, which are both negative factors for part accuracy. However, the 5-axis milling and shot peening after the deposition help to assure the dimensional accuracy and eliminate stress build-up [Sachs, et al., 1997]. Generally speaking, processes based upon laser or drop-on-demand technology and those followed by an additional subtractive method can provide better accuracy than those based upon heat or

continuous deposition technology without an additional subtractive method. Furthermore, in order to improve part accuracy, the machine scanning/leveling/sweeping accuracy should also be further improved, and materials with smaller shrinkage during phase change are needed.

The amount of energy and material in Rapid Prototyping must be precisely controlled in order to make parts with desired dimensional accuracy and mechanical property. In processes such as FDM, precise flow control of the viscous fused material (wax, ABS, etc.) is essential to achieve good accuracy and surface finish. Ways to control the material flow include using an extrusion tip with a smaller aperture, providing accurate material temperature control, optimal depositing routes, etc. On the other hand, the energy applied to the building material is also very critical. For example, in the SL process, the curl distortion of the H-part built with SL-5170 resin is shown to be strongly correlated with the surface exposure index (an index proportional to the applied laser energy per unit area for each layer). In order to build a part with less curl distortion, the building parameters must be very carefully designed to control the exposure to a certain level. More exposure will result in larger distortion while too small exposure may result in delamination.

### ***B. Material Diversity***

Among the current RP processes, the powder based technologies including SLS and 3D-P are typical processes that can use a wide variety of materials, including plastic, wax, ceramic, and even metal powders. Both of SLS and 3DP can directly build metal functional parts. However, the green parts made by these two processes need to be further

**Table 2.1** Comparison of some Rapid Prototyping processes

Processes	SL	FDM	SLS	3D-P	LOM	SDM
Machine	SLA-250 SLA-350/ - 3500 SLA-500/ - 5000	FDM 1650 / 2000 FDM 8000 FDM Quantum	Sinterstation 2000 / 2500	DSPC (Direct Shell Production Casting), Z402	LOM-1025/- 2030H	No commercial machine available
Technology to make and bind each layer	Curing photo- polymer resin with laser beam	Controlled extrusion and deposition of fused material	Sintering powders with high power laser beam	Binding powders with printed binder	Cutting contour of each layer with high power laser beam, then stacking with adhesives	Molten drop ejection deposition, milling, and shot peening
Source of energy	UV laser beam	Heat	High power laser beam	Binder /particle reciprocity	High power laser beam	heat
Material amount control in each layer	Sweeping /leveling	Precise deposition from nozzle	Depositing /leveling and pressing	Leveling/pres sing plus printing binder	Sheet stacking	Depositing from ejection nozzle in drops
Material	Liquid photo- polymer	Nylon/ABS/A BSi/ Wax Filament	Nylon/ poly- carbonate/ca sting wax powder	Almost any kind of powder plus binder	Sheet paper/Polyeste r backed with adhesives	Various kinds of metals
Support	Need support	Need support	Self- supporting	Self- supporting	Self- supporting	Need support
Post processing	Post-curing	None	May need HIP or infiltration depending on applications	Sintering/Firi ng ; may need infil- tration depending on application	None	None
Layer thickness	0.002" - 0.020"	0.002" - 0.030"	0.003"- 0.020"	*	0.002" - 0.015"	*
Build Size	10"x10"x12 " to 20"x20"x24 "	10"x10"x10" to 23.6"x19.7"x 23.6"	φ12 " x15" to 15"x13"x16. 7"	16"x16"x16"	10"x15"x14" to 22"x32"x20"	N/A
Accuracy	0.0018"	0.005"	0.005"	*	0.01"	0.01"

**Table 2.1** (continued)

Tooling capability	QuickCast (investment casting), RTV molding, Keltool, AIM (injection molding), spray metal tooling	RTV molding, spray metal tooling, sand casting, and investment casting	Direct tooling, investment casting, RTV molding	Direct investment shell casting, direct tooling	Sand casting, investment casting, injection molding	Direct metal tooling
--------------------	--	--	---	---	---	----------------------

\* no data source at hand

sintered in order to remove the binder material. The sintered parts are porous which need to be further processed to become fully dense. In 3DP, the printed parts are post-processed using techniques borrowed from metal injection molding to produce metal parts with greater than 92% of theoretical density. These parts may be infiltrated with low melting point alloys to produce fully dense parts [Das, 1997]. In SLS/HIP process, the component is produced by selectively consolidating metal powders with a laser beam layer by layer. While producing each layer, a gas impermeable, very high-density skin (>98% density) is formed at the boundary of the part by providing high laser energy at a low scanning speed. The interior of the part is processed (with slightly less laser energy) to a high density typically exceeding 80%. Thus the part is shaped and canned in-situ. The encapsulated part is evacuated, sealed, and post-processed by containerless hot isostatic pressing (HIP) to full density. A fine machining step may be applied if necessary.

On the other hand, though SL provides good accuracy and surface finish, its materials of coverage are very limited. To obtain metal or functional parts, some secondary process is needed, such as QuickCast® and RTV molding.

### ***C. Build Size/Speed***

Many of the existing commercial RP processes have the capability to increase part build size and improve build speed without great technological differences. However, there exist some restricting factors, such as the maximum achievable building speed, inaccuracy caused by thermal stress, material cost, and part strength. It is clear that processes with higher building speeds, less distortion caused by stress, cheaper materials, and stronger part strength are better able to increase the build size. It will be very difficult for processes with drop-on-demand deposition, such as the Model Maker process, to substantially increase their build size without technical break-through. On the other hand, for the SL process, the build speed and build size may be substantially improved, provided that the laser power is increased and that the distortion is reduced. Another example of speed-improving/size-enlarging is the introduction of FDM Quantum by Stratasys, utilizing the MagnaDrive scanning technology which is much faster than the previous motion system.

### ***D. Application***

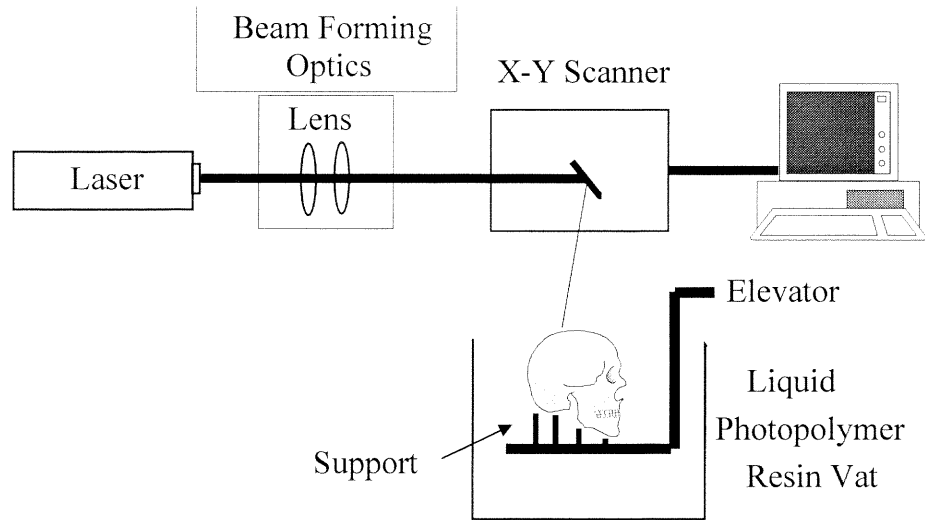
All current RP processes can build prototypes for visualization purpose. The materials of these prototypes include cured photo-polymer resin, plastic, wax, wood, and metal. Most RP processes can also directly build plastic functional parts, such as SL, FDM, etc. However, only a few processes can directly build metal functional parts while the other processes need a secondary process. As mentioned above, the SLS process can build

metal parts with the post-processing technology of HIP or metal infiltration. For most of the other RP processes, RTV molding and casting (sand casting and investment casting) are the most used secondary processes to make metal parts from prototypes.

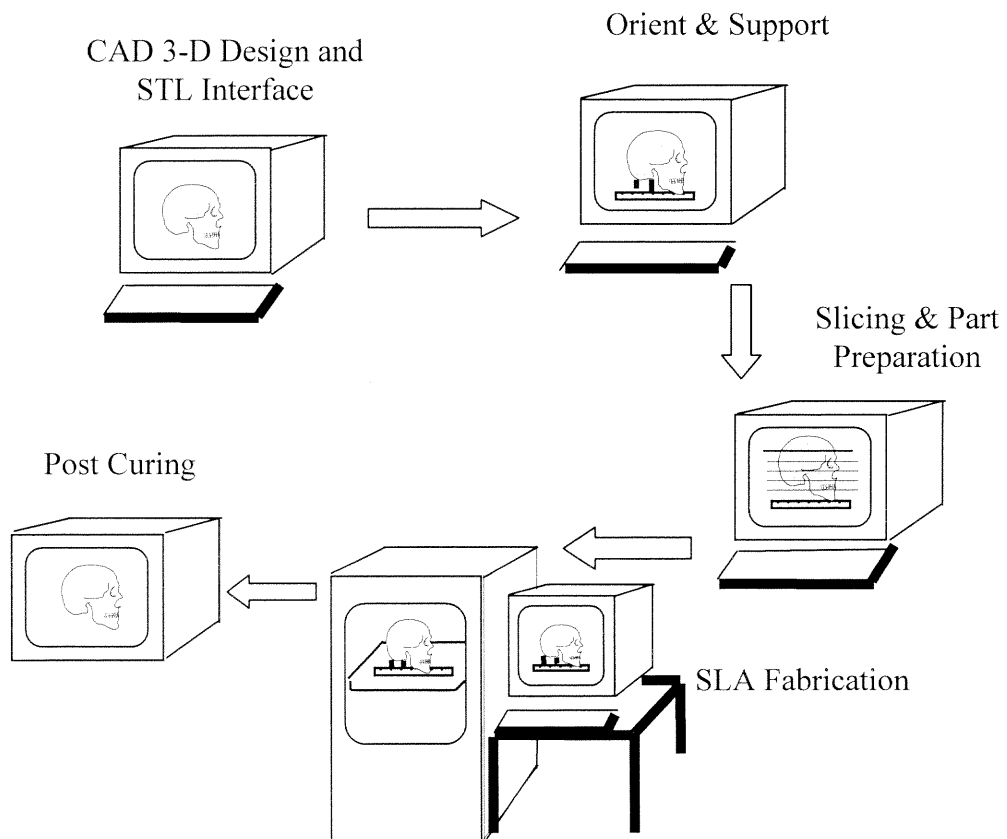
## **2.2 Stereolithography Apparatus**

SLA was firstly commercialized in 1988. It is one of the most widely used processes today. It is an optical fabrication process that translates CAD solid model data into a physical model by successively laser-curing liquid photopolymeric resin to build the cross sections of a part. The computer controlled SLA system consists of an open-topped vat of photocurable polymer resin, computer controlled automatic elevating platform and leveling device, ultraviolet (UV) or visible wavelength laser and optical mirror system. A schematic illustration of the SLA machine is shown in Fig.2.3. The process of producing an SLA prototype starts from a 3D CAD design. In the pre-processing, a three-dimensional object is developed using a CAD system and its surface is approximated by triangular facets in STL format. The object is then sliced into a number of two-dimensional cross-sections. The part is built from bottom to top by a computer controlled laser and elevator. The process of production of an SLA prototype is shown in Fig.2.4.

As noted above, SLA builds a part by controlling a laser beam to selectively cure liquid photopolymer layer by layer. So, the principle of polymerization and exposure of laser beam play very important roles in SLA technology. In the following sections, the principles of photo polymerization and exposure of laser beam to SLA will be reviewed in order to gain solid understanding of the process.



**Figure 2.3** The Stereolithography Apparatus system



**Figure 2.4** Fabrication sequence of an SL prototype



### 2.2.1 Photocurable Resin and Photo Polymerization

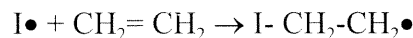
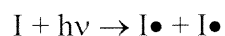
The materials used in SLA method are photocurable polymer resins. They are cross-linked liquid thermoset polymers and photoinitiators, such as acrylate resin or epoxy resin. Epoxies are attractive because of their higher mechanical strength and low volumetric shrinkage compared to acrylate. The requirements for this resin systems are:

- high reactivity, in order to achieve high degrees of polymerization,
- an unchanged viscosity, in order to allow an equal layering,
- good in susceptibility to aging, because the material consumption compared to the fill volume of the work container is proportional small,
- low sensibility against process parameter variability,
- low toxicity,
- low contraction, and
- high rigidity and impact toughness.

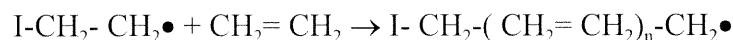
The forming of photocurable thermosets resin is more complicated.

Polymerization is the process of linking small liquid monomers into larger solid polymers

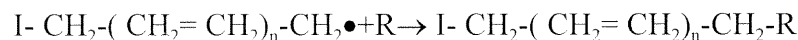
Initiation:



Propagation:



Termination:



**Figure 2.5** Photopolymerization process: initiation, propagation, and termination

using the catalyst energy of absorbed photons. The radicals may be generated either thermally or photochemically. In SLA, the forming of thermoset polymers is photoinitiated radical polymerization. Actinic photon is the catalyst for transformation of the liquid monomer to solid polymer. Three essential steps in polymerization for SLA are initiation, propagation, and termination. A radical process of photopolymerization of ethylene is shown in Fig.2.5.

### 2.2.2 Laser Exposure

SLA is able to rapidly direct focus radiation of appropriate power and wavelength onto surface of a liquid photocurable resin to solidify resin for a two dimensional layer of a part. The use of laser beam with a continuous wave emitting radiation of power  $P_L$  at a suitable wavelength  $\lambda$  is the source of radiation with very high radiance to provide a tightly focused spot on the surface of the photopolymer located at a substantial distance. The excellent features of a SLA part is highly relied on the features of laser. For examples, the minimum feature size of a part is determined by the diameter of the focused laser spot on the photopolymer surface. The resolution of a part depends on the angular accuracy of the galvanometers, the ability to control the intensity distribution, and the laser power.

The solidification of the liquid resin depends on the optical energy per unit area, or known as the exposure, deposited during motion of the focused spot on the surface of the photopolymer. When the exposure is less than a critical value,  $E_c$ , the resin remains liquid. When the exposure is greater than  $E_c$ , the resin polymerizes. When the exposure is

equal to  $E_c$ , the polymer is at the gel point, corresponding to the transition from the liquid phase to solid phase. The critical exposure energy at locus of points ( $y^*$ ,  $z^*$ ) is:

$$E_c = \sqrt{\frac{2}{\pi}} [P_L/W_o V_s] \exp [-(2y^{*2} / W_o^2 + z^* / D_p)] \quad (2.1)$$

where  $P_L$  is laser power,  $W_o$  is Gaussian half width,  $V_s$  is scan speed, and  $D_p$  is penetration depth of resin where the irradiance is about 37% or  $1/e$  of the surface irradiance. After algebra operation eq. (2.1) becomes:

$$2y^{*2} / W_o^2 + z^* / D_p = \ln \left\{ \sqrt{\frac{2}{\pi}} [P_L/W_o V_s E_c] \right\} \quad (2.2)$$

Note that  $W_o$ ,  $D_p$ ,  $P_L$ ,  $V_s$ , and  $E_c$  are all constants, eq. (2.4) can be written in the form

$$a y^{*2} + b z^* = c \quad (2.3)$$

where  $a$ ,  $b$ , and  $c$  are all positive constants. Equation (2.3) is a parabolic cylinder equation. Figure 2.6 shows a schematic view of a cured line having the parabolic cross-section.

In SLA, the relationship between the thickness of the exposed layer and the applied energy is called the “working curve” of a given resin. The equation representing the working curve is

$$C_d = D_p \times \ln \left( \frac{E}{E_c} \right) \quad (2.4)$$

where  $C_d$  is the maximum cure depth or thickness of the solidified layer,  $D_p$  is the penetration depth,  $E$  is the exposure energy used to solidify the resin mixture and  $E_c$  is the

critical exposure at which solidification starts to occur. The equation (2.4) states five fundamental points of the laser exposure of the SLA process:

- The cure depth is proportional to the natural logarithm of the exposure on the centerline of the scanned laser beam.
- The semi-log plot of  $C_d$  versus  $E$  is a straight line. This line is known as working line of a given resin.
- The slope of the working curve is penetration depth,  $D_p$ , of that resin at the laser wavelength.
- The intercept of the working curve is  $E_c$ , the critical exposure, of that resin.
- The  $D_p$  and  $E_c$  are resin parameters, and independent of laser power.

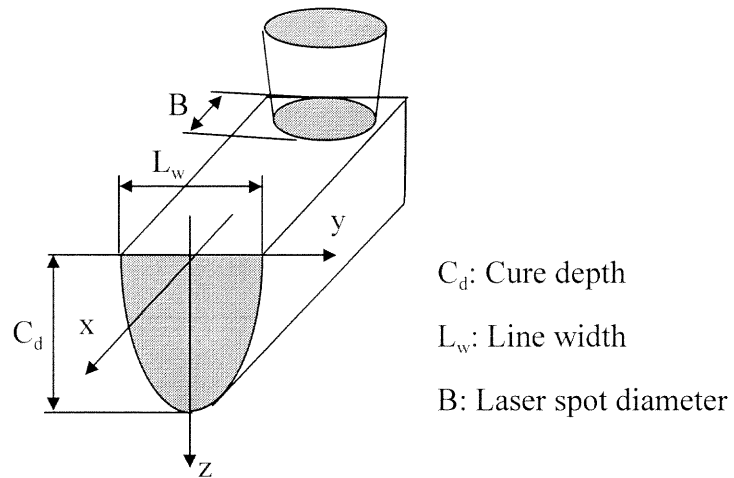
The maximum linewidth can be derived from eq. (2.2). Let  $z^* = 0$ , and linewidth,  $L_w$ , =  $2y^*$  plus working curve. Eq. (2.2) becomes

$$L_w = W_0 [2 C_d / D_p]^{1/2} \quad (2.5)$$

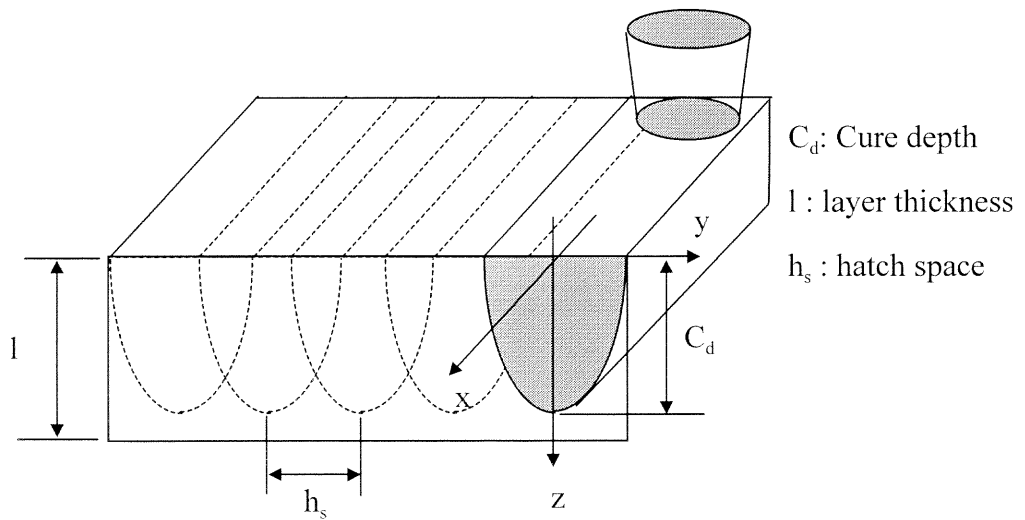
where  $W_0$  is the Gaussian half-width of laser irradiance distribution,  $L_w$  is defined as the full-width of a laser cured line. The laser spot diameter is  $B = 2W_0$ . The cured linewidth becomes

$$L_w = B \sqrt{C_d / 2D_p} \quad (2.6)$$

The cured linewidth is directly proportional to the laser spot diameter,  $B$ . The cured linewidth is also proportional to the square root of the ratio of the cured depth to the resin penetration depth ( $C_d / D_p$ ). Thus curing deeper will also result in increased linewidth. The scan of a line and a layer, and working equation and cure are shown in Fig.2.6. and Fig.2.7.



**Figure 2.6** Laser exposure of a line



**Figure 2.7** Laser exposure of a layer

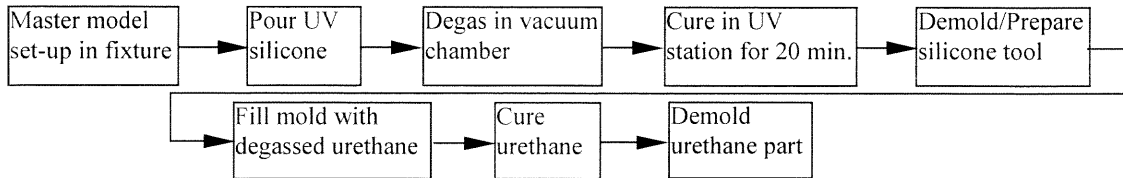
## **2.3 Rapid Tooling Research and Development**

Rapid Tooling (RT) is the process of directly or indirectly employing RP technology in tool, die and mold fabrication. These tools may serve the purpose of forming a prototype part in the end use material for design evaluation, or producing a product that only a small quantity is to be manufactured [Ashley, 1997]. Direct RT methods involve directly producing tools with RP processes and some post processing, such as SLS with low melting point alloy infiltration or hot isostatic pressing. Indirect RT methods involve secondary processes by utilizing RP patterns in conventional casting, metal spraying, or RTV molding [Aubin, 1997].

### **2.3.1 Direct Rapid Tooling**

Processes capable of directly making tools include SLS, 3D-P, SDM, LENS [Karapatis, et al., 1998], and direct ACES (Accurate Clear Epoxy Solid parts) Injection Molding (AIM) [Decelles, 1998]. Low melting point metal infiltration is an important step in some direct RT technologies. It is used to obtain fully dense metal parts from sintered or burnt green patterns made by SLS or 3D-P. Infiltration results in much less shrinkage than HIP technology. However, the disadvantage of infiltration is that it takes longer time. As compared to SLS and 3D-P, the SDM and LENS processes can directly build metal parts with almost no post-processing.

The AIM process is good for making 20-100 prototype parts. It is used to directly inject thermoplastics at up to 300°C into an ACES core and cavity built with an SL photo-polymer having the glass transition temperature of about 75°C [Jacobs, 1997]. The



**Figure 2.8** UV based silicone molding process

key to success in this process is cooling. Currently, Georgia Institute of Technology is working on injection molding with SL patterns, similar to the AIM process [Dawson, 1998].

### 2.3.2. Indirect Rapid Tooling

The indirect rapid hard tooling involves secondary steps by using an RP pattern combined with conventional metal casting, such as investment casting and sand casting, etc., and metal spraying, metal electrodeposition, etc. to produce a metal coating to form cores and cavities in the production of complicated metal molds or EDM electrodes, which are typically difficult to machine due to complex geometry or hard material property.

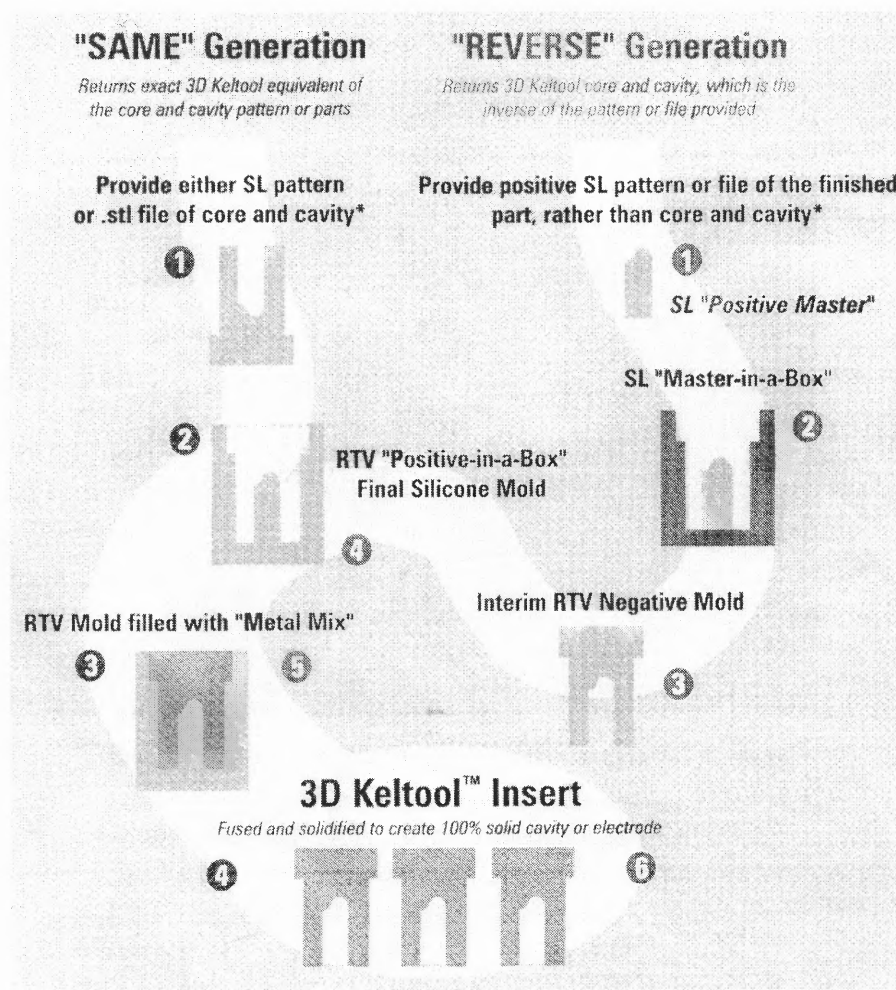
#### *A. UV Silicone Molding*

Silicone RTV molding is a widely used soft tooling process. The recently introduced UV silicone molding is very similar to the traditional RTV molding except that the curing of silicone mold or urethane part is achieved by UV light. The process is shown in Fig.2.8. In the process, the UV cured system utilizes a stable photo-initiator that only reacts to UV radiation. Since temperature is not a factor in this curing process, there are no thermal expansion concerns, no oven temperature stability problems, and no exothermic reactions

to breakdown in the silicone mold. The shrinkage for the UV silicone and UV urethane is stable, consistent and predictable (0.3%). Also, with the photo-initiator acting as the catalyst, the curing speed is a fraction of the time it takes for thermal or addition cure systems. A silicone mold measuring 4"x5"x7" is cured by UV light within 15 minutes.

### ***B. 3D Keltool Powder-Metal Sintering***

The 3D Keltool powdered metal sintering process is a proprietary process of 3D systems for rapid metal hard tooling. The procedure (see Fig.2.9) is as follow [Ashley, 1997;



**Figure 2.9** The 3D Keltool processes (Jacobs, 1996b)



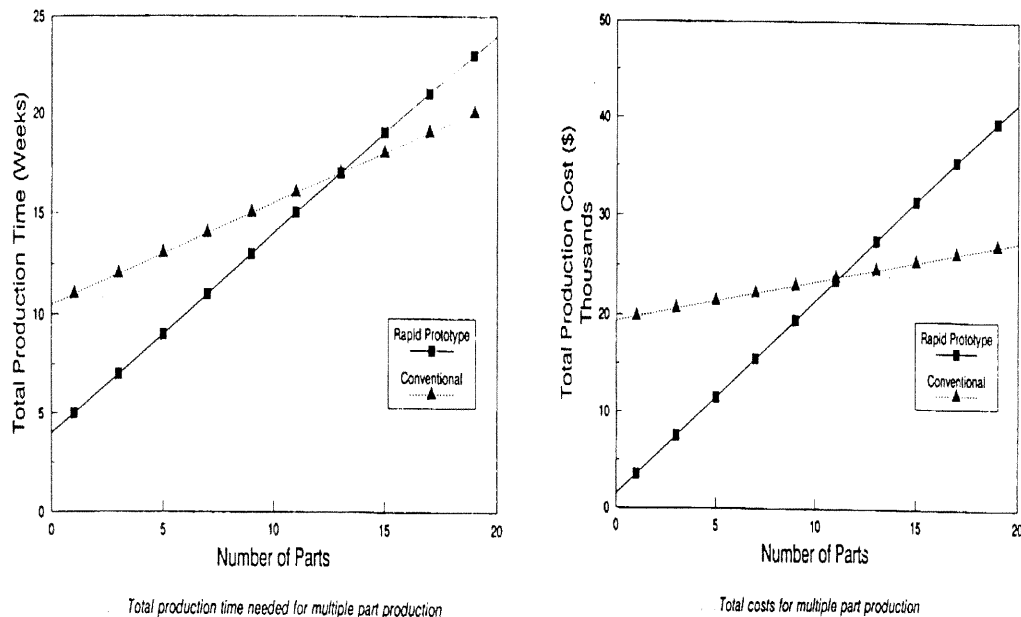
Raetz, 1998]. An positive ACES SL pattern is used to make a precision RTV silicon mold. This temporary mold is then filled with a patented mix of metal particles and a proprietary binder material. After curing and demolding, the green part is fired in a hydrogen reduction furnace that removes the binder and sinters the powders to form a semi-porous metal part. Toxic gases generated in the fusing and sintering process need to be carefully handled. The fused part, which has 30 percent void space, is infiltrated with copper. The end result is roughly machined to form a mold cavity that is essentially 100 percent solid. The shrinkage of the 3D keltool is 0.8 percent. 3D keltool metal inserts are typically manufactured in three weeks, so it saves time. The process saves money in the range from 25 percent to as much as 40 percent compared with traditional CNC machined steel tools. The tool life is excellent. For neat plastics, as many as 10 million injection molded parts have been produced from a single keltool insert. For glass filled resins, lifetime of 500,000 to 1,000,000 parts per tool have been achieved [Jacobs, 1997].

### ***C. QuickCast Tooling***

The use of SL pattern in sand casting has shown a good yielding rate. But this old technology is less popular than the shell investment casting because of its relatively poor production quality. The early attempts to use SL solid patterns to replace investment casting wax patterns met with limited success. The build style and low viscosity epoxy resin of QuickCast provide a solution for increase of the investment casting yield rate. After the SL pattern is postcured, it is invested with ceramic slurry for desired thickness. After the ceramic shell is dried, the investment ceramic shell with SL pattern is put into a flash oven to burnout the pattern, creating the cavity. The shell is then ready for pouring

molten metal. After the molten metal is solidified, the shell is broken to recover the metal prototype.

Investment casting process with the SL models provides the designer with the ability to produce truly functional prototypes quickly. This investment casting process using SL patterns eliminates the initial tooling need associated with conventional production and thus allows the designer to fabricate a functional part at a fraction of the cost and time. Metal casting lead times are also reduced to as little as 2-3 weeks. This process is particularly useful if only one or two parts are to be made for design testing and qualification. Fig.2.10 compares the total time and cost versus number of parts required of the rapid prototyping using SL patterns with those required of the conventional process (Sarkis, 1994; Yao, et al., 1996).



**Figure 2.10** Total production time and cost vs. number of parts

### ***D. Spray Metal Tooling***

Spray metal tooling is an economic way to produce short-run evaluation prototypes made of production materials. The use of RP master for spray metal tooling has resulted in a shorter turnaround time. The spray metal tooling process is as follows. When a RP master is ready to be molded, the RP master is secured on a parting surface and is sprayed with a sealer and release agent. Then an electric arc spraying gun coats the master with zinc alloy. The spraying process is complete when a shell of desired thickness is achieved. The shell is then fit into a mold form, and the back is filled. The type of backing depends on the type of molding process to be used. For example, aluminum-filled epoxy backing would be used for light pressure applications such as vacuum forming, reaction injection molding. A low-melt castable alloy backing can be used for high pressure injection molding applications, or resin transfer molding. Fig.2.11 shows a mold generated by spraying metal on an SLA generated part.



**Figure 2.11** Spray metal tooling (ProtoTech Engineering, Inc., IL)

## 2.4 Accuracy Comparison among Current Rapid Tooling Techniques

One of the main problems with rapid tooling techniques at the present is the inability to hold tight tolerances, especially on larger tools. Jacobs [1998] has shown that when tools are produced by a process which involves tool material phase change, such as from liquid to solid or from solid to liquid, there usually exists an associated random shrinkage of the material. The variation in accuracy is directly proportional to the amount of shrinkage. A modified version of this prediction model initiated by Jacobs determines the tolerances for a number of rapid tooling techniques.[Mueller, 1998].

Currently used rapid hard tooling processes such as 3D Keltool™ [Raetz, 1998], 3-dimensional printing (3DP) [Sachs, et al., 1997; Sachs, et al., 1990] and RapidTool™ [Bourell, et al., 1994], first bind metal powders by various techniques to generate a green part. Afterwards the part is debinded, sintered, and infiltrated with copper or other metals to produce functional metal parts. The powder metallurgy approaches involve random noise shrinkage during the sintering process and thus the generated metal parts suffer dimensional uncertainty and they usually have rough surface finish. Comparing with those powder metallurgy tooling processes, the rapid electroforming tooling (RET) process developed in this dissertation generates metal tools with better accuracy and finer surface finish [Yang and Leu, 1999]. This is because the geometry and surface finish of the pattern are accurately duplicated during the electroforming process [Spiro, 1968], and other deformation sources can be accurately controlled through process modeling and simulation as described in chapter 6 of this dissertation. An accuracy based comparison among these rapid metal tooling processes is given in Table 2.2 [Karapatis, 1998; Zhou and He, 1998; Yang and Leu, 1999].

**Table 2.2** Accuracy based comparison among rapid metal tooling processes

	Main process	Shrinkage	Surface finish	Accuracy (mm)
SLS	Sintering	4%	Rough	0.1
3-DP	Sintering	5%	Rough	0.1
LENS	Melting	N/A	Rough	0.5
3D Keltool	Sintering	0.6%	Fine	0.05
RET	electroforming	0	Extra-fine	0.005

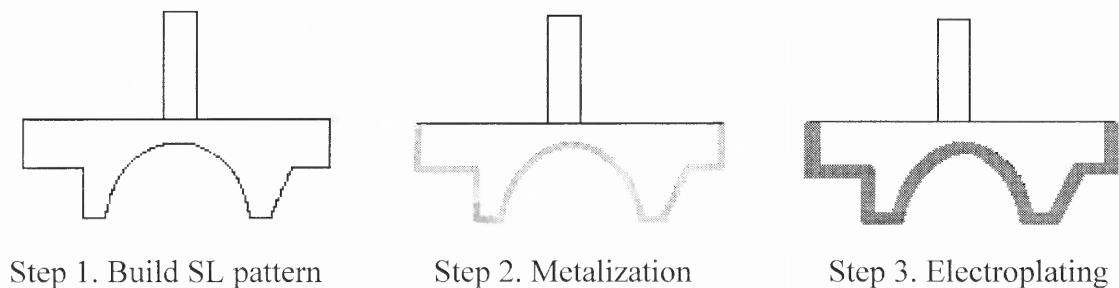
### RESEARCH OBJECTIVES, ISSUES AND APPROACHES

This chapter first introduces the developed rapid tooling processes, namely the rapid electroplating tooling and rapid electroforming tooling. The main problems encountered in electroforming tooling process are stated. The research objectives, issues, approaches and tasks are then presented.

#### 3.1 Tooling Approaches

##### 3.1.1 Electroplating Tooling

Electroplating tooling is studied for use in rapid fabrication of electrical discharge machining (EDM) electrodes using RP patterns. A positive SL model is electroplated with copper to form EDM electrodes without further post-processing or finishing. The basic steps, as shown in Fig.3.1, include fabrication of RP pattern, metalization to make it electrical conductive, and electroplating. A feasibility study of EDM tooling using electroplated stereolithography models has been performed and presented in Chapter 4.



**Figure 3.1** Electroplating tooling using RP pattern.

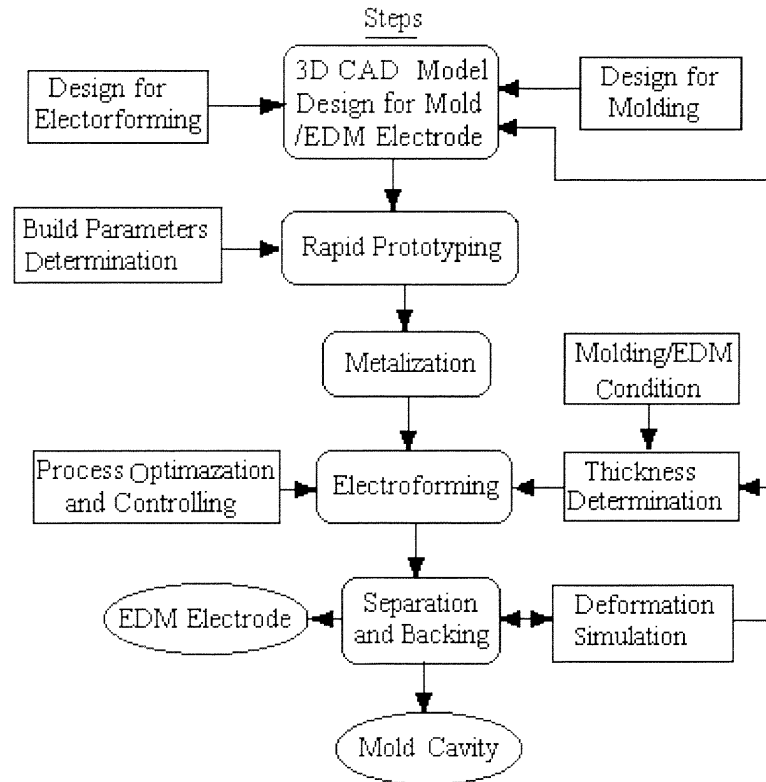
### 3.1.2 Electroforming Tooling

Electroforming is the use of electrodeposition of metal onto a master to replicate the master in a reversed format to produce a thin metal shell. The master, which has the required shape, dimension, accuracy and roughness, is sinked into an electrolyte bath as the cathode and is deposited a desired layer of metal, normally copper or nickel. This metal shell is called electroform. If the master is nonconductive, it needs to be metalized before electroforming. The master is separated from the electroform to form the mold cavity. Electroforming was mainly used to copy antique masterpieces in the last century. Currently, it is widely used in the manufacturing, electronics, aerospace, automotive, instrumentation industries and for copy of art articles. Electroforms most commonly are made of copper, nickel, iron, or silver, and electroforms of thickness up to 16 mm (5/8 inch) have been deposited successfully [Dibari, 1996]. Metals deposited by electroforming have their own distinct properties [Degarmo, 1984]. Dimensional tolerances are very good, often up to 0.0025 mm (0.0001 inch), and surface finishes of 0.05  $\mu\text{m}$  (2 microinch) can be obtained quite readily if the master is adequately smooth. The main obstacle to the development of electroforming is the manufacturing of the master. Electroforming has been used for dies and molds fabrication [Spiro, 1968]. With the development of the electroforming technology, alloy such as Ni-Co can be deposited onto the master to form an alloy shell so that the strength and hardness of the mold can be largely improved [Li, et al., 1992; Stephenson, 1966].

The emergence of RP technologies has brought about new opportunities in the utilization of electroforming for making of molds, dies, EDM electrodes and hollow bodies as disclosed in the dissertation. Masters can be made using RP machines described

in Chapter 2. After the RP master is metalized, an electroform is made from the master with the interface layer conforms intimately to the master. However, separation of the electroform from the master may not be easy and the difficulty increases as the form complexity increases. Traditionally, the master is removed by extraction (pull-off), heat-softening, melting or chemical dissolution. Separation of an RP master by mechanical pull-off has been found impractical, however, since extreme care and skills are required during the pulling off process in order not to damage the metal shell. The pulling force may break the master thus leaving some master relic in the metal shell, especially when the master is brittle and intricate in shape. Pull-off can not be used if the master is enveloped in the metal shell such as a hollow-body electroform of complex shape. Dissolving the RP master in a chemical solution to separate the metal shell by causing delamination of the interface layer may be possible but the time taken may be excessive. Melting, incineration or heat softening may be applied to wax or polymer RP master for separating the electroform from the master. A major problem is that these materials have much higher coefficients of thermal expansion than the electroformed metal. During the process of heating up the electroformed object, the expansion of the RP master can significantly deform the metal shell. Bocking [1997] described the use of thermal cycling (without detailed information) to separate a polyurethane master from a metal shell, but stated that removal of an SL master is more difficult than removal of a polyurethane part because an SL part is more brittle and tends to fracture during the removal process and thus an SL part is used as a master to create a vacuum cast mold used to produce a polyurethane master for electroforming.





**Figure 3.2** The tooling process being investigated

Figure 3.2 illustrates the electroforming tooling process being investigated for fabrication of dies, molds and EDM electrodes. The basic process is as follows:

- A CAD model is generated and transformed into STL/SLI file format. This file is input into an RP machine to build the electroforming master.
- The master is metalized and then placed in an appropriate electroplating solution and metal is deposited upon the master by electrolysis.
- When the required electroform thickness has been deposited, the master is then removed from the metal shell by burnout.

- The metal shell is backed with low melting alloy to form a mold cavity or an EDM electrode.
- If a thin walled hollow body is required, the master is removed from the metal shell and the shell is post-processed to form the hollow object.

In this doctoral dissertation study, the EDM electrodes are electroformed with copper and the molds are electroformed with nickel. The RP pattern is made by SL. The RP pattern is removed by burnout. The coefficient of SL resin is about one magnitude larger than that of the electroformed nickel or copper. The thermal expansion of the SL pattern results in thermal stress that could deform or even crack the electroform. The electroformed copper shell is backed with tin-lead (Metspec 217) alloy whose melting temperature is 103 °C and the electroformed nickel shell is backed with tin-lead-bismuth (Metspec 281) alloy which melts at 138.5 °C. The coefficient of thermal expansion of Metspec 281 is  $15 \times 10^{-6} / ^\circ\text{C}$ , which is very close to that of the nickel valued at  $14 \times 10^{-6} / ^\circ\text{C}$ .

### **3.2 Research Objectives, Issues and Approaches**

The currently popular rapid hard tooling processes utilize the metal powder sintering and infiltration method to produce metal parts. These powder metallurgy processes involve phase changes and consequently random shrinkage during the phase change [Paul, 1998; Zhou, 1998]. The random shrinkage implies that the approaches based on one form or another of powdered metallurgy are doomed to suffer dimensional uncertainty. Moreover, the produced parts always have rough surface finish. Comparing with the other rapid tooling processes, the described method of integrating stereolithography with

electroforming has much smaller random shrinkage and it generates metal tools with better accuracy and finer surface finish (Yang and Leu, 1999).

The *objective of this research* is aimed to understand and optimize the described rapid electroforming tooling process for the purpose of producing metal molds, EDM electrodes, and thin walled hollow bodies with intricate shapes and accurate dimensions rapidly, accurately and cost-effectively. The new process has the potential of being widely used in manufacturing, aerospace, automotive, instruments, electronics and consumer products.

In order to achieve this objective a number of *research issues* are addressed in this dissertation study. They are:

- Identification of inaccuracy factors in the tooling process and methods for accuracy improvement. The accuracy of the formed mold cavity or EDM electrode is influenced by RP masters, materials, geometry, and process parameters.
- Modeling of thermal stress induced by the burnout processes. Based on the observation of our previous experiments (refer to Chapter 5), the largest inaccuracy source is the deformation caused by burnout of the SL master. The thermally induced stress could even crack the thin nickel or copper shell. The thermal model and structure model will be established to analyze the distortion. The analysis result is used to determine a optimal electroform thickness and to guide the structure design and optimization for the SL parts.
- Process development and implementation. The design methods of 3D CAD masters for electroforming tooling will be studied through experimentation and analysis. The

implementation and optimization methods take into consideration of tooling time, cost and tooling accuracy.

To deal with the above research issues, the *research approaches* taken are:

- Experimental investigation: Determine the main inaccuracy factors through process development and understanding. The experimental work demonstrates that the main inaccuracy factor is the thermal expansion of SL master during the separation process.
- Analytical modeling: Thermomechanical modeling of the process of incineration of SL master. The governing equation and the initial and boundary conditions will be established to provide a theoretical model of the burnout process.
- Numerical simulation: Finite element method (FEM) will be used to numerically simulate the thermally induced deformation and distortion of the metal shell in the burnout process using the established thermomechanical model.
- Experimental verification: The simulated results will be experimentally verified to check the predictions of the established theoretical model.

### 3.3 Research and Development Tasks

Based on the research objective and related issues, the following research tasks are performed:

- ***Process Development and Understanding***

The tooling process needs to be established and understood for this rapid tooling approach. The problems and related research issues are identified during the process

development period. The main considerations include SFF part design, separation, backing and inaccuracy identification.

- ***Property Specifications of the Materials***

The accuracy of tools generated by the proposed tooling process is mainly determined by the properties of the materials used. The deformation and distortion generated at the burnout process depend greatly upon the thermal and mechanical properties of the cured SL resin and the electroformed metal. The used SL resin in this study is SL 5170. The electroformed metal may be nickel or copper. The properties of these materials are essential for the analysis of thermal stress induced during the incineration process.

- ***Analytical Modeling of Thermal Stress in the Burning out Process***

Thermomechanical modeling of the burnout process is established to solve the thermal stresses induced during the burnout process. The governing equation and the initial and boundary conditions are established to provide a theoretical model of the burnout process.

- ***Numerical Simulation***

Analytical calculation of the thermal stress is extremely difficult. To solve this problem, finite element analysis (FEA) is used to simulate the thermal stress resulted from the burnout process. The finite element model is implemented in ANSYS, a commercial software package for multi-physics modeling and analysis.

- *Experimental Verification*

In order to verify the thermomechanical model results obtained through numerical analysis, strain gages are used to measure thermal stresses resulted from burnout of electroformed objects. The measured thermal stresses are compared with the analysis results to verify the finite element based thermomechanical model.

- *Design and Optimization Approaches*

Finally this dissertation provides design and optimization studies for RP master and electroform thickness to minimize the manufacturing time and cost while satisfying the tooling accuracy requirement.

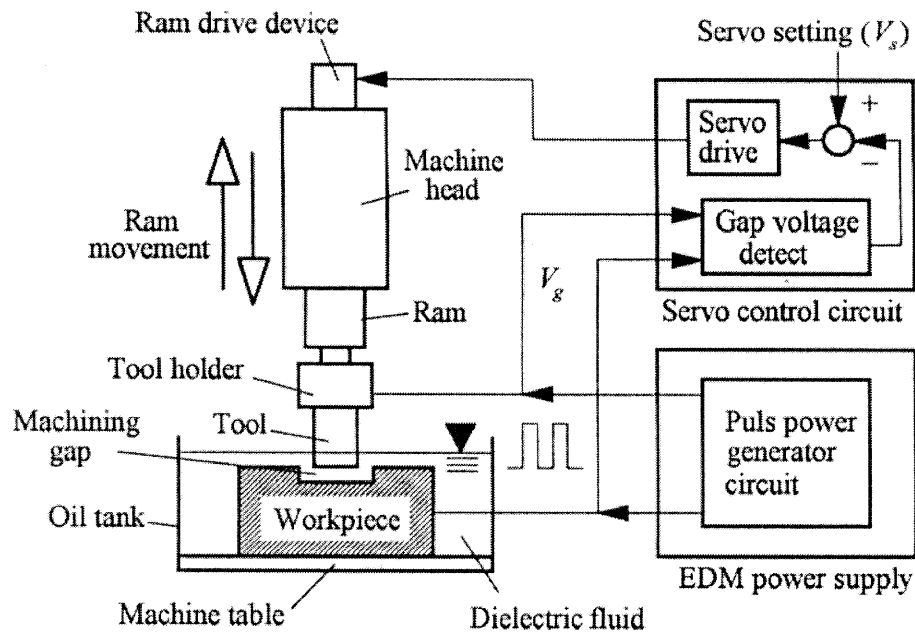
## CHAPTER 4

### ELECTROPLATING TOOLING FOR EDM ELECTRODES

This chapter presents an experimental study on using electroplated stereolithography (SL) models as electrodes for electrical discharge machining (EDM). The experimental results reveal that under roughing, semi-roughing and finishing EDM machining, a copper-plated SL-generated model works as well as a regular copper electrode until the thickness of the copper layer becomes the depth of the largest crater burned on the copper layer by the electrical discharge. The performance charts of copper-plated SL electrodes vs. those of regular solid copper electrodes have been generated. The EDM process parameters whose values sharply change when the epoxy surface gets burned are recorded and analyzed to provide information for further design of control systems for auto-retracting of SL electrodes. The plating thickness required to prevent burning of the SL electrode is discussed. The process can potentially provide a cost-effective route for rapid tooling of EDM electrodes.

#### 4.1 EDM Principles and Its Tooling Background

Electrical discharge machining (EDM) has been widely used for tool making. A basic setup of an electrical discharge machine is shown in Fig.4.1. The pulse power generator circuit provides a pulsed direct-current output to the electrode/workpiece system. The main sequence of events in a pulse cycle includes the ignition phase, the main discharge phase, and the melting and expulsion phase (Rajurkar and Pandit, 1986). These three stages signify a large number of physical processes and their interactions which take



**Figure 4.1** A Basic EDM Machine

place within the restricted spark gap, usually 10-250  $\mu\text{m}$ . The application of a voltage between the workpiece and tool electrode results in ionization and formation of a conductive channel when a breakdown voltage has been reached. When this occurs, a plasma column is generated between the two closest points of the two electrodes. The generation of the plasma is followed by fast moving electrons which strike the anode. The kinetic energy of the electrons is converted into thermal energy upon the impact. The anode surface heats rapidly to melting and even evaporation temperatures. The heating of the cathode due to the impact of ions is less rapid. At the same time, the electrical discharge causes shock waves in the fluid which are responsible for expulsion of metal from the workpiece. The dielectric fluid in the region of the discharge undergoes pyrolysis which generates hydrogen and acetylene black. The tool wear is caused mainly at the beginning of the sparking phase, i.e., the ignition phase (Weck and Dehmer, 1992).



After this phase, the electrode has little wear due to the buildup of acetylene black on its surface (Poco, 1994).

EDM has been widely used to form cavities in the production of complicated dies and molds which are typically difficult to machine using traditional chip removal techniques due to complex geometry or hard material. There are several advantages of using EDM, such as zero contact force between the tool and workpiece. Because EDM causes virtually no mechanical stress on the workpiece, it is possible for this technique to machine parts that are extremely fine and brittle. The more complicated the geometry of the die or mold, the more difficult it is to fabricate the corresponding electrode by conventional machining. With the increase of die and mold complexity, EDM electrode manufacture is becoming even more time consuming and expensive. If new rapid and economical EDM tooling methods can be achieved, EDM could be more widely used in the die and mold industry.

Various routes for generating EDM electrodes have been investigated worldwide. The application of SFF to the production of EDM electrodes seems to be a promising route. There could be considerable savings in cost and time by integrating SFF with EDM die and mold manufacture. Currently, there are several rapid routes being studied for fabrication of EDM electrodes, such as net shape casting, SL patterns coupled with electroplating, abraded-graphite electrodes, and metal sprayed electrodes (Ryall, 1995). Among them, the metal-plated EDM electrode from an SL part is relatively new and unproven. Arthur, Cobb and Dickens (1995) reported an experimental study using an SL model based electrode and electroplating process. Their experimental results showed that the copper-plated SL electrode may suffer premature damage and catastrophic failure.

Arthur, Carol, Dickens and Cobb (1997) stated that copper-plated SL electrodes could only be used as 'finishing' electrodes due to electrode damage when used in the 'roughing' process.

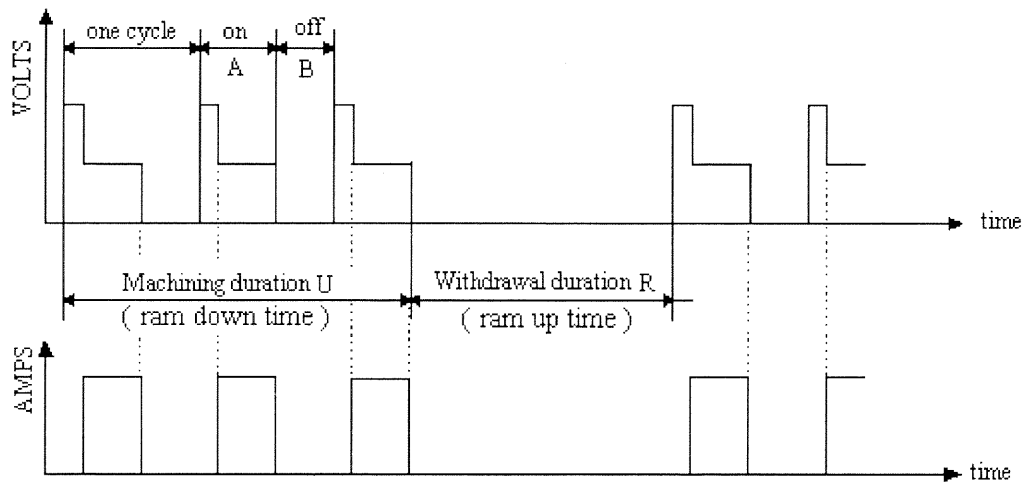
An experimental study using copper-plated electrodes from SL models to replace regular copper electrodes for the EDM process has been conducted as described in this chapter. The experimental results indicate that the copper-plated electrode normally works like a regular copper electrode under roughing, semi-roughing, and finishing conditions. The SL electrode could be damaged, however, when the plating thickness of the copper layer is equal to or smaller than the depth of the largest crater burned by the electrical discharge on the copper layer. If the EDM process still continues after the epoxy surface gets burned, the workpiece surface will be damaged. We term the crater depth burned by the EDM sparking as the critical thickness of plating. The EDM performance charts including the material removal rate (MRR), tool end wear (TEW), tool wear ratio (TWR) and surface finish ( $R_a$ ) of copper-plated electrodes are compared with those of regular copper electrodes. The comparison reveals that the performance of the copper-plated electrode is almost the same as that of the regular copper electrode before the copper layer of the SL electrode reaches its critical thickness. When the critical thickness is reached, the values of EDM process parameters change sharply. These changes can be detected and used to design a control system for automatic retraction of the SL electrode when the epoxy surface gets burned.

## 4.2 The Experiment

### 4.2.1. EDM Machining Parameters

The EDM machining process progressively generates the inverted shape of a tool electrode by pulsed electrical spark discharges across the machining gap between the workpiece and the tool electrode. The parameters of a pulse cycle consist of an on-time A and an off-time B, which are usually expressed in microseconds. When EDM machining is processed for a certain time (the machining duration, U), the discharge is turned off and the ram is retracted for a short while (the withdraw duration, R) to allow more dielectric fluid moving into the cavity to improve flushing and to avoid arc damage to the workpiece (Wang, Rajurkar and Akamatsu, 1995). Each machining duration U may have thousands of discharge pulses. The gap voltage and current waveform of the discharge pulse and the definition for the parameters A, B, R and U are illustrated in Fig.4.2.

Table 4.1 lists EDM machining parameters associated with the Charmilles Technologies EDM machine Roboform 100 used in our experimental study, where M, V, P and A are the main parameters set by the EDM control system when an E setting is assigned. The E setting is associated with a certain grade of surface finish. B, R and U are the secondary parameters which affect material removal rate. Most commercial EDM machines have an adaptive controller which is usually turned on in order that the burning process adapts to the machining condition. The values of B, R and U continuously change as the machining proceeds and can be instantaneously displayed on the EDM machining control page.



**Figure 4.2** Gap voltage and current waveforms of EDM pulses and definition of A, B, R and U

**Table 4.1** The EDM machining parameters

Parameter	Descriptor	Unit	comment
E	generator setting		setting associated with a required surface finish
M	machining mode		1:standard, 2:low wear, 3:very low wear, 4:microfine.
V	machining voltage	volt	sign of $V = +$ : The electrode is polarized positively. Sign of $V = -$ : The electrode is polarized negatively.
P	power available	watt	determines the maximum current
A	pulse duration (on time)	$\mu\text{s}$	pulse width in microseconds
B	interval between two pulses (off-time)	$\mu\text{s}$	If $B=0$ its value will be automatically optimized as the machining proceeds.
R	withdrawal time duration of pulsation	s	If $R=0$ its value will be automatically optimized as the machining proceeds.
U	machining time duration of pulsation	s	If $U=0$ its value will be automatically optimized as the machining proceeds. If $U=9$ the pulsations are stopped.

In order to investigate the feasibility of using the copper-plated SL electrode under various machining conditions, a series of E settings for roughing, semi-roughing and finishing are chosen, including E 403 whose nominal roughness is 400 microinches, E 342 whose nominal roughness is 200 microinches, and E 293 whose nominal roughness is 112 microinches. These E settings have default parameter values provided by the manufacturer as listed in Table 4.2 (Charmilles technologies, 1990). The result of the TWR which stands for tool wear ratio is also listed in this table.

**Table 4.2** Default process parameters for the selected E settings

E	M	V	P	A	B	R	U	TWR
403	3	+2	11	400	50	0.2	1.65	0
342	1	+5	9	50	12.8	0.2	0.8	2.5
293	1	+5	6	50	12.8	0.2	0.8	0.85

The volume of material removal is directly proportional to the amount of energy applied. This energy is controlled by the spark amperage and the on-time duration. Under the E settings for EDM finishing, the power generator provides much smaller discharge energy, shorter pulses, and smaller machining duration (Wang, Rajurkar and Ahmed, 1990). This results in very small and shallow craters, thus leading to fine surface finish. The surface finish is the result of overlapping tiny craters being formed by the random impacts of thousands of sparks. The E settings for EDM roughing indicate that the power generator provides greater energy, longer pulses, and larger machining duration. The longer the pulses, the more the workpiece material is melted away. Correspondingly,

deeper and broader craters are created on the workpiece resulting in a rougher surface finish. The E settings for semi-roughing have parameters and resulting surface finish between roughing and finishing.

#### **4.2.2 Preparation of Stereolithography Electrodes**

Several techniques for deposition of metal material onto an epoxy substrate are available. Among them, metallizing SL substrates by electroless plating, metal spraying of copper or nickel onto an SL model, or using vapor deposition and subsequently electroplating techniques have demonstrated good potential and appear to offer viable production routes. To easily facilitate surface and volume measurements, the SL models used in this experiment have a simple rectangular prism geometry of 0.75" x 0.75" x 4" and are made from SL5170 epoxy resin. The models are metallized using electroless nickel plating and subsequently copper-electroplated with a thickness of 0.02 inch (0.5 mm) which can be made fairly uniform, without the need for any further treatment. Future experiments will use complex profiles which are representative of a range of commercial EDM tools.

#### **4.2.3 Performance Attributes**

This experiment is intended to obtain a series of performance comparison charts of copper-plated SL electrodes versus those of regular copper electrodes. The performance attributes of EDM electrodes, which are listed in Table 4.3, include the material removal rate (MRR), tool end wear (TEW), tool wear ratio (TWR), and surface finish ( $R_a$ ) of the machined cavity. MRR is the volume of metal removal from a workpiece per unit time. The depth of each cut measured with a dial gauge multiplying the cut area is equal to the

volume removed. TWR is the wear volume of the electrode over the removed volume of the workpiece. Prior to each cut, the overall length of an electrode is measured with a height gauge and the reading recorded. After each cut, the electrode is measured to determine its overall length. This length is then subtracted from the measurement made prior to the cut, and the remainder indicates the amount of TEW.

**Table 4.3** EDM process performance attributes

Attribute	Descriptor	Measurement	Units
MRR	Material removal rate	Volume/Time	inch <sup>3</sup> /min
TEW	Tool end wear	height worn	inch
TWR	ool wear ratio (electrode: workpiece)	Vol. <sup>electrode</sup> /Vol. <sup>workpiece</sup>	%
R <sub>a</sub>	average surface roughness (workpiece)	microns	μ inch

#### 4.2.4 The Experimental Steps

The comparison of the performance attributes of copper-plated SL electrodes versus those of regular copper electrodes is determined by burning each electrode 10 minutes under the same machining condition and then measuring the process performance using the attributes described above. After an SL electrode has been burned 10 minutes, the process is stopped and the electrode and workpiece are taken out to measure the TEW, TWR, MRR and R<sub>a</sub>. After that, a regular copper electrode is used to do the same experiment. In order to check repeatability of the experiment, eight tests are performed for each E setting, with the use of one SL electrode and one regular copper electrode in each test.

During each burning process, we also examine the EDM machining control page which displays in real time the machining process parameters and machining conditions. This real-time monitoring of the machining control page can provide us useful information for detecting the possible burn of the copper layer of the SL electrode. This will be discussed in section 4.4.

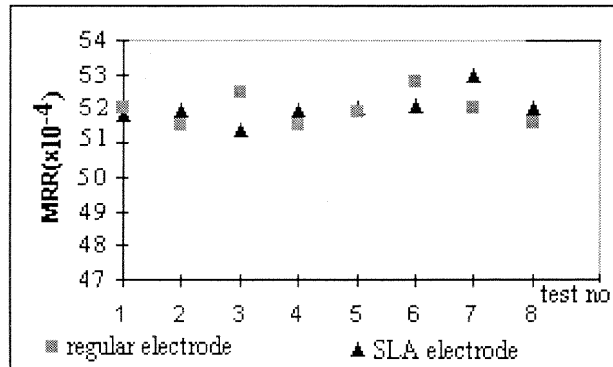
## **4.3 Experimental Results**

### **4.3.1 Roughing**

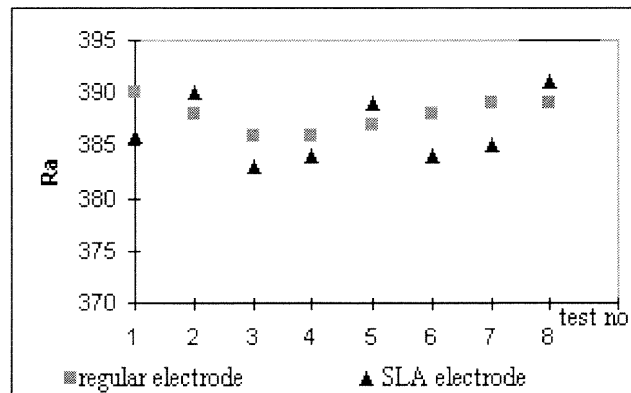
There are several E settings in the EDM machine for roughing, and the tool wear ratios of some of these E settings are essentially zero. The E 403 setting is selected to demonstrate the performance of the SL electrode versus that of a regular electrode under rough machining. The default machining parameters of the E 403 setting are listed in Table 4.2. The experimental results reveal that there exist almost no TEWs for both the copper-plated SL electrode and the regular copper electrode. So the TWRs for both the copper-coated SL electrode and the regular copper electrode are also zero. The results are consistent with the technology data provided by the EDM manufacturer who states that the tool wear is zero under the E 403 setting (see Table 4.2). This indicates that copper plated SL electrodes are excellent for EDM roughing.

The other performance attributes MRR and  $R_a$  are measured and presented in Fig.4.3 and Fig.4.4, respectively. These results lead to the conclusion that the performance of the copper-plated SL electrode is approximately the same as that of the regular copper electrode under rough machining, if the SL electrode does not get burned.





**Figure 4.3** Material removal rate of copper-coated SL electrode vs. regular copper electrode using E 403 setting

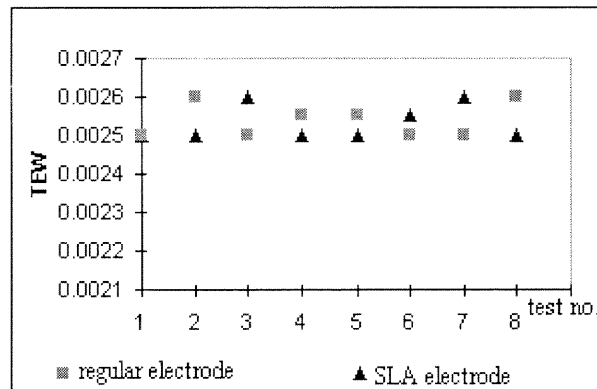


**Figure 4.4** Surface finish of copper-coated SL electrode vs. regular copper electrode using E 403 setting

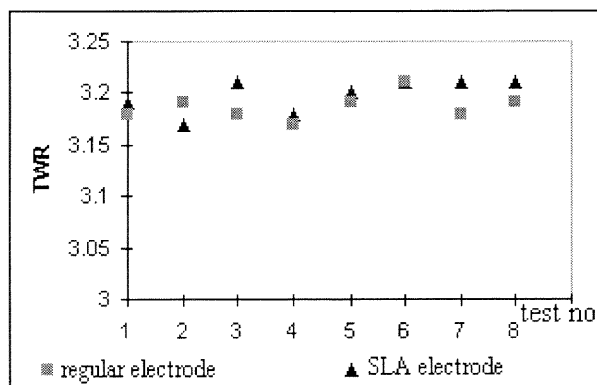
### 4.3.2 Semi-Roughing

The E 342 setting is then used to investigate the performance of the SL electrode versus that of the regular electrode under the semi-roughing condition. The default process parameters of the E 342 setting are listed in Table 4.2. The performance attributes TEW, TWR, MRR and  $R_a$  are measured and shown in Fig.4.5, Fig.4.6, Fig.4.7 and Fig.4.8, respectively. Like in roughing, these figures indicate that the copper-plated SL electrode works as well as the regular copper electrode under semi-rough machining. Because the tool wear is relatively high under the E 342 setting, the copper layer on the surface of the

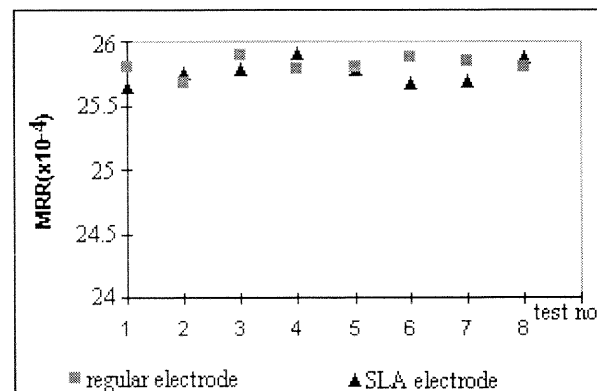
SL electrode gets burned after 30-40 minutes of the EDM process. This problem is discussed in section 4.4.



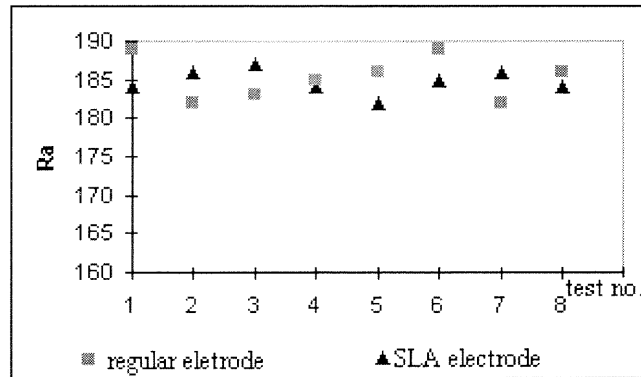
**Figure 4.5** Tool end wear of copper-plated SL electrode vs. regular copper electrode using E 342 setting



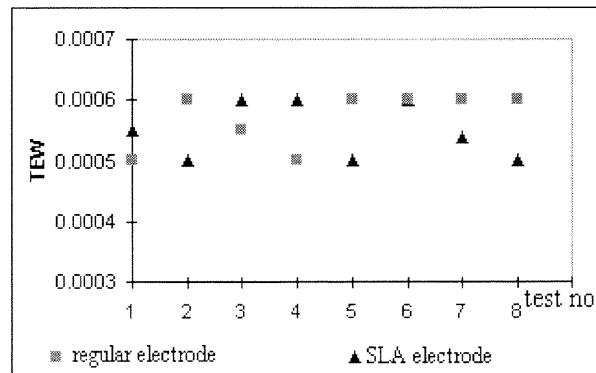
**Figure 4.6** Tool wear ratio of copper-coated SL electrode vs. regular copper electrode using E 342 setting



**Figure 4.7** Material removal rate of copper-coated SL electrode vs. regular copper electrode using E 342 setting



**Figure 4.8** Surface finish of copper-coated SL electrode vs. regular copper electrode using E 342 setting

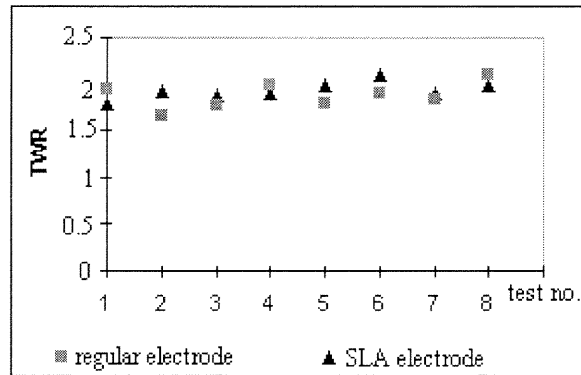


**Figure 4.9** Tool end wear of copper-coated SL electrode vs. regular electrode using E 293 setting

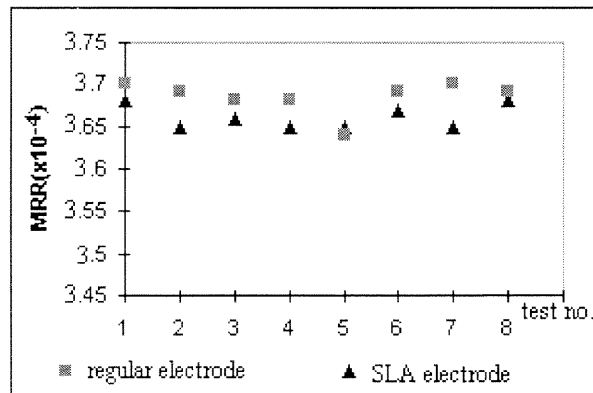
### 4.3.3 Finishing

The E 293 setting is used to see the performance of SL electrode versus that of regular electrode in finishing. The default process parameters of the E 293 setting are listed in Table 4.2. Eight pairs of data for each performance attribute are measured and presented in Fig.4.9, Fig.4.10, Fig.4.11 and Fig.4.12, respectively. From these figures, we again observe that the performance of the copper-plated SL electrode is close to that of the regular copper electrode under finishing. Because the TEW of 10 minutes of EDM burning is very small in the finishing operation, no burn of the copper layer is observed in

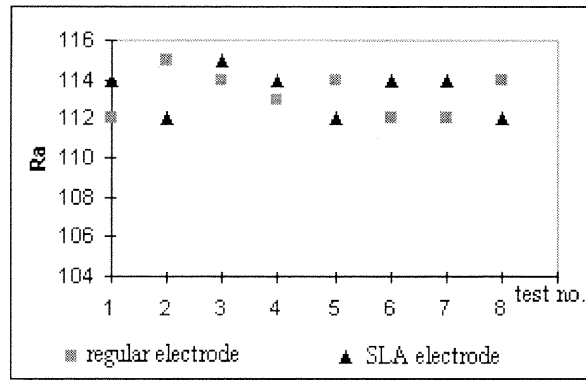
the experiment. Of course, if the machining lasts until the moment that the thickness of the copper layer left on the epoxy surface is smaller than the depth of the largest crater created by the EDM spark, the epoxy surface is expected to get burned.



**Figure 4.10** Tool wear ratio of copper-coated SL electrode vs. regular copper electrode using E 293 setting



**Figure 4.11** Material removal rate of copper-coated SL electrode vs. regular copper electrode using E 293 setting



**Figure 4.12** Surface finish of copper-coated SL electrode vs. regular copper electrode using E 293 setting

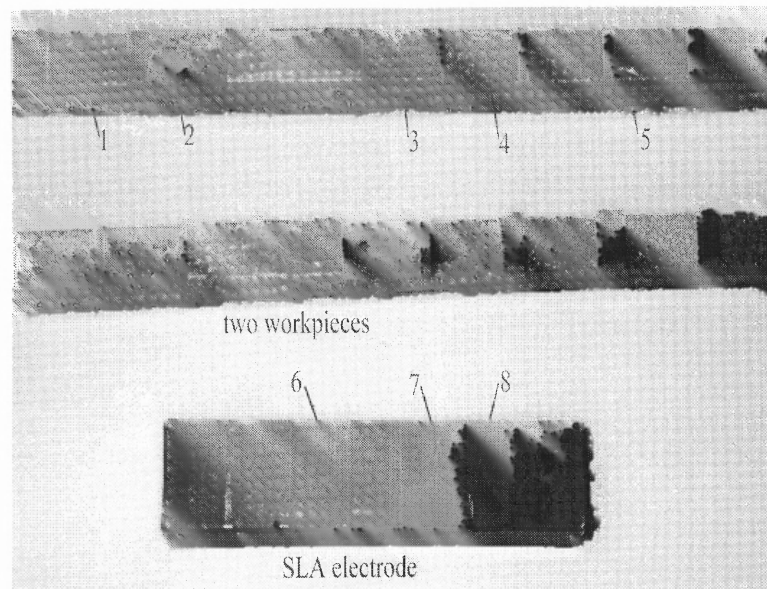
#### 4.4 Discussion of Workpiece Damage and Plating Thickness

##### 4.4.1 Workpiece Damage

A copper-plated SL electrode can be used for EDM provided that the thickness of the copper layer on the SL model is larger than the depth of the largest crater created by an electrical discharge. In Fig.4.13, areas 1 and 3 illustrate the semi-roughing and roughing surfaces of the workpiece, respectively, generated by successful EDM. If the thickness of the copper layer left on the epoxy surface is equal to or smaller than the depth of the largest crater produced on the copper layer, the epoxy surface gets burned. If the SL electrode is not retracted promptly under this condition, the workpiece will be damaged. Spots 2, 4 and 5 in Fig.4.13 show damaged spots on the workpiece due to the burns of the copper layer of the SL electrode at spots 7, 6 and 8, respectively.

Arthur, Carol, Dickens and Cobb (1997) stated that bulk removal of the workpiece material is not possible using SL electrodes due to excessive heat build-up in the copper layer which may result electrode damage. We note that the thickness of the plated SL

electrode used in their study is 0.175mm. Our experiment shows that the copper layer may be burned under the E 403 setting if its thickness is about 0.28mm, the critical thickness of this setting, or less. To prevent the burn of the copper layer, the plating thickness must be larger than 0.28mm for the E 403 setting. Thus, the SL electrode can be an excellent candidate for EDM roughing if the plating thickness of the SL electrode can be larger than the critical thickness under an E setting which does not cause tool wear.

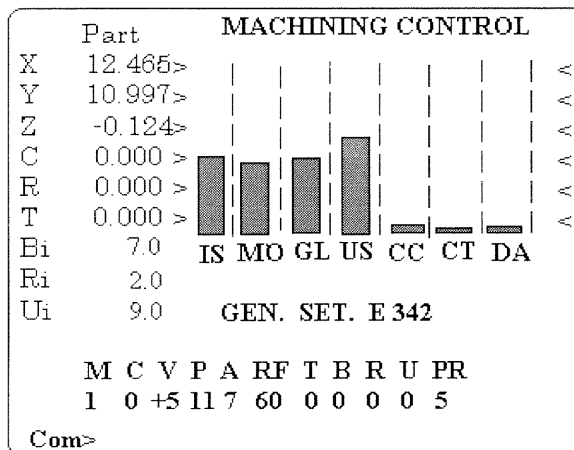


**Figure 4.13** The tested workpieces and the SL electrode

#### 4.4.2 Damage Monitoring

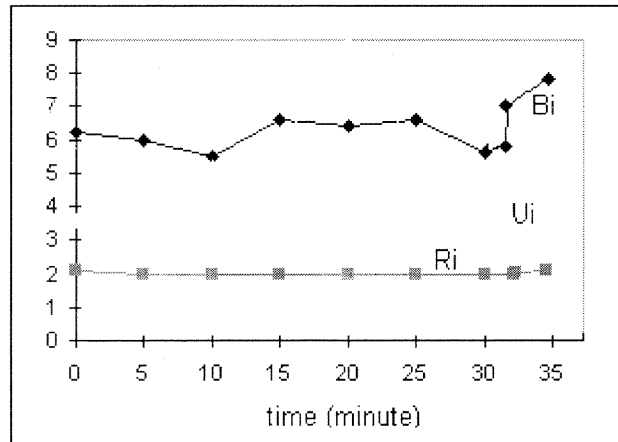
When an SL electrode is used, a monitoring system should be available to detect the damage of the workpiece. During our experiment, we observe that when the epoxy surface gets burned, the values of some of the EDM process parameters, which can be

displayed on the machining control page (refer to Fig.4.14) in real time, change sharply. On-line monitoring of the machining parameters under the E 342 setting is performed, and the data of Bi, Ri, Ui, IS, MO and GL are recorded as shown in Fig. 4.15 and Fig. 4.16. Clearly, the physical signals of some of these parameters can be used to effectively monitor the EDM process.

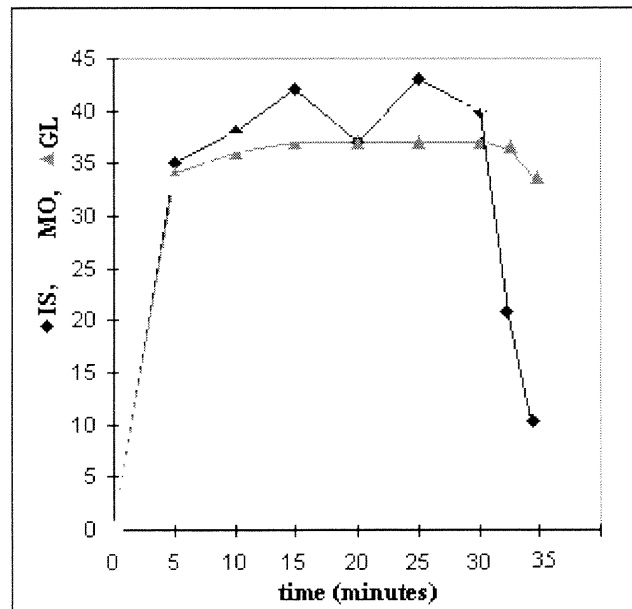


- Bi Instantaneous off-time
- Ri Instantaneous withdrawal time duration
- Ui Instantaneous machining time duration
- IS Instantaneous efficiency, computed between two pulses
- MO Average efficiency, computed over a period of 8 pulses
- GL Global efficiency: average efficiency since the mode is selected
- US Stability; when stable, the indicator is at the center
- CC Short-circuit rate
- CT Contamination factor
- DA Abnormal discharge rate

**Figure 4.14** Machining parameters displayed on-line in the machining control page



**Figure 4.15** Ri, Ui and Bi versus time under E 342 setting when the SL electrode is used



**Figure 4.16** IS, MO and GL vs. time under E 342 setting when the SL electrode is used

#### 4.4.3 Plating Thickness

The relationship between electrodeposition thickness and the machining length of the workpiece cavity can be expressed as

$$T_c = S_f(TWR \cdot W_d + C_t) \quad (4.1)$$



where  $T_c$  is the electroplating thickness needed for a copper layer on an electrode,  $W_d$  is the length of the workpiece cavity to be generated. TWR is the tool wear ratio for a specific EDM machining setting, and  $S_f$  is safety factor ( $S_f > 1$ ).  $C_t$  is the critical thickness, which must be larger than the depth of the deepest crater burned on the surface of the SL electrode. For the E 342 setting in our experiment,  $C_t$  is 0.0006-0.0008 inch.

An important factor for the success of copper-plated SL electrodes for EDM is the plating method. Important are plating thickness and its uniform distribution, plating surface finish, and uniform grain size of the plating material. They depend on the electrodeposition technology which is not considered in this chapter.

#### 4.5 Closure

The feasibility study of using copper-plated SL electrodes for roughing, semi-roughing, and finishing is conducted. The experimental results reveal that a copper-plated SL electrode can be potentially used for EDM like a regular copper electrode. The EDM process does not “know” of the plating, until the moment that the thickness of the copper layer left on the epoxy surface of an SL electrode is equal to or smaller than the depth of the largest crater created by the electrical discharge. To avoid damage to the workpiece, a monitoring and control system needs to be developed in order to auto-retract the ram of an EDM machine when the copper layer reaches its critical thickness. In practice, proper selection of the EDM setting, such as selecting E 403 for roughing, plus ability to perform plating larger than the critical thickness, will be essential to enable the plated SL electrode working well.

This tooling process has the advantages of fast, simple and cost-effective. However, due to the property of electroplating, the metal layer plated on the master can not be uniformly distributed on the entire surface if the surface consists of some slots, cavities and sharp corners. This makes the approach feasible only when the surface of the EDM electrode is smooth without slots, cavities, or sharp corners. The SL electrode could be damaged when the plating thickness of the copper layer is equal to or smaller than the depth of the largest crater burned by an electrical discharge on the copper layer. If the EDM process still continues after the copper layer gets burned, the workpiece will be damaged. The plating with thick copper layer can prevent the burning of the RP master, but the thicker the copper layer plated on the surface of the master, the less uniform the copper distributed on the entire surface of the electrode, especially if the electrode consists of cavities, sharp corners and complex surfaces. This results in the loss of accuracy of the EDM electrode. Non-uniformity of the plating thickness is due to the non-uniformity of current density distributed between the surface of the anode and the surface of the cathode (workpiece) when the anode does not have the same (but reversed) geometry of the workpiece.

## CHAPTER 5

### RAPID ELECTROFORMING TOOLING

This chapter describes a rapid tooling process that integrates solid freeform fabrication (SFF) with electroforming to produce metal tools including molds, dies, and electrical discharge machining (EDM) electrodes. An SFF part is metalized by electroless plating and then placed in an electroplating solution, where metal is deposited upon the part by electrolysis. When the desired thickness of metal has been reached, the SFF part is removed from the metal shell by heating. The shell is then backed with other materials such as alloy or aluminum to form a mold cavity, an EDM electrode, or other desired parts for tooling. The case studies for mold tooling and EDM electrode fabrication are performed and experimental data are recorded. Based on those experimental data analysis, the geometry and material properties of the SFF part, the properties of the electroformed metal, and the process parameters are significant factors that cause inaccuracy in the manufactured tools. Thermal stresses induced during the burnout process that removes the SFF part from the electroform is one of the major sources for inaccuracy of this tooling process.

#### 5.1 Introduction of Electroforming Tooling

##### 5.1.1 Electroforming and Rapid Electroforming Tooling

Electroforming was invented by M. H. Jacobi of the Academy of Science of St. Petersburg, Russia in 1838. It was initially used to copy antique masterpieces in the last

century. Currently, electroforming is widely used in manufacturing, electronics, aerospace, automotive, and art reproduction. Electroformed parts most commonly are made of nickel, iron, copper, or silver, and thickness up to 16 mm (5/8 inch) has been deposited successfully. However, a variety of other types of materials have been used. Metals deposited by electroforming have their own distinct properties. Dimensional tolerances are very good, often up to 0.0025 mm (0.0001 inch), and surface finishes of 0.05 mm (2 microinches) can be obtained quite readily if the pattern is adequately smooth. The main obstacle to the development of the electroforming is the manufacturing of the pattern. In some less technology advanced countries, electroforming is widely used to copy the shape of an imported complex part. The copied shell is used as the mold cavity.

Electroforming has been used to make dies, molds and EDM electrodes by electrodeposition of metal onto a pattern to replicate the pattern in a reversed format to produce a metal shell. The pattern, which has the required shape, dimension, accuracy and roughness, is sunk into an electrolyte bath as the cathode and is deposited a required layer of metal, normally copper or nickel. If the pattern is nonconductive, it needs to be metalized before electroforming. The metal shell is then separated from the pattern to form the mold cavity. Electroforming can be used to reproduce the reversed shell of a wide variety of parts and shapes, the principal limitation being that it must be possible to separate the pattern from the metal shell, similar to the situation that it must be possible to remove the molding part from the mold cavity. Electroforming has been used for dies and molds fabrication. With the development of the electroforming

technology, an alloy, such as Ni-Co, can be deposited onto the pattern to form a shell so that the strength and hardness of the mold can be largely improved.

The integration of SFF technologies with electroforming has explored a new way for rapidly making of molds, dies, EDM electrodes and hollow bodies as discussed in this chapter. Masters can be made using the RP processes discussed in Section 2.1, such as SLA, SLS, Model Maker, FDM, etc. The process for electroforming tooling has been described in 3.1.2. The main problem is that during the separation stage, the thermal expansion of the SFF part could deform or even crack the electroform due to the fact that the coefficient of thermal expansion of the SFF part is one about magnitude larger than the electroformed metal. This will be demonstrated in an experimental investigations described in this chapter.

### **5.1.2 Advantages and Disadvantages of Rapid Electroforming Tooling**

The advantages of electroforming tooling are as follows [Spiro, 1968]:

- The metallurgical properties of an electroformed metal can be controlled over a wide range by choice of suitable metals, adjustment of the plating bath compositions, and variation of conditions of deposition.
- Electroforming can accurately copy the shape of the pattern, so the dimensional and geometric accuracy can be very good, being limited only by the accuracy of the pattern produced by RP machines.
- Reproduction of fine details is so good that it can not be matched by other mass production methods. Shapes can be made that are not possible using any other fabrication methods.

- Sandwiches of various metals can readily be built as required, thus varying properties in a controlled fashion.
- There is no direct relationship with electroforming time and part volume or area, but the only constraint is the size of the electrolyte bath.
- Multiple mold cavities can be electroformed in the same electrolyte bath at the same time.
- The electroform and the electrolyte solution can be easily reused in the next electroforming run so there is little environmental impact.

The disadvantages of electroforming are as follows:

- Many metals deposited are in a state of internal stress [Stein, 1996], which may give rise to difficulty in separating of the deposited metals (when an SFF pattern is removed using mechanical means) and in maintaining the dimensional accuracy of the finished part.
- Because of the exactness of reproducibility, scratches and imperfections in the pattern will also appear in the pieces processed from it.
- Material is deposited onto the protruding parts of a cathode than into its recesses. It is difficult to form a homogeneous, i.e. non-fissured deposit into the apex of a sharp re-entrant angle (corner weakness).
- Electroforming cost is often relatively high. However, it becomes competitive when a large number of products are produced using the electroformed tools, in comparison with machining part-by-part.

### 5.1.3 Introduction of Electroless Plating

The SL patterns used for rapid electroforming tooling are not electrically conductive. Before the electroforming process, the patterns need to be made electrically conductive. Electroless plating can produce uniform pinhole-free metal film on the entire surface regardless of the complexity of part geometry, so the SL patterns are metalized using electroless plating in this dissertation study.

Electroless plating refers to autocatalytic or chemical reduction of aqueous metal ions plated to a base substrate [Duffy, 1980]. Components of the electroless bath consists of metal ions, reducing agents, complexing agents, and bath stabilizers operating in a specific metal ion concentration, temperature and pH range. Unlike conventional electroplating, no electrical current is required for deposition. The electroless bath provides a deposit that follows all contours of the substrate exactly, without building up at the edges and corners. A sharp edge receives the same thickness of deposit as does a narrow slot. In electroless plating, metal ions are reduced to metal by the action of chemical reducing agents, which are simply electron donors. The metal ions are electron acceptors, which react with electron donors.

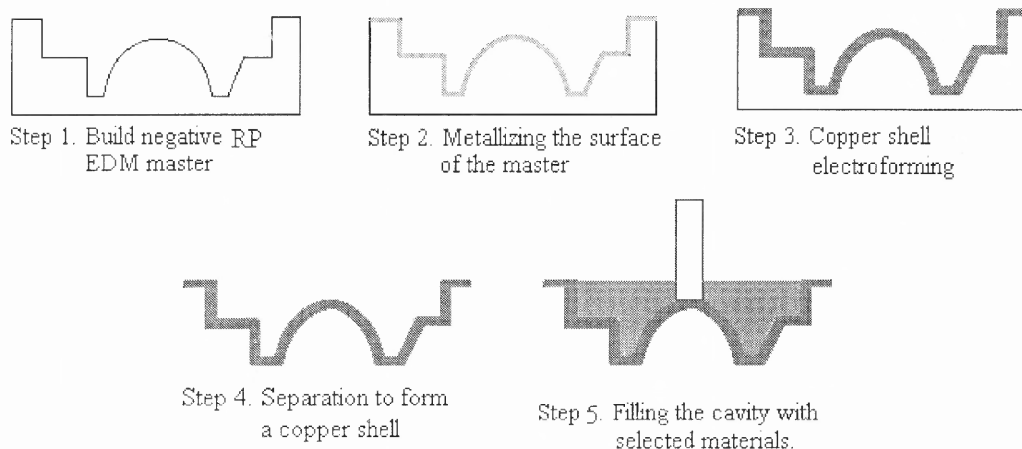
The electroless plating used in this study is electroless nickel. Electroless nickel offers unique deposit properties including uniformity of deposit in deep recesses, bores, and blind holes. It also provides unique physical characteristics, including excellent corrosion, wear and abrasion resistance, ductility, lubricity, solderability, electrical properties, and high hardness.

## 5.2 Rapid Electroforming Tooling of EDM Electrodes

### 5.2.1 Tooling Process

The selection of electroforming metals is determined by tool requirements. Three most widely used electroforming metals are copper, nickel and iron. The electrical and thermal conductivity of the electroformed metal are most important attributes for EDM electrode, so copper electroforming is used for EDM tooling. Cyanide, fluoborate and sulfate plating baths are three widely used baths, but sulfate is the most typical one. The typical formulation of copper sulfate solution is:

- Copper sulphate,  $\text{Cu-SO}_4 \cdot 5\text{H}_2\text{O}$ : 20-35 oz/gall (125-220g/l)
- Sulphric acid,  $\text{H}_2\text{SO}_4$ : 6-12 oz/gall (40-75 g/l)
- Temperature: 20 to 42 °C
- Voltage less than 6v.
- Current density: 3.2 to 16.2 amp per sq dm.



**Figure 5.1** EDM tooling process using SL master and electroforming



The process of making EDM electrodes using SL masters and electroforming is illustrated in Fig.5.1. The negative (complementary) geometry of the EDM electrode is prototyped by stereolithography as the master. The master must be rigid enough to withstand the electroforming stress induced during the building up of the copper layer. The electroforming stress is largely determined by the electroforming process parameters and it varies from compressive to tensile stress in a widely range[Safranek, 1986]. Using stress reducer additives and optimal electroforming parameters, the stress can be controlled under 1 MPa. Before electroforming of the SL master, metalization of the SL surface is needed to make it electrically conductive. Several techniques for metalization of nonconductive materials are available [Duffy, 1980]. Electroless plating, an autocatalytic or chemical reduction of aqueous metal ions to a base substrate, can produce uniform pinhole-free metal film on the entire surface regardless of the complexity of part geometry, so the SL parts are metalized using electroless nickel plating in our experiment. The metalized SL parts are then copper electroplated to the required thickness. At the separation process, prevention of the electroform deformation is extremely important. The RP master built with ceramic and other difficult-to-melt materials are preferred to be separated using extraction mechanically. Melting, burning out, or heat softening can be applied to wax and thermoplastic RP masters. SL resin is a thermosetting material, so burning out of the SL master is the preferred separation method. The SL master is completely incinerated at the temperature of 560 °C. During the burning out process, the heat results in expansion of the master. This may crack or deform the electroformed metal shell. The thickness of the electroformed copper shell needs to be optimized to minimize the cost while the stress exerted on the metal shell due

to the expansion of the master does not crack the copper shell or cause unacceptable deformation. Because the EDM electrode does not contact the workpiece during the electrical discharge machining process, the strength of the electrode is not important. A low melting alloy with good electrical and thermal conductivity can be used to backfill the shell to form an EDM electrode.

### **5.2.2 Performance Testing**

SL models with a simple rectangular cavity of 1 in x 1 in x 1 in, made from SL 5170 epoxy resin, are electroformed and the finished EDM electrodes are used to test the electrical discharging machining performance versus the conventional, machined solid EDM electrode. The experimental method used in Chapter 4 are adopted here to test the performance of the electroformed EDM electrodes. The comparison of the performance attributes of the copper-electroformed electrode versus those of the machined copper electrode is determined by burning each electrode 10 minutes under the same EDM condition and then measuring the process performance attributes of tool wear ratio (TWR), material removal rate (MRR, unit:  $\text{in}^3/\text{min}$ ), and surface finish ( $R_a$ , unit:  $\mu\text{in}$ ). In order to check the repeatability of the experiment, eight tests are performed for each machining setting, with the use of one electroformed electrode and one regular copper electrode in each test. The performance investigation reveals that an electroformed EDM electrode can be used for EDM like a regular copper electrode for roughing, semi-roughing, and finishing until the moment that the thickness of the copper layer is equal to or smaller than the depth of the largest crater created by an electrical discharge. The performance of copper electroformed electrode versus regular copper electrode under

roughing, semi-roughing and finishing are listed in Table 5.1, 5.2 and 5.3, respectively. In order to facilitate the comparison, the performance data for electroplated EDM electrodes are also listed in those tables.  $E_1$ ,  $E_2$ ,  $E_3$  in those tables represent electroformed, electroplated and regular EDM electrodes, respectively.

### 5.2.3 Case Study

Two EDM electrodes of the same geometry, as illustrated in Fig.5.2, are made by this tooling process with the smallest copper layer thickness of 0.08 in (2 mm) and 0.16 in (4 mm), which are presented as electrode 1 and electrode 2, respectively. The cavity of the master is 0.45 in (11.4 mm) deep. Both SL cavities are polished to the surface finish of 48  $\mu$ in. After polishing, each dimension, as marked in Fig.5.2(a), is measured three times and the average is recorded as listed in Table 5.4. Copper sulfate bath is used for electrodeposition of copper onto the SL patterns. The electroformed electrodes show that the corners with zero radius are well electroformed, although the thinnest copper layer (required smallest thickness) always in these positions. Both masters are electroformed at room temperature to avoid the thermal expansion of the master. Incineration is used to remove the SL master from the electroformed copper shell. After the electroformed masters are heated about 560 °C and then kept for one hour, the SL resin is completely burned away. After the burning of the SL resin, the dimensions of the finished EDM electrodes are measured using the same method as measuring the SL master and the values are recorded in Table 5.4 to compare with the corresponding data measured on the SL master. The dimensional deviation of the electrode with 4 mm thick copper shell is always smaller than that of the electrode with 2 mm thick copper shell. It means that the

thinner the copper layer, the lower the dimensional accuracy resulted from the burning deformation. The % deviation is defined as the percent ratio of the deviation over the corresponding dimension of the SL master. The copper shell is backed with a tin-lead alloy whose melting point is 103 °C. The surface finish of the two finished EDM electrodes are measured using Mitutoyo surface scale and both the average surface finish are about 50  $\mu\text{in}$ . The finished electrode are used to machine a hard steel workpiece using the settings of machining parameters typically used for EDM roughing. The burned cavity with a depth of 0.4 in (10 mm), as shown in Fig.5.2(d) is machined in 3 hours 24 minutes.

**Table 5.1** Performance Data of Electroformed ( $E_1$ ) and Electroplated ( $E_2$ ) Electrodes vs. Regular Solid Copper Electrode ( $E_3$ ) Using E 403 Setting

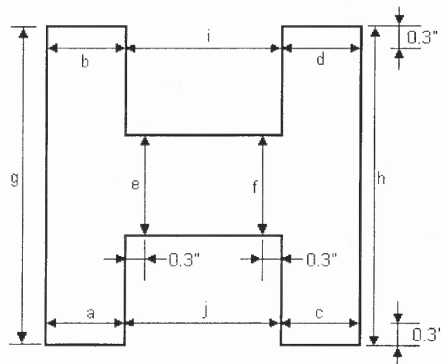
Test No.		1	2	3	4	5	6	7	8
TWR	$E_1$	0.02	0.01	0.01	0.02	0.02	0.01	0.02	0.01
	$E_2$	0	0	0	0	0	0	0	0
	$E_3$	0	0	0	0	0	0	0	0
MRR ( $\times 10^{-3}$ )	$E_1$	5.15	5.13	5.16	5.16	5.12	5.13	5.17	5.16
	$E_2$	5.18	5.19	5.14	5.14	5.22	5.21	5.18	5.21
	$E_3$	5.21	5.15	5.24	5.15	5.18	5.28	5.21	5.18
Ra	$E_1$	385	392	384	389	386	389	392	382
	$E_2$	386	390	383	384	389	384	385	391
	$E_3$	390	388	386	386	387	388	389	389

**Table 5.2** Performance Data of Electroformed ( $E_1$ ) and Electroplated ( $E_2$ ) Electrodes vs. Regular Solid Copper Electrode ( $E_3$ ) Using E 342 Setting

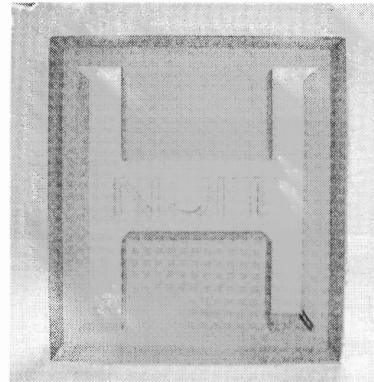
Test No.		1	2	3	4	5	6	7	8
TWR	$E_1$	3.31	3.32	3.33	3.30	3.32	3.18	3.24	3.38
	$E_2$	3.19	3.18	3.21	3.18	3.20	3.21	3.21	3.21
	$E_3$	3.18	3.19	3.18	3.17	3.19	3.21	3.18	3.19
MRR ( $\times 10^{-3}$ )	$E_1$	2.94	2.92	2.93	2.78	2.84	2.91	2.93	2.95
	$E_2$	2.93	2.94	2.87	2.98	2.88	2.94	2.95	2.96
	$E_3$	2.96	2.95	2.96	2.96	2.98	2.96	2.97	2.98
Ra	$E_1$	187	188	189	186	182	186	184	185
	$E_2$	184	186	187	184	182	185	186	184
	$E_3$	189	182	183	185	186	189	182	186

**Table 5.3** Performance Data of Electroformed ( $E_1$ ) and Electroplated ( $E_2$ ) Electrodes vs. Regular Solid Copper Electrode ( $E_3$ ) Using E 293 Setting

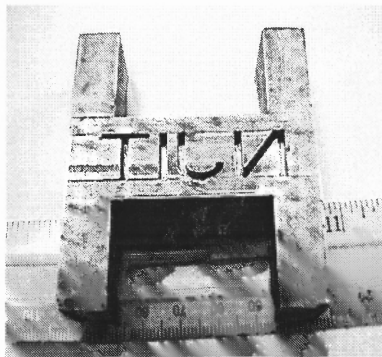
Test No.		1	2	3	4	5	6	7	8
TWR	$E_1$	8.09	8.12	8.06	8.02	8.05	8.10	8.07	8.03
	$E_2$	7.92	7.92	7.89	7.93	7.98	8.10	7.94	8.12
	$E_3$	7.95	7.66	7.78	8.00	7.89	7.96	7.83	8.09
MRR ( $\times 10^{-3}$ )	$E_1$	0.54	0.53	0.52	0.55	0.53	0.54	0.54	0.53
	$E_2$	0.53	0.54	0.55	0.53	0.54	0.54	0.53	0.54
	$E_3$	0.55	0.56	0.54	0.57	0.54	0.55	0.54	0.55
Ra	$E_1$	116	114	118	110	112	114	113	116
	$E_2$	114	112	115	114	112	114	114	112
	$E_3$	112	115	114	113	114	112	113	114



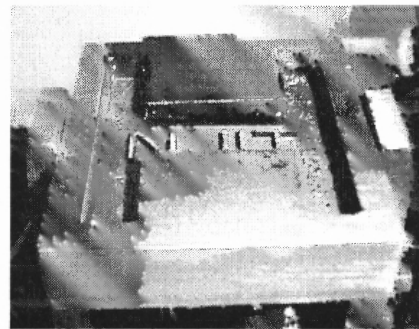
(a) Dimensions measured.



(b) SL master.



(c) Finished EDM electrode



(d) EDMed workpiece

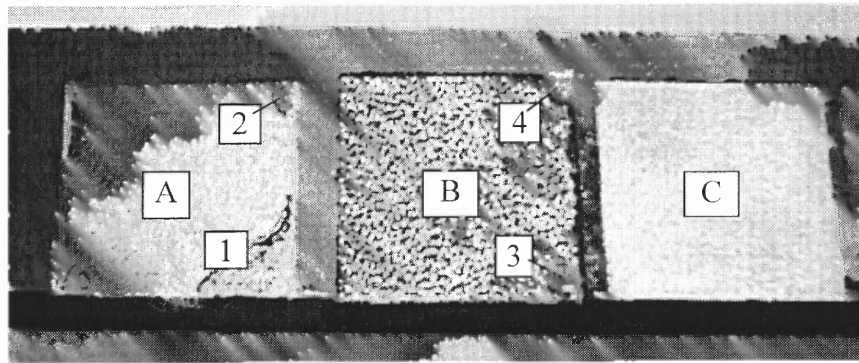
**Figure 5.2** Electroformed Electrode and EDM Generated Workpiece

**Table 5.4** Dimensional data of SL parts vs. those of electroformed copper shell  
(unit:mm)

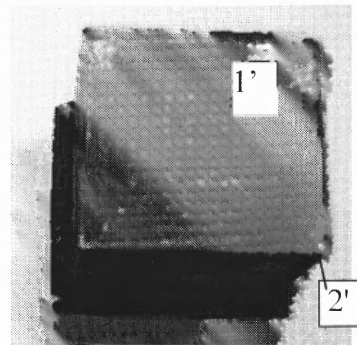
	A	B	C	D	E	F	G	H	I	J
Master 1	11.562	11.595	11.585	11.575	17.996	17.983	61.107	61.132	38.095	38.085
Electrode 1	11.552	11.580	11.572	11.562	17.978	17.960	61.074	61.095	38.181	38.176
Deviation 1	0.010	0.015	0.013	0.013	0.018	0.023	0.033	0.037	0.086	0.093
% Deviation	0.09	0.13	0.11	0.11	0.10	0.13	0.05	0.06	0.24	0.26
Master 2	11.639	11.638	11.618	11.610	17.886	17.902	61.229	61.212	38.120	38.090
Electrode 2	11.632	11.628	11.603	11.600	17.871	17.888	61.201	61.180	38.173	38.142
Deviation 2	0.009	0.010	0.015	0.010	0.015	0.014	0.028	0.031	0.054	0.052
% Deviation	0.08	0.09	0.10	0.09	0.08	0.08	0.05	0.05	0.14	0.13

#### 5.2.4 Electroforming Thickness

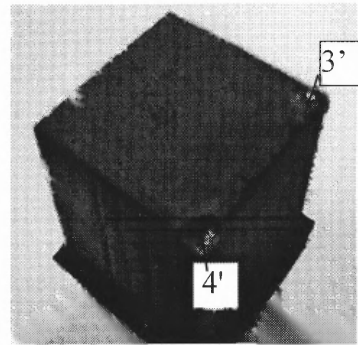
The copper-electroformed electrode can be used for EDM provided that the thickness of the copper shell is larger than the depth of the largest crater created by an electrical discharge. This depth is termed critical thickness. The critical thickness is a function of the discharge energy, which in turn is a product of the pulse current, gap voltage during the current pulse, and current pulse time. In Fig. 5.3(a), areas A, B and C illustrate the semi-roughing, roughing and finishing surfaces of a workpiece, respectively, generated by the EDM process. If the copper layer gets burned, the workpiece will be damaged. Spots 1,2, 3, and 4 in Fig.5.3(a) show damaged areas on the workpiece due to the burns of the copper layer of the electrode of Fig. 5.3(b) at spots 1', 2', and the electrode of Fig.5.3(c) at spots 3' and 4', respectively. These electrodes with thin copper layers are used to detect the critical thickness.



(a) Damaged workpiece



(b) Electrode for area A



(c) Electrode for area B

**Figure 5.3** Critical thickness investigation

The thickness of electroforming for successful EDM is a function of tool wear ratio (TWR) and the critical thickness corresponding to its machining condition. TWR is the ratio of the volume of tool wear over the eroded volume of workpiece. From the definition of TWR, the electroforming thickness of copper layer is directly proportional to the depth of the workpiece cavity to be machined. The relationship between electroforming thickness and the machining depth of the workpiece cavity is expressed as:  $T_c = S_f(TWR \cdot W_d + C_t)$ , where  $T_c$  is the electroforming thickness needed in order for a copper-electroformed electrode not to get damaged,  $W_d$  is the depth of the workpiece cavity to be machined. TWR is the tool wear ratio for a specific EDM machining setting,  $C_t$  is the critical thickness,  $S_f$  is safety factor ( $S_f > 1$ ). The critical

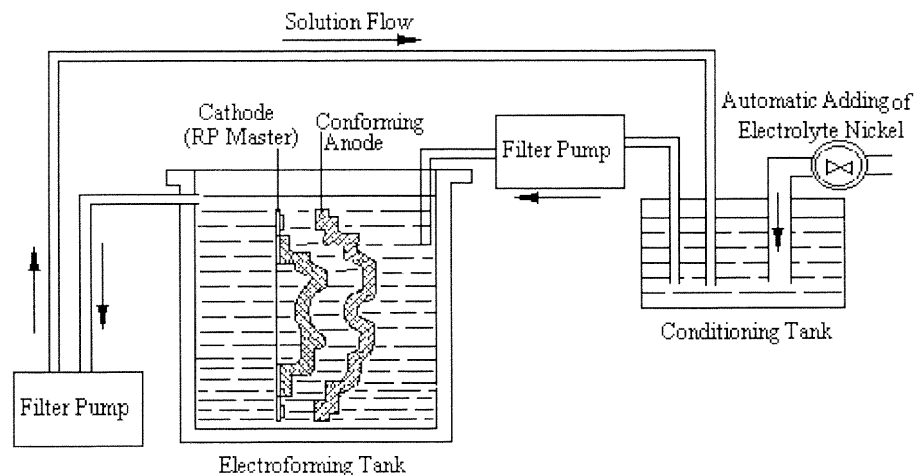
thickness must be larger than the depth of the largest crater which can be generated on the surface of the electrode. It is a function of the discharge energy, which in turn is a product of the pulse current, gap voltage during the current pulse, and current pulse time (Rajurkar and Pandit, 1986).

### 5.3 Rapid Electroforming Tooling of Molds

#### 5.3.1 Tooling Process

The reasonable hardness, tensile strength, ductility and good corrosion of electroformed nickel make electroforming most suitable for production of molds and dies of complex shapes. Generally speaking, the mechanical, chemical and thermal properties of electroformed nickel are similar to those of stainless steel, especially the highly wear and corrosion resistant properties. So nickel is very suitable for electroforming mold tooling.

There are six basic types of nickel baths being used currently for electroforming: Watts bath with or without addition agents, hard nickel, chloride, cobalt-nickel,

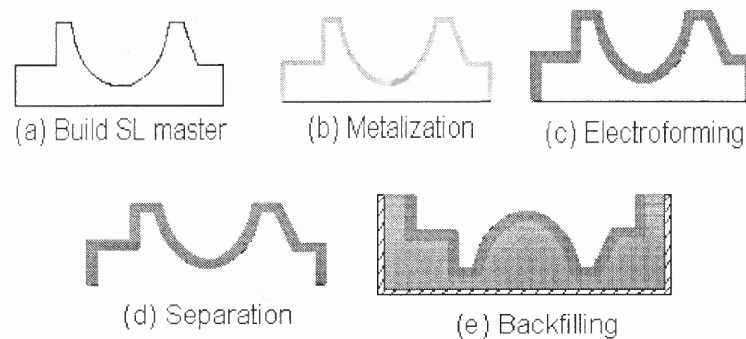


**Figure 5.4** Typical setup of nickel electroforming



fluoborate and sulfamate [Spiro, 1968]. Because sulfamate bath can produce electroformed nickel with nice mechanical and thermal properties, it is widely used. Fig. 5.4 illustrates a typical setup for sulfamate nickel electroforming. The sulfamate bath is used for this dissertation project.

As illustrated in Fig. 5.5, the mold tooling process is very similar to the tooling process for making EDM electrodes. A CAD model is created and sliced layer by layer to produce a STL/SLI file which is transferred to the SLA machine to build the SL master. The master is post-cured, sanded and finished to be used as an electroforming master. The master is then metallized using nickel electroless plating, with a thickness of about 0.0002 in. The metalized master is then put into the electroforming bath as a cathode to deposit a layer of metal which is thick enough to resist the deformation caused by the separation and backfilling. Separation is done by burning out the SL master. The deformation in the separation is largely determined by the electroforming thickness and the geometry of the SL master. Backfilling of the mold is more critical in manufacturing an electroformed mold cavity compared with manufacturing an electroformed electrode

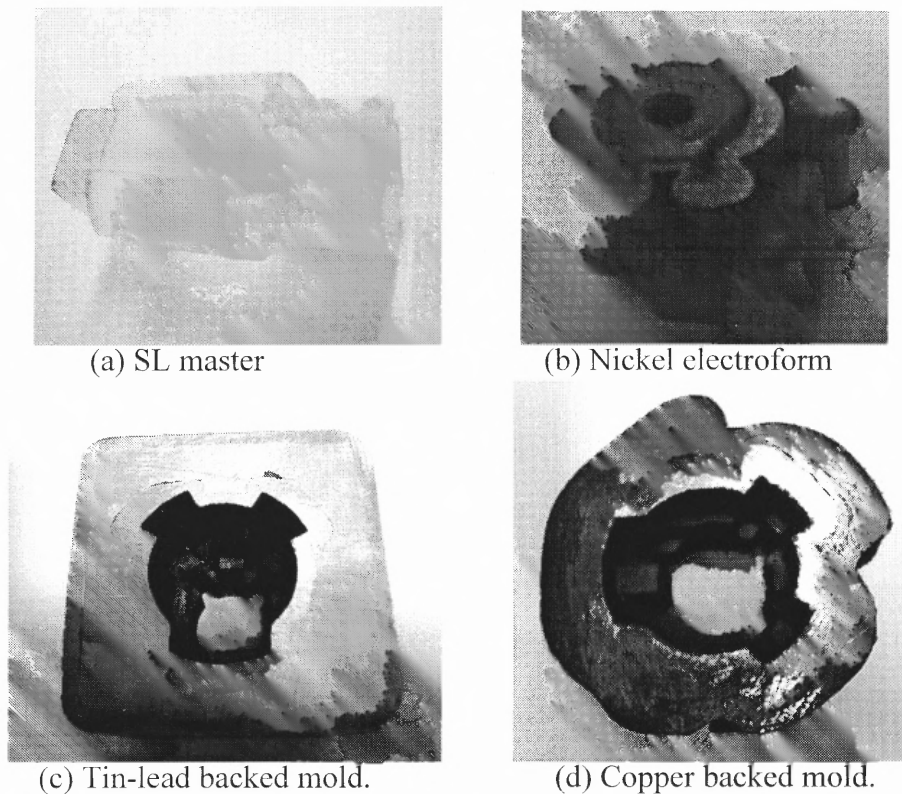


**Figure 5.5** Mold tooling process using RP master and electroforming

due to the high strength required in the subsequent injection molding process. The harder the backfilled metal, the higher the strength of the mold cavity. However, a harder metal usually has a higher melting temperature, and casting with a high melting temperature metal tends to generate larger thermal stresses which cause larger deformation in the electroformed metal shell. To reduce the injection molding cycle time, conformal cooling lines may be put around the nickel shell before the backfilling process.

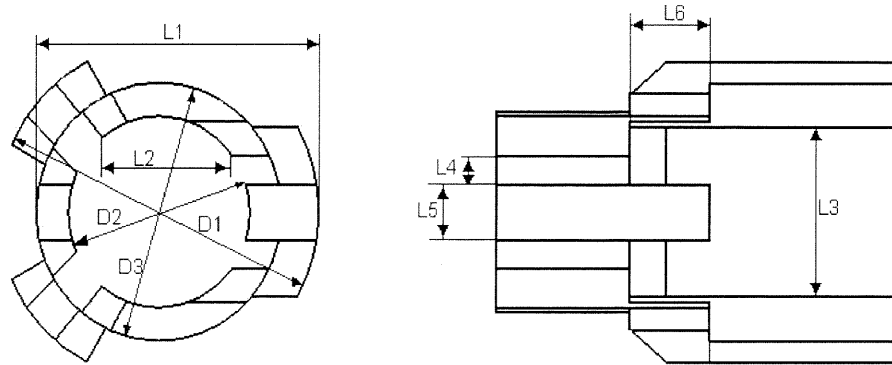
### 5.3.2 Case Studies

Using the mold tooling process, the SL master shown in Fig. 5.6(a) is used to produce a nickel electroform shown in Fig.5.6(b). The electroform is then backed with tin-lead



**Figure 5.6** Nickel electroformed molds with fine features

alloy or copper to fabricate the mold cavities shown in Fig.5.6(c) and Fig.5.6(d), respectively. The geometry of the master is difficult to machine due to the sharp corners and very small features. The masters are polished to have a surface finish of  $48\ \mu\text{in}$ . Each dimension (see Fig. 5.7) of the polished masters 1 and 2 is measured three times using a three axis coordinate measuring machine (CMM) and the average is recorded as listed in Table 5.5. Metallizing the masters with nickel to a thickness about  $0.0002\ \text{in}$  by nickel electroless plating, the masters are nickel-electroformed with the sulfamate electrolyte to form the nickel shell with a thickness of  $0.08\ \text{in}$  ( $2\ \text{mm}$ ). The mechanical properties of the electroformed nickel is about the same as that of stainless steel. The nickel electroformed shell ( $0.08\ \text{in}$  thick) from SL master 2 is then backed with  $0.08\ \text{in}$  thick of copper to a total metal thickness of  $0.18\ \text{in}$  ( $4\text{mm}$ ) also by electrodeposition. The electroformed masters are then put into an incinerator to burn out the SL resin at  $560\ ^\circ\text{C}$ . After burning, each dimension is measured three times using CMM and the average is recorded as listed in Table 5.5. Table 5.5 shows that the dimensional deviation of the mold 1 is larger than that of the mold 2. This is because that metal shell 2 is copper backed so that it is more rigid than nickel shell 1 to withstand thermal expansion of the SL master. The surface finishes of both of the cavities are measured at the values about  $49\ \mu\text{in}$ , which are about the same as that of the SL masters. The nickel shell 1 is put into a metal box and backfilled with molten bismuth-tin-lead alloy whose melting temperature is  $138.5\ ^\circ\text{C}$ . The dimensional deviation generated by this metal casting process is very small due to the low melting temperature of the backfilled metal.



**Figure 5.7** Dimensions measured

**Table 5.5** Dimensional data of SL parts versus electroformed mold cavities (unit: mm)

	D1	D2	D3	L1	L2	L3	L4	L5	L6
Part 1	30.503	23.421	16.828	27.033	10.932	15.225	2.578	5.108	7.661
Mold 1	30.579	23.477	16.868	27.089	10.947	15.245	2.583	5.113	7.666
Deviation 1	0.076	0.056	0.040	0.066	0.015	0.020	0.005	0.005	0.005
% deviation	0.25	0.24	0.24	0.21	0.14	0.13	0.20	0.10	0.07
Part 2	30.490	23.365	16.982	28.021	11.059	15.254	2.497	5.09	7.686
Mold 2	30.533	23.396	16.998	28.053	11.069	15.266	2.499	5.095	7.688
Deviation 2	0.039	0.031	0.018	0.032	0.010	0.012	0.002	0.005	0.002
% deviation	0.12	0.13	0.11	0.11	0.09	0.08	0.10	0.10	0.03

#### 5.4 Tooling Accuracy

The evaluation criteria for a tooling process include accuracy, surface finish and strength.

Widespread applications can be achieved when the following levels of properties can be

attained repeatedly: accuracy $\geq 0.01\text{mm}$ , roughness $\leq 1\mu\text{m}$ , and strength $\geq 300\text{Mpa}$  [Rees, 1995].

As stated before, surface finish of  $0.05\ \mu\text{m}$  can be obtained quite readily if the master is adequately smooth. Our experiment also showed that the surface finishes of the electroforms are almost the same as the surface finishes of the masters. So the surface finish of tools produced by the proposed tooling process can satisfy the surface requirements.

Physical, thermal and mechanical properties of electroformed copper and nickel have been widely studied [Spiro, 1968; Safranek, 1968; Sample and Knapp, 1968; Safranek, 1986]. The properties of these electroformed materials are varying in a large range depending on electrolyte solutions and operating conditions. Typically, the properties of the electroformed nickel is similar to that of the stainless steel, and the properties of the electroformed copper can match the properties of the rolled copper sheet. The strength of the electroformed copper for EDM electrode is less important than that of the electroformed nickel for mold because EDM electrode will not stand high mechanical loads but mold sometimes does. The electroformed nickel has typical yield strength ranging from 400 to 580 MPa.

As the experimental investigations demonstrate, identifying deformation sources and exploring methods to calculate and minimize the deformation to improve the tooling accuracy is the main task in this Ph.D dissertation study. The factors which affect the accuracy of a tool include the accuracy of the RP master, the deformation caused by electroforming stress, thermal expansion of master during electroforming, thermal expansion caused deformation and distortion of the metal shell when the electroformed

part is separated using burning, thermal stress caused deformation when backing metal shell with molten metals. The accuracy of a master is largely determined by the SL machine and can be improved through optimizing the building parameters. Stress reducer additives and optimal electroforming process parameters can dramatically reduce or even eliminate the internal stress of the electroformed metals [Stein, 1996]. Electroforming of SL parts is operated in room temperature to eliminate the thermal expansion of the master in our experimental work. With the various techniques which have been developed, electroforming can make part with dimensional tolerance as small as 0.0001 inch (0.0025 mm) [Degarmo, 1984].

The experimental case studies reveal that after the burnout of the SL masters, the largest dimensional deviations corresponding to dimension J (see Fig.5.2a and Table 5.4) of the two copper electroforms with the thickness of 2 mm and 4 mm are 0.093 mm (0.26% relative deviation) and 0.052 mm (0.13% relative deviation), respectively. The largest dimensional deviation corresponding to dimension D1 (see Fig.10 and Table 3) of the nickel electroformed shell with the thickness of 2 mm is 0.076 mm(0.25% relative deviation) and the largest dimensional deviation of the 2 mm nickel shell backed with 2 mm copper is 0.043 mm(12% relative deviation). These figures demonstrate that the thicker, the smaller the dimensional deviation. All the SL masters are electroformed at room temperature so the deformation due to electroforming is very small compared with the thermal expansion caused by the master burnout process. If there exists large dimensional deviation, the electroform at this portion may experience permanent deformation during the burnout process. The coefficient of thermal expansion of nickel is  $14 \times 10^{-6} /K$  and that of copper is  $17 \times 10^{-6} /K$ . The coefficient of thermal expansion of SL

5170 is temperature dependent. From the ambient temperature to about 75 °C, it is about  $90 \times 10^{-6}$  /K and when the temperature is higher than 75 °C, it is about  $181 \times 10^{-6}$  /K. When it is heated above 100°C, the strength of the SL material reduces rapidly as the temperature rise but it still has its strength until it reaches its burning point. This is the properties of thermosetting polymers. Because the thermal coefficient of the epoxy resin is much larger than the thermal coefficient of nickel and copper, thermal stresses are generated during the pattern burnout which deforms or even cracks the metal shell. If the thermal stress is larger than or equal to the yield strength of the electroformed metal, the electroform generates permanent deformation. We predict that the above deviations are due primarily to the thermal expansion of the SL pattern which deforms the electroform during the burnout process.

Backfilling the electroformed shell with molten metals is another main source of tooling inaccuracy. The strength of the EDM electrode is not important because the EDM electrode does not contact the workpiece during electrical discharge machining. Low melting alloys with good electrical and thermal conductivity can be used to backfill the shell to form an EDM electrode with little thermal deformation. A fully backed electroformed mold cavity with high strength metals will significantly improve the durability of the electroformed mold and increase the ability of the mold to resist deformation during the injection molding process. However, high strength metals always have high melting points. Our investigation shows that when aluminum with melting temperature of 667 °C is backfilled to the cavity of a copper shell, the copper shell deforms severely. One way to reduce the thermal deformation caused by backing with molten metal is by preheating the electroformed metal shell to about the same

temperature of the molten metal before pouring the molten metal. The preheating can also improve the flowability of the molten metal. In our current study, we use low melting alloys Metspec 281 whose melting temperature is 138.5 °C to back the nickel shell to form mold cavities, and Metspec 217 whose melting temperature is 103 °C to back copper shell to form EDM electrodes. Metspec series products are bismuth-tin-lead alloy manufactured by MCP Systems, Inc. The thermal deformation generated by back filling with these molten metals are very small. Therefore the thermal deformation at the backfilling process is not conducted in this study. The investigation of inaccuracies caused by burning out of SL masters is the challenge research issue and must be thoroughly studied to achieve successful tooling approach.

### **5.5 Environmental Performance of the Rapid Electroforming Tooling**

SFF processes have some good environmental characteristics. The waste streams are less in SFF processes than in conventional manufacturing processes such as machining. Worn tools and scraps seldom occur in SFF processes and equipment. Cutting fluids, which are the major source of hazard in machining [Sheng, et al., 1998], are not used in SFF processes. Comparing with conventional manufacturing processes, SFF processes have distinguishing features in process mechanisms, materials, energy use, etc. From the lifecycle point of view, a part produced with a SFF process generally goes through the following stages: (a) inputting the building material into the system, (b) building the part layer by layer, (c) shape replication and sintering or burning (for tooling processes) and (d) post-processing. When the user finishes using the part fabricated by SFF, the part goes to the disposal stage: to be landfilled, incinerated, or recycled. While the material,



part usage and part disposal are not exactly part of a process, their inclusion provides a holistic view of the environmental performance of an SFF process. Thus, factors taken into account in process environmental performance should include the material extraction stage, energy consumption and process wastes in the fabrication and replication stages, and the disposal stage. In terms of these environmental factors, a general comparison between conventional machining process and SL process is given in Table 5.6.

**Table 5.6** Comparison of Machining with SFF Processes [Luo, et al., 1999a]

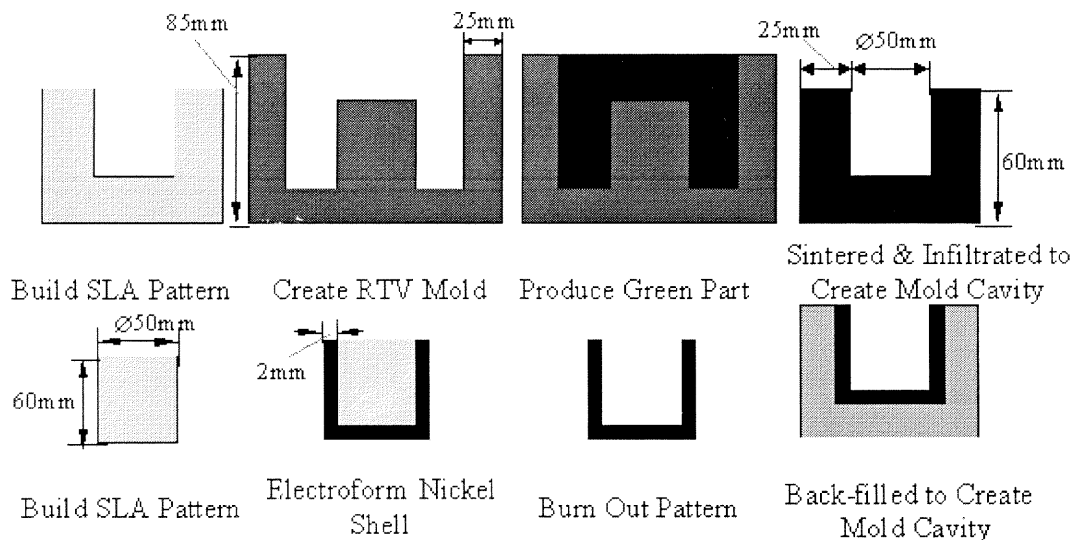
	Materials	Material Utilization	Energy Source	Process Residues	Disposal
Machining	metals, alloys, ceramics, etc.	material-removal process. Material Utilization Rate (MUR) is 60% - 90%	electromotor power (mechanical energy)	material chips, tool scraps & chips, cutting fluids, fluid vapor	Landfill, recycling
SLA	liquid photo-polymers, etc.	material-additive process. MUR almost 100%	UV laser (chemical energy)	material chips, removed support structures	Incineration, Landfill

A method for assessing the environmental performance of rapid prototyping and rapid tooling processes has been established [Luo, et al., 1999b]. In this method, each process is divided into a number of life stages. The environmental effect of each process stage is analyzed and evaluated based on an environmental index utilizing the Eco-indicators that were compiled by PreConsultants of the Netherlands. The effects of various life stages are then combined to obtain the environmental performance of a process. In the assessment of SFF processes, the material use in the fabrication of a part,

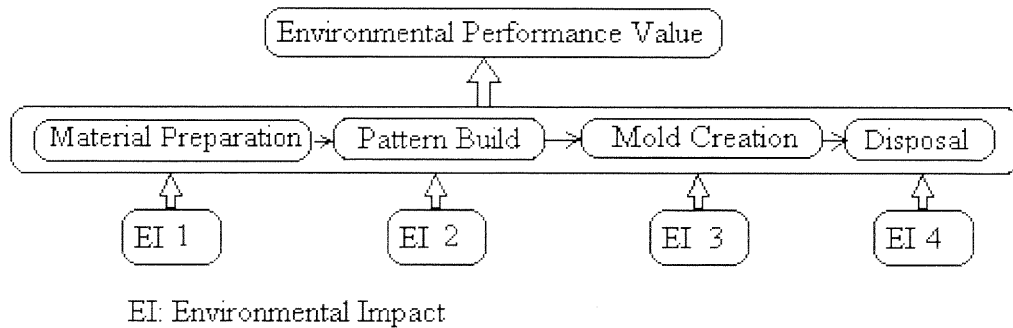
energy consumption, process wastes, and disposal of a part after its normal life are considered.

3D Keltool and the rapid electroforming tooling (RET) process are two indirect rapid tooling processes that require a master pattern built by SL process. 3D Keltool process [Raetz, 1998] can be used to rapidly create injection molds or die casting inserts. It begins with an SL pattern. The pattern is used to produce an RTV silicone rubber mold. Once the RTV mold is produced, it is then filled with a mix of tooling steel powder, tungsten carbide powder and epoxy binder. After this material has cured in the mold, this “green part” is sintered in a hydrogen-reduction furnace and the binder material is burning off. The final step is to infiltrate the sintered part with copper.

Figure 5.8 illustrates the concepts of these two indirect tooling processes. When a cylindrical metal mold cavity is required to be manufactured, both 3D Keltool and RET processes have this function, although they differ from each other in the type and amount of materials use and specific intermediate steps. The model introduced by Luo, et al.



**Figure 5.8** Indirect tooling processes



**Figure 5.9** Lifecycle environmental performance model of indirect RT process [Luo, et al., 1999b]

[1999b] is used to assess the environmental performance of the 3D Keltool and RET processes from the lifecycle viewpoint.

In order to evaluate indirect RT processes, the volume of final tool should be accounted in order to estimate the amount of intermediate material consumed. The cylindrical mold cavity with dimensions of diameter 50mm and height 60mm in Fig. 5.8 is used as an example for the following assessment.

SLA 250 is used to fabricate the master patterns for the two RT processes. The environmental impact for unit volume ( $\text{cm}^3$ ) SL material consumed is 0.0104. Since 3D Keltool uses the negative pattern and SFF-Electroforming uses positive pattern, different volumes of materials used yield different impact values for this stage. Here we assume the dimensions of the mold is 100mm diameter and 90mm height. The volume of material used by the 3D Keltool process to build the pattern is  $589.4\text{cm}^3$  and that used by the RET process is  $117.2\text{cm}^3$ .

In the mold creation stage, material consumption, and energy consumption during the sintering or burning step should be considered. In this stage, 3D Keltool typically consumes silicone rubber to build an RTV mold, uses mixed steel powder and epoxy

binder to create the green part, and uses copper infiltration to create the final solid mold. The environmental indices for unit volume ( $\text{cm}^3$ ) of silicone rubber, mixed steel, epoxy binder and copper are 0.0101, 0.133, 0.0104 and 0.757 respectively. The volumes of RTV mold can be calculated. The volumes of steel and epoxy binder are 70% of 30% of the mold volume respectively. Since the void volume of mold after sintering is 30% [Raetz, 1998], the volume of infiltrated copper should be 30% of the mold volume. Therefore the material consumption impact in this stage can be estimated based on Eco-indicators and the volume of materials used in this stage. Supposedly, the RET process uses nickel to electroplate a certain thickness of nickel shell, and then backfills the shell with aluminum. For unit volume ( $\text{cm}^3$ ) of nickel and aluminum, the environmental indices are 0.757 and 0.0486, respectively. The nickel shell thickness is typically 2mm. So the volume of nickel and aluminum used also can be calculated. Hence we can get the material consumption impact in this stage for RET process. The results can be seen in Table 5.7. Sintering & infiltration in the 3D Keltool process and burning off in the RET process require energy. The energy consumption is estimated based on the melting point or burning point, the specific heat and the assumed furnace efficiency.

In the disposal stage, the 3D Keltool process produces wastes such as SL material and silicone. The RET process only has residue of SLA material. If the process residue are all disposed to landfill, the environmental impact can be assessed by considering the impact indices and the volume disposed. The results are shown in Table 5.7. In addition, we expect that the disposed tools can be recycled by material recovering. The mixed metal of the tool made by 3D Keltool is less preferable than laminated nickel and aluminum used in the electroforming tooling process. The impact indices for recycling

unit volume ( $\text{cm}^3$ ) of mixed steel, nickel, and aluminum are -0.0226, -0.312, and -0.035 respectively. The assessment results for the above two indirect RT processes are listed in Table 5.7.

**Table 5.7** Environmental Performance of RT Process [Luo,et al., 1999b]

<b>Process</b>	<b>Project</b>	
3D KelTool RET	Environmental effect for RT processes	
<b>Base SFF process</b> SLA	<b>Environmental impact index</b> Eco-indicator	
	3D KelTool	SFF-Electroforming
<b>Pattern build</b>		
• Material use	6.13 (epoxy resin)	1.22 (epoxy resin)
• Energy use	12.38 (energy used in pattern building)	2.46 (energy used in pattern building)
<b>Mold creation</b>		
• Material use	193.7 (silicon rubber + mixed steel powder + epoxy binder + infiltrated copper)	46.21 (nickel + aluminum)
• Energy use	0.707 (energy used in sintering and infiltration processes)	0.0191 (energy used in burning off process)
<b>Disposal</b>		
• Process residues landfill	0.088 (epoxy resin + silicon rubber)	0.033 (epoxy resin)
• Material recovery	-64.49 (mixed steel + copper)	-26.67 (nickel + aluminum)
<b>Total impact</b>	148.52	23.24

From the above assessment, we can see that the environmental performance of a rapid tooling process depends on several factors. First, the selection of the base SFF process is an important factor. It is desirable to select an SFF process that has good environmental performance. Secondly, the tooling materials, and process residues can further impact on the environmental performance due to the use of natural resources and possible generation of process residues. Finally, the method of disposal or recovery of tool material will also influence the total environmental performance of a process.

### **5.6 Discussion of Tooling Time and Cost-effectiveness**

Die and mold manufacturing must be considered as a total system that includes: a) part design for near net shape (NNS) manufacturing, b) production of prototypes for visualization, testing and evaluation, c) process modeling for optimum mold design, d) CNC machining, e) manufacturing of EDM electrodes, f) EDM machining, g) Surface conditioning and polishing, and h) dimensional control of electrodes, dies, and the NNS formed products [Altan, et al., 1993]. In a survey conducted of the U.S. injection molding industry [Shanahan, 1993], the total mold manufacturing time varied between 1,200 to 3,800 hours, depending on mold size, geometry and complexity. The time spent for each manufacturing step, as a percent of the total, was in the range of: 10-20% for design, 14-17% for tool path generation, 8-16% for rough machining, 27-39% for finishing machining, 13-23% for finishing, and 4-6% for try-out.

There exists part design and try-out for both conventional machining approach and RET process for making tools. Taking the example of the mold shown in Fig. 5.6(c), the geometry of the mold is so complex that the shape of the mold cavity can not be

generated by CNC milling itself due to the sharp corners and narrow slots. In order to generate the mold cavity by machining, CNC rough machining, semi-roughing, and EDM machining are needed to generate the final shape as shown in the figure. The generation of the EDM electrodes is also a difficult task due to its complex geometry. The minimum time for manufacturing this mold by conventional machining would be more than 1,200 hours, i.e. about 50 days, three shifts per day.

However, the mold shown in Fig. 5.6(c) was manufactured by RET process in less than one week. It takes 12 hours to generate the SL pattern, 24 hours to electroform the pattern, 4 hours to burnout the pattern and 6 hours to back the metal shell. The total net time is about 46 hours. If the overhead time of the RET process for generating this mold is about 40%, the total time then becomes 64 hours, i.e. less than 3 days.

The rate for machines used for manufacturing the mold cavity is difficult to estimate. So we only consider the labor rate for making the mold cavity. Suppose the labor rate is \$10 per hour. The labor cost for making the mold by conventional machining would be  $1200 \text{ (hour)} \times 10 \text{ (\$/hour)} = \$12,000$ . However, the labor cost for making the mold by RET process is about  $64 \times 10 = \$640$ .

The actual cost for making the mold in our case study is \$ 702. The cost is distributed as follows: \$122 for SL pattern generation, \$400 for electroforming, \$60 for burnout process and \$120 for backing process.

## 5.7 Closure

Solid freeform fabrication combined with electroforming for generation of metal molds and EDM electrodes is developed in this chapter. Case studies of EDM and mold tooling

indicate that the described methods are viable for rapid tooling of molds and EDM electrodes. Compared with the rapid tooling processes involving metal powder sintering, the described process of integrating stereolithography with electroforming eliminates the dimensional uncertainty associated with the occurrence of random shrinkage during sintering and it generates metal tools with better accuracy and finer surface finish. The electroforming thickness affects the mechanical properties and dimensional accuracy of the mold. Thermal stress caused by burnout of the SL masters is identified as one of the major sources of inaccuracy factors. The another major inaccuracy factor is the deformation generated by solidification when backfilling the electroform with molten metals. Burnout of the SL resin from the electroforms is an efficient and convenient method, however, the thermal stress induced during the burnout process is critical for generating accurate tools. The thermal stress problem is studied in the next chapter.



### THERMOMECHANICAL MODELING AND ANALYSIS

Based on experimental data analysis, the geometry and material of the SFF part, properties of the electroformed metal, and process parameters are significant factors that cause inaccuracy in the manufactured tools. Thermal expansion of the SL part during burnout process can significantly deforms or even cracks the thin electroformed metal shell. In this chapter, the material properties of the SL resin and the electroformed metal, namely copper and nickel, are first presented. A thermomechanical model is then derived. Finite element analysis (FEA) based numerical simulation using ANSYS software is then modeled to simulate the thermal stress induced by the burnout. In order to verify the modeling and numerical simulation, thermal stress measurements using strain gages are performed. Finally, discussions and conclusions are given. The objective of this chapter is to provide a thermomechanical model and an FEA based numerical simulation method that can be used to determine the geometry of the SFF part and the electroform thickness for minimizing the manufacturing time and cost while satisfying the tooling accuracy requirement.

#### 6.1 Properties of Tooling Materials

Accuracy of tools generated by the proposed tooling process is mainly determined by the properties of the materials used. Especially the deformation and distortion generated during the burnout process are greatly determined by the thermal and mechanical properties of the cured SL resin and the electroformed metals. The SL resins in this study

include SL 5170 and SL 5210. The electroformed metals include nickel and copper that are used for mold tooling and EDM electrode tooling, respectively. The properties of these materials are essential for the analysis of thermal stress induced during the burnout process.

### 6.1.1 Properties of Stereolithography Resin

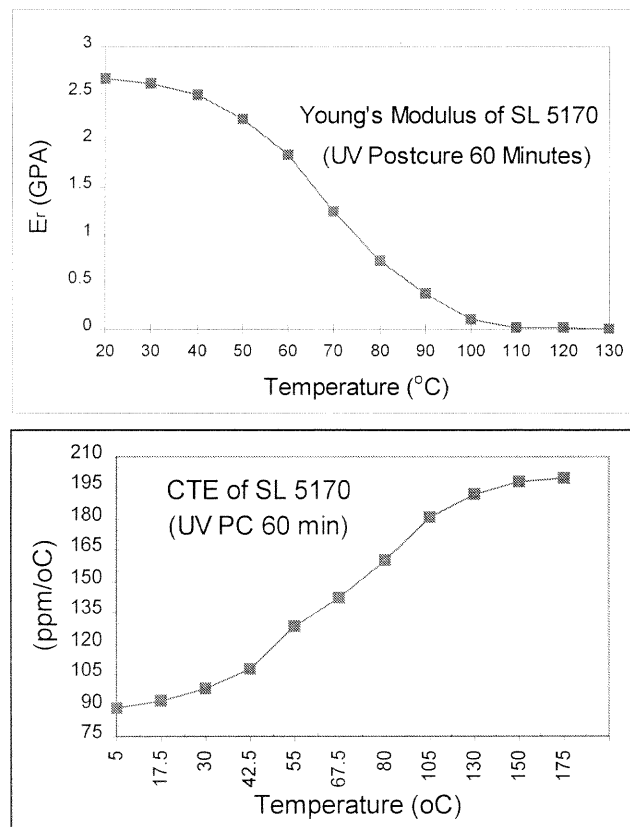
Cibatool SL 5170 is an epoxy-based resin that offers the greatest degree of accuracy available in any rapid prototyping process. Parts are strong, durable and multifunctional. SL 5170 fits a wide range of applications from form, fit and function to optical stress analysis, and as parts for secondary tooling applications. SL 5170 has several material properties that exceed or are comparable to medium impact polystyrene. The typical mechanical properties of SL 5170 at 20 °C are listed in Table 6.1. Thermal properties of SL 5170 are listed in Table 6.2. Most of those properties are a function of the temperature. Fig. 6.1 illustrates the Young's modulus and coefficient of thermal expansion (CTE) of SL 5170 versus the variation of temperatures.

**Table 6.1** Mechanical properties of SL 5170 at 20 °C (UV Post Cured 60 minutes)

Measurement	Method	Value
Density		1.22 g/cm <sup>3</sup>
Ultimate strength	ASTM D 638	59-60 MPa (8,600-8,800 psi)
Young's modulus	ASTM D 638	2,500-2,650 MPa (353-367 Ksi)
Elongation at break	ASTM D 638	7-19%
Flexural strength	ASTM D 790	107-108 Mpa (15,500-15,700 psi)
Flexural modulus	ASTM D 790	2,920-3,010 Mpa (423-436 Ksi)
Poison ratio	ASTM D 638	0.40

**Table 6.2** Thermal properties of SL 5170 (UV Post Cured 60 minutes)

Measurement	Method	Temperature range	Value
Glass transition temp	DMA, 4°C/min	-100 to 200 °C	65-90°C (149-184°F)
Heat deflection temp	ASTM D 648	-100 to 200 °C	55°C (131°F) @ 66 psi 49°C (120°F) @ 264 psi
Thermal expansion coefficient	TMA	5 to 220 °C	See Fig.11
Thermogravimetric analysis (Weight loss in %)	TGA	247 °C 458 °C 537 °C	1.3% 84.3% 94.1%
Specific heat			1758.8 J/kg·°C (0.42 Btu/°F·lb)
Thermal conductivity	VDE 0304		0.2002 W/m·°C

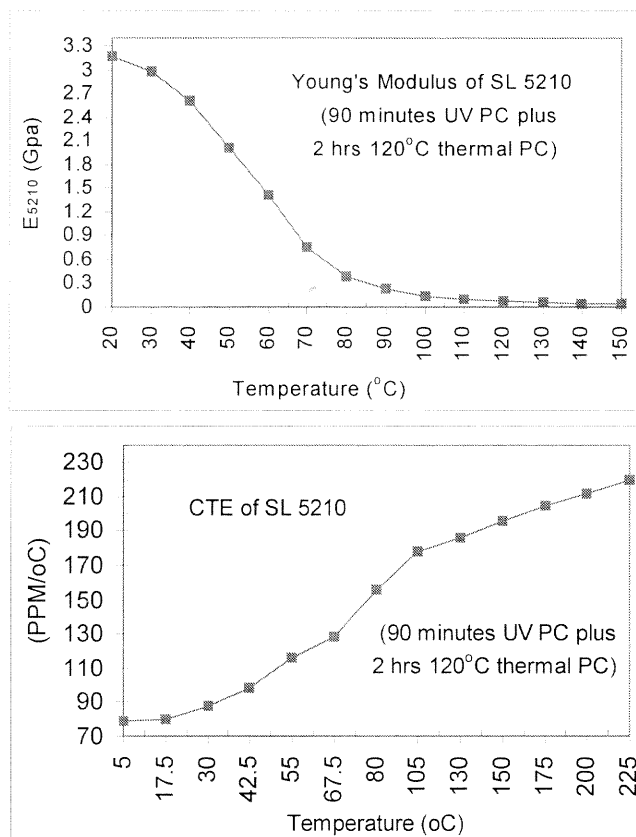
**Figure 6.1** Young's modulus and coefficient of thermal expansion of SL 5170 vs. temperatures

Cibatool SL 5210 is an advanced vinyl ether/acrylate based resin which is a perfect solution for functional prototypes which demand high temperature or water immersion testing. Capable of withstanding temperatures in excess of 100°C (212°F), SL 5210 offers the highest heat resistance of any previously released material by Ciba Company. SL 5210 is ideal for under-the-hood testing, underwater testing, wind-tunnel models, housings for electrical assemblies, high temperature RTV molding, water pumps, working prototypes and visual models. The typical mechanical properties of SL 5210 at 20 °C are listed in Table 6.3. Thermal properties of SL 5210 are listed in Table 6.4. Fig.6.2 illustrates the Young's modulus and coefficient of thermal expansion (CTE) of SL 5210 versus temperatures.

**Table 6.3** Typical mechanical properties of SL 5210 at 20 °C

Measurement	Method	Value*	Value**
Ultimate strength	ASTM D 638	15 Mpa (2,220 psi)	45 Mpa (6,500 psi)
Young's modulus	ASTM D 638	1,455 Mpa (211,000 psi)	3,020 Mpa (438,000 psi)
Elongation at break	ASTM D 638	1.2%	1.6%
Flexural strength	ASTM D 790	44 Mpa (6,400 psi)	74 Mpa (10,700 psi)
Flexural modulus	ASTM D 790	1,724 Mpa (250,000 pi)	3,061 Mpa (444,000 psi)
Density	ASTM D 792	1.2098 g/cm <sup>3</sup>	1.2112 g/cm <sup>3</sup>
Poison ratio	ASTM D 638	0.42	0.41

\* 90 minutes of UV postcure. \*\* 90 minutes of UV postcure + 2 hours @ 120°C thermal postcure.



**Figure 6.2** Young's modulus and coefficient of thermal expansion of SL 5210 vs. temperatures

**Table 6.4** Thermal properties of SL 5210

Measurement	Method	Value*	Value**
Glass transition temp	DMA	70.25 °C (158°F)	92°C (198°F)
Heat deflection temp	ASTM D 648	47°C(117°F) @ 66 psi 46°C(115°F) @264 psi	99°C (210°F) @ 66 psi 74°C (165°F) @ 264 psi
Thermal expansion coefficient	TMA	5 to 220 °C	See Fig.12
Thermogravimetric analysis (Weight loss in %)	TGA	247 °C 458 °C 537 °C	1.1% 83.8% 93.4%
Specific heat		1716.2 J/kg·°C (0.41 Btu/°F·lb)	1758.8 J/kg·°C (0.42 Btu/°F·lb)
Thermal conductivity	VDE 0304	0.2001 W/m·k	0.2003 W/m·k

\* 90 minutes of UV postcure. \*\* 90 minutes of UV postcure + 2 hours @ 120°C thermal postcure.

**Table 6.5** Mechanical and thermal properties of electroformed copper at 20 °C

	Electroformed copper (sulfate solution)	Annealed wrought copper
Ultimate Strength (Mpa)	360 - 380	280
Yield Strength (Mpa)	198 - 210	178
Tensile Modulus (Gpa)	100 - 110	90
Vickers Hardness	118 - 120	110
Internal Stress (Mpa)	-0.55 - 0.8	
Poison Ratio	0.3	0.3
Density (g/cm <sup>3</sup> )	8.9	8.96
Melting Temperature (°C)	1080	1080
CTE (ppm/°C)	17	16.8
Thermal conductivity (W/m·°C)	399	399
Specific heat (J/kg·°C)	383	382

### 6.1.2 Properties of Electroformed Copper

The properties of electroformed metals differ appreciably not only from the properties of castings, forgings or rolled sheet, but also from the procedures and process parameters used for electrodepositing the metals. Careful control of the electrodeposition condition and environment are essential for obtaining required material properties [DiBari, 1996]. The metal deposition control aspects include adjusting the composition of the plating solution, monitoring the impurity level, controlling the PH value, temperature and current density, monitoring and controlling stress continuously by automatically tuning process parameters and adding stress reducing agents, adjusting the concentration of organic additives to control the electrochemical characteristics of individual metal layers. Current

density, solution composition and pH value are key factors that determine the mechanical and thermal properties of the electroform [Safranek, 1962; Safranek, 1986]. Higher current density increases the deposition rate, but it decreases the strength and increases the electroforming stress.

The sulfate plating bath is used for the dissertation work. The typical mechanical and thermal properties of electroformed copper from sulfate plating bath and annealed wrought copper at 20 °C are listed in table 6.5 [Safranek, 1962; Safranek, 1986]. Mechanical and thermal properties of electroformed copper versus temperature are listed in Table 6.6.

**Table 6.6** Mechanical and thermal properties of sulfate electroformed copper vs. temperature

Temperature (°C)	Ultimate strength (MPa)	Yield strength (MPa)	Young's modulus (GPa)	CTE ppm/°C
20	370	200	100	17
100	362	193	97	17
200	348	182	90	17.1
300	316	166	81	17.2
400	284	130	72	17.2
560	228	110	66	17.3

### 6.1.3 Properties of Electroformed Nickel

The mechanical and thermal properties of electroformed nickel are influenced by current density, pH values, and solution composition [DiBari, 1991]. The typical mechanical and thermal properties of electroformed nickel from sulfamate bath and annealed wrought

nickel at 20°C are listed in table 6.7 [Sample and Knapp, 1962]. Mechanical and thermal properties of electroformed nickel versus temperature are listed in Table 6.8.

**Table 6.7** Mechanical and thermal properties of electroformed nickel at 20 °C

	Electroformed nickel (sulfamate solution)	Annealed wrought nickel
Ultimate Strength (Mpa)	640 – 650	420
Yield Strength (Mpa)	486 – 498	168
Tensile Modulus (Gpa)	280 – 290	160
Vickers Hardness	192 – 195	154
Internal Stress (Mpa)	-5 –10	
Poison Ratio	0.28	0.29
Density (g/cm <sup>3</sup> )	8.8	8.7
Melting Temperature (°C)	1450	1450
CTE (ppm/°C)	12.6	13.3
Thermal conductivity (W/m·°C)	91	91
Specific heat (J/kg·°C)	446	446

**Table 6.8** Mechanical and thermal properties of sulfamate electroformed nickel vs. temperature

Temperature (°C)	Ultimate strength (MPa)	Yield strength (MPa)	Young's modulus (GPa)	CTE ppm/°C
20	650	488	286	12.6
100	640	446	276	13.2
200	560	360	245	13.6
300	450	282	193	13.9
400	360	188	158	14.1
560	240	156	124	14.2



## 6.2 Failure Criteria

Failure refers here to the situation that stresses existing on the metal shell generate plastic deformation. Nickel and copper used in this tooling study are ductile and capable of undergoing an appreciable amount of yielding or permanent deformation, while the SL resin that is brittle prior to fracture can suffer only a small amount of yielding.

For the three dimensional case, it has been demonstrated that three planes of zero shear stress exist, that these planes are mutually perpendicular, and that on these planes the normal stresses have maximum or minimum values. These normal stresses are referred to as principal stresses, usually denoted as  $\sigma_1$ ,  $\sigma_2$ , and  $\sigma_3$  with the  $\sigma_1$  represents the largest and  $\sigma_3$  the smallest normal stresses. The three principal stresses are the three roots of the following equation:

$$\sigma_p^3 - I_1\sigma_p^2 + I_2\sigma_p - I_3 = 0 \quad (6.1)$$

where

$$I_1 = \sigma_x + \sigma_y + \sigma_z \quad (6.2a)$$

$$I_2 = \sigma_x\sigma_y + \sigma_x\sigma_z + \sigma_y\sigma_z - \tau_{xy}^2 - \tau_{yz}^2 - \tau_{xz}^2 \quad (6.2b)$$

$$I_3 = \begin{vmatrix} \sigma_x & \tau_{xy} & \tau_{xz} \\ \tau_{xy} & \sigma_y & \tau_{yz} \\ \tau_{xz} & \tau_{yz} & \sigma_z \end{vmatrix} \quad (6.2c)$$

In this study, the most widely used theory, the maximum shear stress theory, proposed by C. A. Coulomb, also referred to as the Tresca yield criterion in recognition of the contribution of H. E. Tresca, is adopted to predict the onset of inelastic behavior for ductile materials, including nickel and copper. This theory predicts that yielding will

start when the maximum shear stress in the material equals the maximum shear stress at yielding in a simple tension test, i.e.

$$|\sigma_1 - \sigma_3| = \sigma_{yp} \quad (6.3)$$

where  $\sigma_{yp}$  represents the yield strength or failure strength of the material under a simple tension test. During the burnout process, if  $|\sigma_1 - \sigma_3| < \sigma_{yp}$ , there will be no permanent deformation, i.e., the loss of accuracy of the tool during burnout can be ignored. In the case of plane (two-dimensional) stress,  $\sigma_3=0$ . The yielding condition is given by

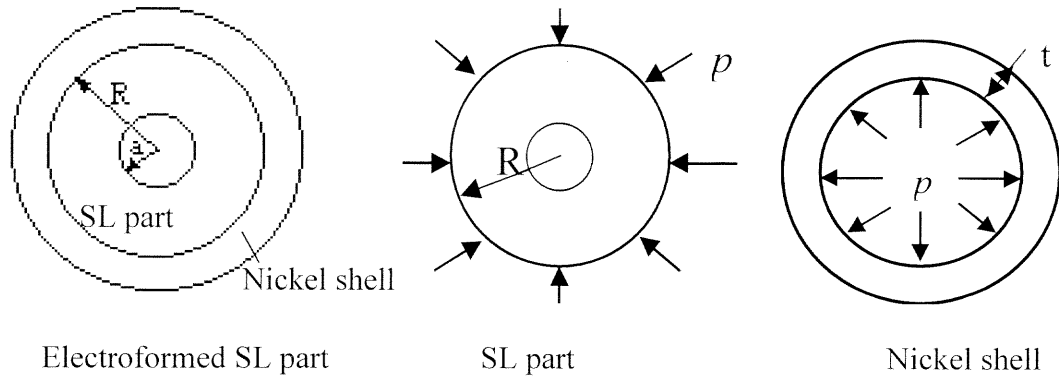
$$|\sigma_1 - \sigma_2| = \sigma_{yp} \quad (6.4)$$

where  $\sigma_2$  is the second principal stress.  $|\sigma_1 - \sigma_3|$  and  $|\sigma_1 - \sigma_2|$  are termed thermal stresses in this dissertation for three-dimensional and two-dimensional cases, respectively. If the thermal stress is smaller than yield strength  $\sigma_{yp}$ , the electroform can withstand the burnout process with little or no permanent deformation. Otherwise, the electroform will yield and generate permanent deformation that is not accepted for the tooling process.

Maximum Principal Stress Theory, credited to W.J.M. Rankine, is adopted to predict the failure of the SL material. According to the maximum principal stress theory, a material fails by fracturing when the largest principal stress exceeds the ultimate strength  $\sigma_u$  in a simple tension test. That is, at the onset of fracture,

$$|\sigma_1| = \sigma_u \text{ or } |\sigma_3| = \sigma_u \quad (6.5)$$

Thus, a crack will start at the most highly stressed point in a brittle material when the largest principal stress at that point reaches  $\sigma_u$ . In finite element analysis, if the SL part fractures, the stress exerted on the electroform will dramatically decrease. In our



**Figure 6.3** Pressure generated at the interface of the SL master and the nickel shell due to heating of the model

study we only query the stresses on the electroform because it is the object that we are mostly concerned of.

### 6.3 Analytical Calculation of Thermal Stresses

The thermal expansion of the SL parts generates thermal stresses which deform or even crack the metal shells during the burnout process. In order to understand the importance of analyzing the thermal stress generated during the burnout process, we first analytically compute the stress for a simple case. Suppose that a cylindrical SL part of circular cross-section, with outer radius of  $R=50$  mm and inner radius of  $a$ , is electroformed with nickel, with variable electroforming thickness  $t$ , as illustrated in Fig.6.3 and is then burned.  $a=0$  stands for the solid SL part. For the burnout process, let us assume that the SL part and nickel shell have a uniform temperature rise from the room temperature  $20^\circ\text{C}$  to  $80^\circ\text{C}$ , i.e.,  $\Delta T=60^\circ\text{C}$ . At this temperature, both the SL resin and nickel shell will expand. Further assuming that the two ends of the cylinders are open and unconstrained, i.e.,

$\sigma_z=0$ . Thus the electroformed cylinder is in a condition of plane stress. Now we can solve the thermal pressure exerted at the interface of the SL resin and the nickel shell using the following formula [Ugurall, 1995]:

$$p = \frac{(\alpha_r - \alpha_n)\Delta T}{\frac{1}{E_r} \left( \frac{R^2 + a^2}{R^2 - a^2} - \nu_r \right) + \frac{1}{E_n} \left( \frac{(R+t)^2 + R^2}{(R+t)^2 - R^2} + \nu_n \right)} \quad (6.6)$$

where Young's modulus of SL resin at 80 °C is  $E_r=390$  Mpa; Young's modulus of nickel is  $E_n=178$  Gpa; Poison ratio of SL resin is  $\nu_r=0.4$  and that of nickel is  $\nu_n=0.28$ ; coefficients of thermal expansion of SL resin and nickel are  $\alpha_r=158 \times 10^{-6}/^\circ\text{C}$ , and  $\alpha_n=14 \times 10^{-6}/^\circ\text{C}$ , respectively.

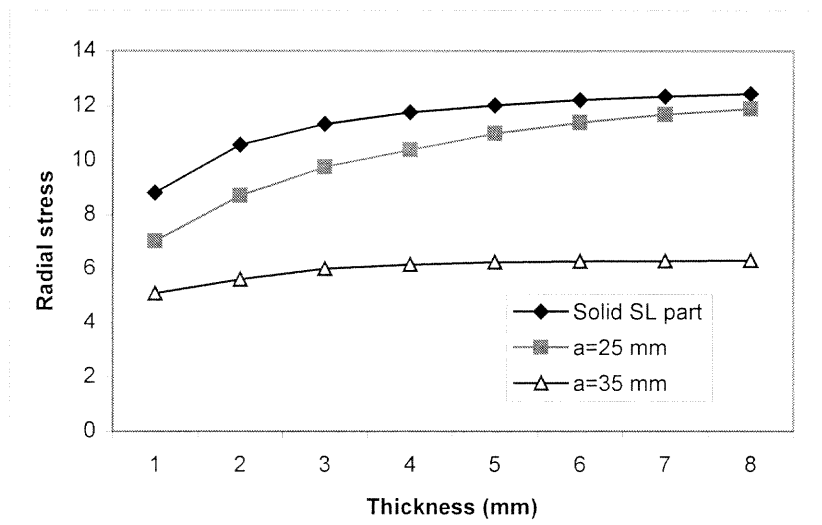
The principal stresses, radial stress ( $\sigma_{rad}$ ) and circumferential stress ( $\sigma_\theta$ ), of the nickel shell are calculated as follows:

$$\sigma_{rad} = -\frac{R^2}{(R+t)^2 - R^2} \left( 1 - \frac{(R+t)^2}{r^2} \right) \cdot p \quad (6.7)$$

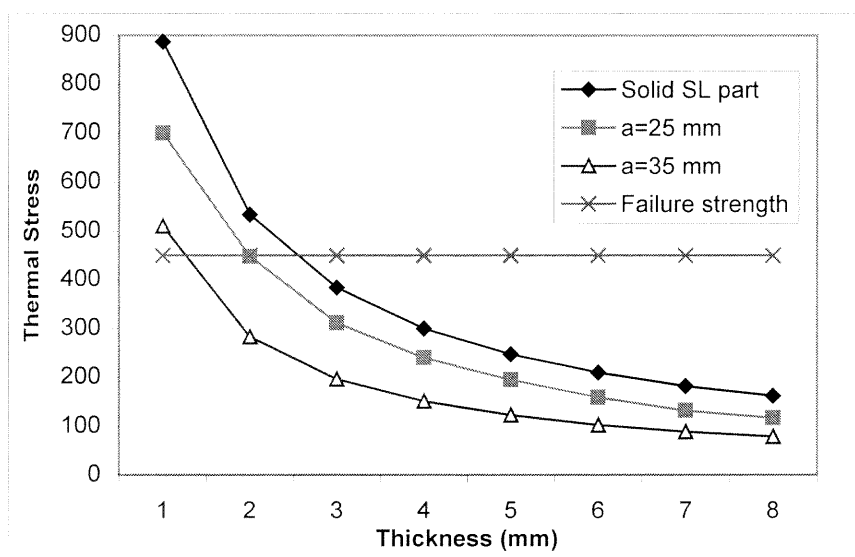
$$\sigma_\theta = \frac{R^2}{(R+t)^2 - R^2} \left( 1 + \frac{(R+t)^2}{r^2} \right) \cdot p \quad (6.8)$$

where  $r$  is the value between  $R$  and  $(R+t)$ . The maximum  $\sigma_\theta$  takes place at  $r=R$ .

Let the electroforming thickness  $t$  vary from 1 mm to 8 mm and calculate the radial stresses at the interface of the SL part and the electroformed nickel shell for  $a=0$ , 25 mm, 35 mm. The calculated results are illustrated in Fig. 6.4(a). It is seen that the larger the nickel shell thickness, the greater the pressure. According to the maximum principal stress theory, the SL master will crack when the principal stress is larger than its ultimate strength, which is 24 Mpa at temperature of 80 °C. It is depicted that the pressure exerted on the SL part will not crack the SL part.



(a) Radial stress at the interface of master and nickel shell

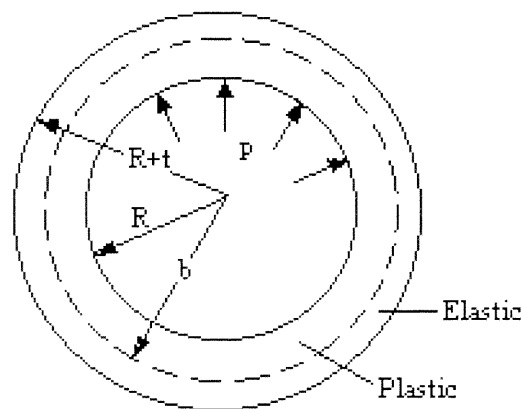


(b) Maximum thermal stress exerted on nickel shell

**Figure 6.4** Radial and thermal stresses vs. electroforming thickness

The maximum circumferential stresses at the inner surface of the nickel shell are calculated and the thermal stress ( $\sigma_{\theta} - \sigma_{rad}$ ) is shown in Fig.6.4(b). The yield strength (450 MPa), also termed the critical stress, of the nickel is also illustrated in this figure. A continuing increase in internal pressure will result in failure of the nickel material at the

interface of the nickel shell and the SL part. When the electroforming thickness of the solid SL part is smaller than 2.8 mm and that of the hollowed SL part with inner radius of 25 mm is smaller than 2 mm, the maximum hoop stress will plastically deform the nickel shell and cause permanent deformation when the part cools down. However, if the electroforming thickness is larger than 1.4 mm for the SL part having an inner radius of 35 mm, the maximum thermal stress will be smaller than the yield strength. As the pressure increases, the plastic zone will spread toward the outer surface of the nickel shell, and an elastic-plastic state will prevail in the shell with a limiting radius  $b$  beyond which the cross section remains elastic, as shown in Fig. 6.5. When the SL is burned out and the pressure is released, the nickel shell unloads elastically. Thus, elastic and plastic stresses are superimposed to produce a residual stress pattern. The plastic deformation directly affects the dimensional accuracy of the mold. Our analysis is to calculate the thermal stress so that the thermal stress exerted on the electroform is smaller than the yield strength of the electroform through building of inner hollow structure for the SFF part and adjusting the electroform thickness.



**Figure 6.5** Partially yielded nickel shell under internal pressure

As stated before, the SL part must be rigid enough to withstand the electroforming stress when building the nickel shell. The typical value of internal electroforming stress ( $\sigma_\theta$ ) can be in the range of  $-5$  to  $10$  Mpa. The pressure  $p$ , due to electroforming stress, exerted on the surface of the SL part can be calculated by

$$p = \frac{(R+t)^2 - R^2}{(R+t)^2 + R^2} \cdot \sigma_\theta \quad (6.9)$$

For  $R=50$  mm, and let  $\sigma_\theta=10$ MPa and  $t=1$  mm, the pressure exerted on the SL part is  $0.198$ MPa. Under this pressure, the part deformation in radial direction can be calculated by:

$$u = \frac{R^3 p}{E_r (R^2 - a^2)} \left( (1 - \nu_r) + (1 + \nu_r) \frac{a^2}{R^2} \right) \quad (6.10)$$

The deformations are  $0.0024$  mm,  $0.0042$  mm and  $0.0096$  mm for solid ( $a=0$ ),  $a=25$  mm and  $a=35$  mm SL parts, respectively.

#### 6.4 Thermomechanical Modeling of the Burnout Process

The analytical calculation of the thermal stress implies that the structure of the SL part and electroforming thickness can control the thermal stress so that it is smaller than the yield strength of the electroformed metal to prevent permanent deformation. Practically, the geometry of the tools is always complex and the distribution of temperatures in the burnt object is not uniform so analytical solution can not handle the thermal stress calculation. A finite element analysis based thermomechanical model needs to be established to analyze the thermal stresses.

Thermal stress induced by burning out the SL part is a multi-materials, non-linear, transient coupled thermal-mechanical problem. Boley and Weiner [1964] proved that the

thermal solution is independent of any changes caused by thermally-induced stress under the condition that the time history of the displacement closely follows the change of temperature, and vice versa. Assume that the burnout process satisfies the condition due to the thermal expansion of the object closely follows the temperature variation, so the thermomechanical coupling problem can be simplified as an uncoupled, transient thermal stress problem. Under this assumption, the modeling of the thermal stress can be divided into two steps: thermal modeling and structural modeling.

#### 6.4.1 Thermal Modeling of the Burnout Process

Thermal modeling is to compute the transient temperature field  $T(x,y,z,t)$  during the burnout process. The governing heat conduction equation is

$$a\left(\frac{\partial^2 T}{\partial x^2} + \frac{\partial^2 T}{\partial y^2} + \frac{\partial^2 T}{\partial z^2}\right) = \frac{\partial T}{\partial t} \quad (6.11)$$

where  $a = \frac{k}{c\rho}$ ,  $k$ ,  $c$ , and  $\rho$  are the heat conductivity, the specific heat, and the material density, respectively. To solve this second-order partial differential equation, there should be one initial condition and six boundary conditions for each volume. Because SL part and electroformed metal are burned together, so there are two volumes and 14 conditions are needed to calculate the temperature distribution  $T(x,y,z,t)$ .

The two initial conditions are that metal shell and the RP part are at the ambient temperature  $T_a$ . That is:

$$T_m(p,0) = T_r(p,0) = T_a \quad (6.12)$$

When an electroformed RP part is put into an oven, the thermal load is the oven temperature  $T_o$ . We assume the oven is preheated to the burnout temperature (560 °C for



SL part) and it is constant during the burning process. This is termed stepped thermal load, as shown in Fig.6.6(a). Another alternative is that we put the electroformed object inside the oven first and then start to heat up the oven in a linear increase function of oven temperature versus time. This is termed ramped thermal load, as shown in Fig.6.6(b). The electroformed object is inside an oven chamber and the hot air is in a perfect thermal contact with the exterior surface of the bi-material electroformed object. Theoretically thermal convection should be taken into consideration, however, the thermal convection effect is negligible for solving this thermal stress problem because the thermal stresses generated by using convection thermal load are very close to the thermal stresses generated by directly employing the oven temperatures as the boundary condition. This is explained in Appendix A. Thus the first boundary condition is defined as that the temperature of the hot air is the same as the temperature of exterior surface of the object being burned, i.e.

$$T(p,t) = f(p,t) \quad (6.13)$$

where the point  $p$  is on the surface of the metal shell, and  $f(p, t)$  is the oven temperature function. There are six faces for a hexagonal element, so this makes six boundary conditions for the governing equation 6.4.

Assuming the metal shell is in perfect thermal contact with the RP part, the heat transfer at the bounding surface of the part and the metal shell is conduction dominated. So the temperature at the bounding surface of the RP part is the same as that at the metal shell surface. In addition, the heat flux leaving metal shell through the contact surface is equal to that entering the RP part. Thus for a point P on the contact surface of the metal and RP part, the boundary conditions are:

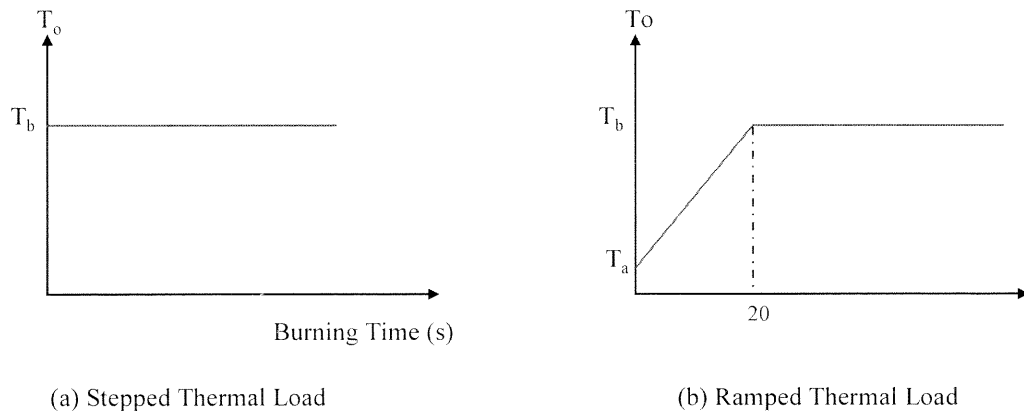
$$T_m(P, t) = T_r(P, t) \quad (6.14)$$

$$k_m \frac{\partial T_m}{\partial n}(P, t) = k_r \frac{\partial T_r}{\partial n}(P, t) \quad (6.15)$$

where subscripts  $m$  and  $r$  refer to the metal shell and RP material, respectively, and  $n$  is the normal of the contact surface at point  $P$ . These make six other boundary conditions at the bounding surface between the RP part and the metal shell. So we have the total of 12 boundary conditions and 2 initial conditions to solve the heat transfer governing equation.

#### 6.4.2 Structure Modeling of the Burnout Process

Structure modeling is used to determine the thermally-induced stress exerted on the metal shell. After the thermal analysis is performed, a structure analysis is made to compute the thermal stress exerted on the metal shell due to the expansion of the SL part. The loads



$T_b$ : Burnout temperature, 560°C for SL part.

$T_o$ : Oven temperature  $f(t)$ .

$T_a$ : Ambient temperature.

**Figure 6.6** Two scenarios of thermal loads

are the computed temperature fields in the previous thermal analysis. The problem is to determine the following fifteen parameters:

6 stress components:  $\sigma_x, \sigma_y, \sigma_z, \sigma_{xy}, \sigma_{yz}, \sigma_{zx}$

6 strain components:  $\varepsilon_x, \varepsilon_y, \varepsilon_z, \varepsilon_{xy}, \varepsilon_{yz}, \varepsilon_{zx}$

3 displacement components:  $u, v, w$

satisfying the following fifteen equations throughout the metal shell:

$$3 \text{ equilibrium equations: } \left. \begin{aligned} \frac{\partial \sigma_x}{\partial x} + \frac{\partial \sigma_{xy}}{\partial y} + \frac{\partial \sigma_{xz}}{\partial z} &= 0 \\ \frac{\partial \sigma_{xy}}{\partial x} + \frac{\partial \sigma_y}{\partial y} + \frac{\partial \sigma_{yz}}{\partial z} &= 0 \\ \frac{\partial \sigma_{xz}}{\partial x} + \frac{\partial \sigma_{yz}}{\partial y} + \frac{\partial \sigma_z}{\partial z} &= 0 \end{aligned} \right\} \quad (6.16)$$

$$6 \text{ stress-strain relations: } \left. \begin{aligned} \varepsilon_x &= \frac{1}{E} [\sigma_x - \nu(\sigma_y + \sigma_z)] + e \cdot \Delta T \\ \varepsilon_y &= \frac{1}{E} [\sigma_y - \nu(\sigma_x + \sigma_z)] + e \cdot \Delta T \\ \varepsilon_z &= \frac{1}{E} [\sigma_z - \nu(\sigma_y + \sigma_x)] + e \cdot \Delta T \\ \gamma_{xy} &= \frac{1}{2G} \sigma_{xy}; \gamma_{yz} = \frac{1}{2G} \sigma_{yz}; \gamma_{zx} = \frac{1}{2G} \sigma_{zx} \end{aligned} \right\} \quad (6.17)$$

where  $e$  is the coefficient of thermal expansion,  $\Delta T$  is the temperature rise. The shear modulus  $G$  relates to Young's modulus  $E$  and Poisson's ratio  $\nu$  by the equation:

$$G = \frac{E}{2(1+\nu)} \quad (6.18)$$

and

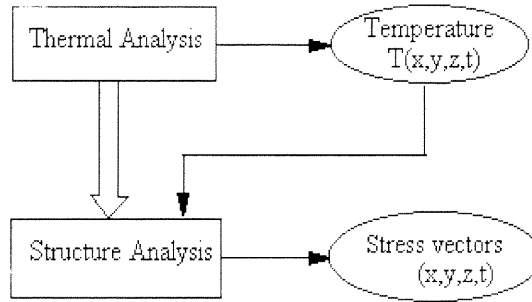
$$\left. \begin{aligned}
 &\varepsilon_x = \frac{\partial u}{\partial x}; \quad \varepsilon_y = \frac{\partial v}{\partial y}; \quad \varepsilon_z = \frac{\partial w}{\partial z} \\
 &\varepsilon_{xy} = \frac{1}{2}\gamma_{xy} = \frac{1}{2}\left(\frac{\partial v}{\partial x} + \frac{\partial u}{\partial y}\right) \\
 &\varepsilon_{yz} = \frac{1}{2}\gamma_{yz} = \frac{1}{2}\left(\frac{\partial w}{\partial y} + \frac{\partial v}{\partial z}\right) \\
 &\varepsilon_{zx} = \frac{1}{2}\gamma_{zx} = \frac{1}{2}\left(\frac{\partial u}{\partial z} + \frac{\partial w}{\partial x}\right)
 \end{aligned} \right\} \quad (6.19)$$

6 strain-displacement relations:

## 6.5 FEM Based Numerical Simulation

### 6.5.1 General

Analytical calculation of the previous thermal stress is extremely difficult. To solve this problem, finite element analysis (FEA) is used to simulate the thermal stress resulted from the burnout process. FEA solves each element through the body of the SL part and metal shell by employing the formulas 6.4 to 6.12 on each element. The simulation procedure can be structured as illustrated in Fig.6.7. The temperature field is first calculated and then it is used as the loads for structure analysis. The maximum thermal stress is compared with the yield strength of the metal shell to determine if the metal shell is yielded. If the thermal stress is larger than the yield stress, either the solid SL part is modified with a hollowed structure or electroform thickness is increased. Another analysis using the new model is performed. This process is repeated until the thermal stress is smaller than the yield strength of the metal. ANSYS 5.4 is the software for thermal stress analysis.



**Figure 6.7** Thermal stress analysis model

From material mechanics, the stress is related to the strains by:

$$\{\sigma\} = [D] \{\varepsilon^{el}\} \quad (6.20)$$

where  $\{\sigma\}$  is stress vector,  $[D]$  is elasticity matrix,  $\{\varepsilon^{el}\}$  equals  $\{\varepsilon\} - \{\varepsilon^{th}\}$ ,  $\{\varepsilon\}$  is total strain vector, and  $\{\varepsilon^{th}\}$  is thermal strain vector. The  $\{\varepsilon^{th}\}$  is:

$$\{\varepsilon^{th}\} = \Delta T [\alpha_x \alpha_y \alpha_z 0 0 0]^T \quad (6.21)$$

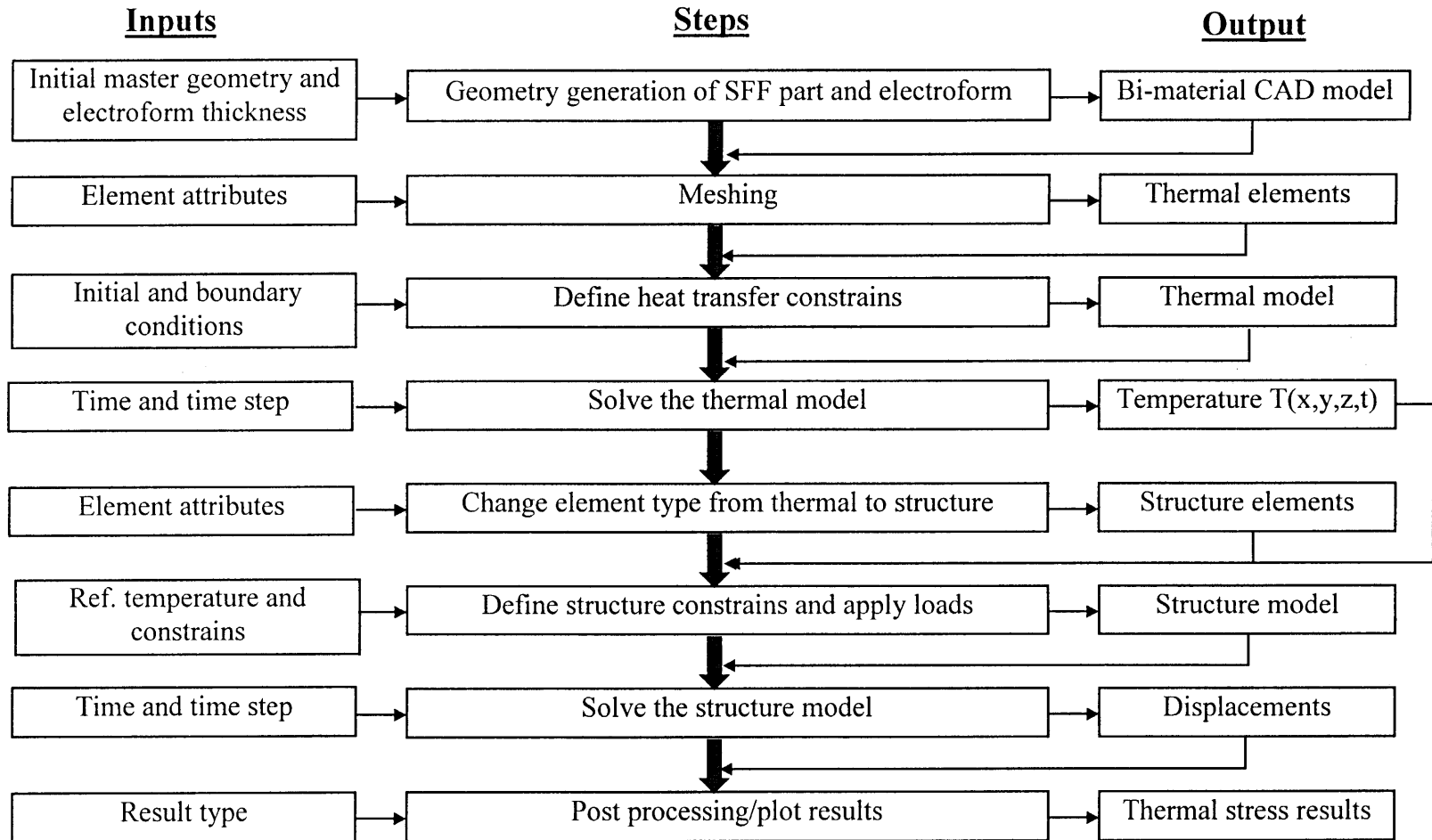
where  $\alpha$  is coefficient of thermal expansion,  $\Delta T$  is temperature rise which is obtained from the thermal analysis. In turn, the strain is related to the nodal displacements by

$$\{\varepsilon\} = [B] \{u\} \quad (6.22)$$

where  $[B]$  is strain-displacement matrix,  $\{u\}$  is nodal displacement vector. Therefore, ANSYS solves the equation 6.20 and the following equation:

$$\{\varepsilon^{el}\} = [B] \{u\} - \{\varepsilon^{th}\} \quad (6.23)$$

The criteria for evaluating the failure of the metal electroform is the maximum shearing stress theory, i.e.  $|\sigma_1 - \sigma_3| < \sigma_{yp}$ . The criteria for fracture of the SL part is the maximum principal stress theory, i.e.  $|\sigma_1| < \sigma_u$ .



**Figure 6.8** ANSYS-based thermal stress simulation model

### 6.5.2 FEM Based Simulation

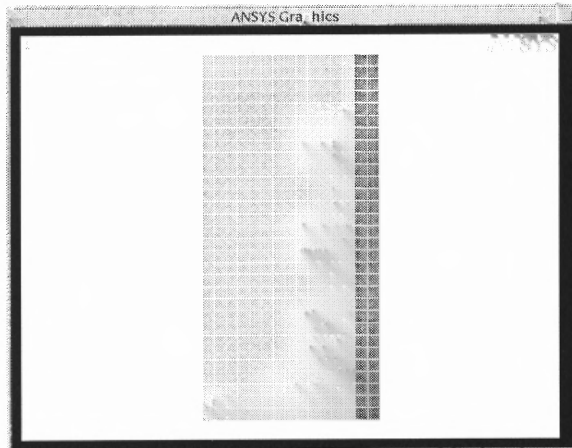
For analyzing thermal stress induced during the burnout process the FEM-package ANSYS 5.4 is used. The analysis of the thermal stress is carried out as shown in Fig.6.8. FEM modeling and analysis consists of three phases: preprocessing, solution, and postprocessing.

During the preprocessing phase, the analysis type, such as transient thermal and mechanical analysis for our case, and the material properties such as Young's modulus, density, coefficient of thermal expansion (CTE), thermal conductivity, etc, are first specified. Most of the properties are a function of temperature, and their values versus temperatures are established in a table. The geometry of the RP part is pre-designed during the mold design stage. For initial analysis, a solid RP part, termed initial RP part, is used to perform the analysis. The geometry of the solid part is directly imported from the CAD package or generated from the geometry modeling module of the ANSYS package. The metal electroform is then generated according to the initial electroforming thickness, normally 2 mm or determined by the mold strength or EDM machining requirements. The bimaterial volumes (or geometry) are herein generated. After the geometry has been created, the geometry model is then meshed. Meshing means creation of finite elements based on the bi-material model geometry. The element type is determined according to the complexity of the geometry of the model so that meshing of the model is possible. Certain correlation between thermal element type and structure element type exists for ANSYS, so the element type has to be suitable for both thermal and structure analysis. Element size is also an important factor for obtaining accurate analysis results. The larger the element size, the less accurate the analysis result.

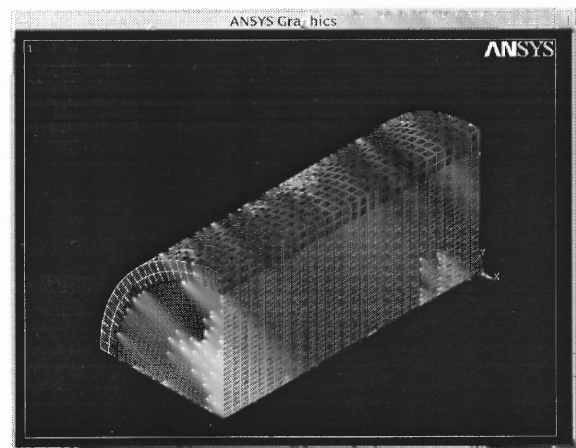
However, fine element size will generate huge nodes and elements that could exhaust the computer capability or take an extensively long time to solve the model. Generally speaking, when the element size reaches a certain value, the analysis difference between this element size and smaller size is ignorable. So convergence study is important to ensure accurate analysis result. During the meshing, the model is divided into nodes and elements to which material properties are assigned. Element type, element size and associated material properties with the element are referred to as element attributes.

The next phase is solution. The initial and boundary conditions, as stated in the thermal modeling section, are defined, and the finite element model for thermal analysis is complete. As thermal problems are transient, time steps have to be defined in order to enable computation of temperature distribution in the bi-material model at different time. After solving the thermal model, the temperature distribution is examined and it has to be reasonable. After the thermal analysis is finished and carefully examined, a structure analysis is made to ascertain the thermal stresses due to the thermal influence. For computing these thermal stresses the type of elements which comprise the finite element model has to be changed into a type that is appropriate for structure analysis. Computed temperatures in the thermal analysis are defined as load to the structure finite element model. Apart from temperatures, moving of the bi-material model is constrained, too. At each time step, the temperatures at that time step are loaded from the ANSYS database and applied to the structure model. Reference temperature is also provided for the solver to compute the thermal expansion (displacement) from which the thermal stresses are derived.

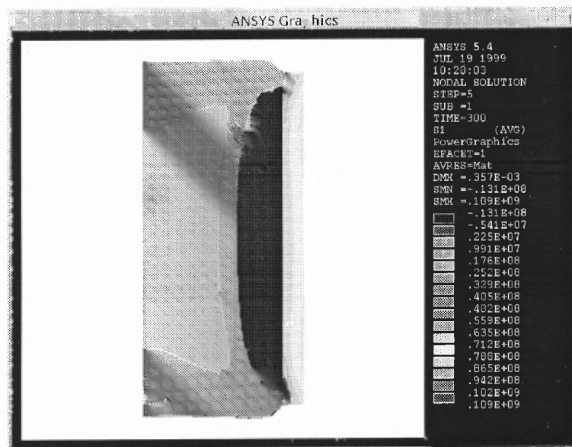




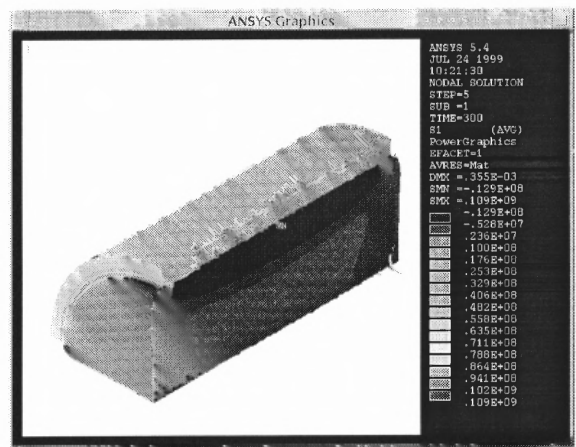
(a) Meshed two dimensional model with element type PALEN55-PLANE42, element size 2 mm.



(b) Meshed three dimensional model with element type SOLID70-SOLID45, element size 2 mm.



(c) First principal stress simulation for model (a).



(d) First principal stress simulation for model (b).

**Figure 6.9** Comparison of meshes and thermal stresses for two and three dimensional models

The postprocessing phase of the ANSYS follows the preprocessing and solution phases. In this phase the calculated results are shown in graphics display and/or tabular report form. The principal stresses are mainly concerned in this study, so the principal stresses are displayed and recorded to evaluate if the thermal stress is smaller than the yield strength of the electroform.

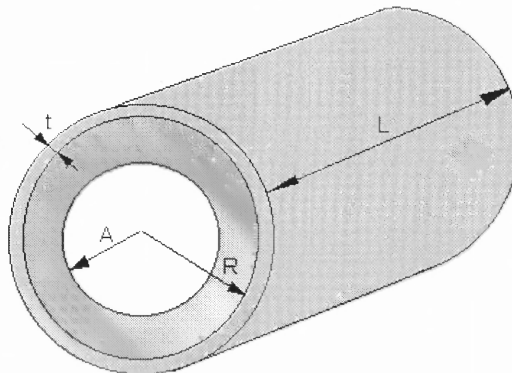
### 6.5.3 Convergence Study

Element size is an important factor for determining if accurate analysis results can be obtained. The larger the element size, the less nodes and elements are generated that lead to less accurate results for the analysis. The finer the element size, the more nodes and elements are generated that could exhausts the computer capacity or take a extensive time to solve the model. When the element size reaches a certain value, the analysis result converges to the actual value with minor variation. To achieve accurate results, poor element size have to be avoided. For the convergence study of the finite element analysis, a 4 mm thick of nickel electroplated solid cylinder SL part with dimensions of  $\phi 50 \times 60$  mm with element size of 1 mm, 2 mm, 3 mm and 4 mm using two and three dimensional models have been carefully examined and the results are listed in Table 6.9. The thermal load is ramped thermal load, as shown in Fig.6.6(b). For two-dimensional case, PLANE55 with four nodes and a single degree of freedom, temperature, at each node is used for thermal element type and its corresponding structural element type is PLANE42 with two degree of freedom, displacements in x and y direction, at each node. For the three-dimensional case, the element type SOLID70, an eight nodes with a single degree of freedom, temperature, at each node, is used for thermal element and its corresponding structure element type is SOLID45 with three degree of freedom, displacement at x, y and z direction. When element size equals to 1 mm for a three dimensional model, ANSYS generates 79320 elements that is beyond the constrain of the ANSYS 5.4 University High Version so no result is given. Meshes generated using 2 mm element size for two and three dimensional models are illustrated in Fig.6.9(a) and Fig.6.9(b), respectively. The corresponding thermal stress simulation results are shown in Fig.6.9(c)

and Fig.6.9(d), respectively. The convergence study indicates that when element size equals to or smaller than 2 mm, the maximum thermal stress converges no matter using two or three dimensional model. In the following analysis, we use 2 mm element size, PLANE55-PLANE42 as element type for two dimensional thermal stress model, and SOLID70-SOLID45 as element type for three dimensional thermal stress model.

**Table 6.9** Convergence of thermal stress with different element type, size and models

Element size (mm)	4		3		2		1	
	2D	3D	2D	3D	2D	3D	2D	3D
Model type	2D	3D	2D	3D	2D	3D	2D	3D
Elements	120	1800	220	4480	450	14400	1740	79320
First principal stress (Mpa)	127	124	120	118	109	109	108	N/A



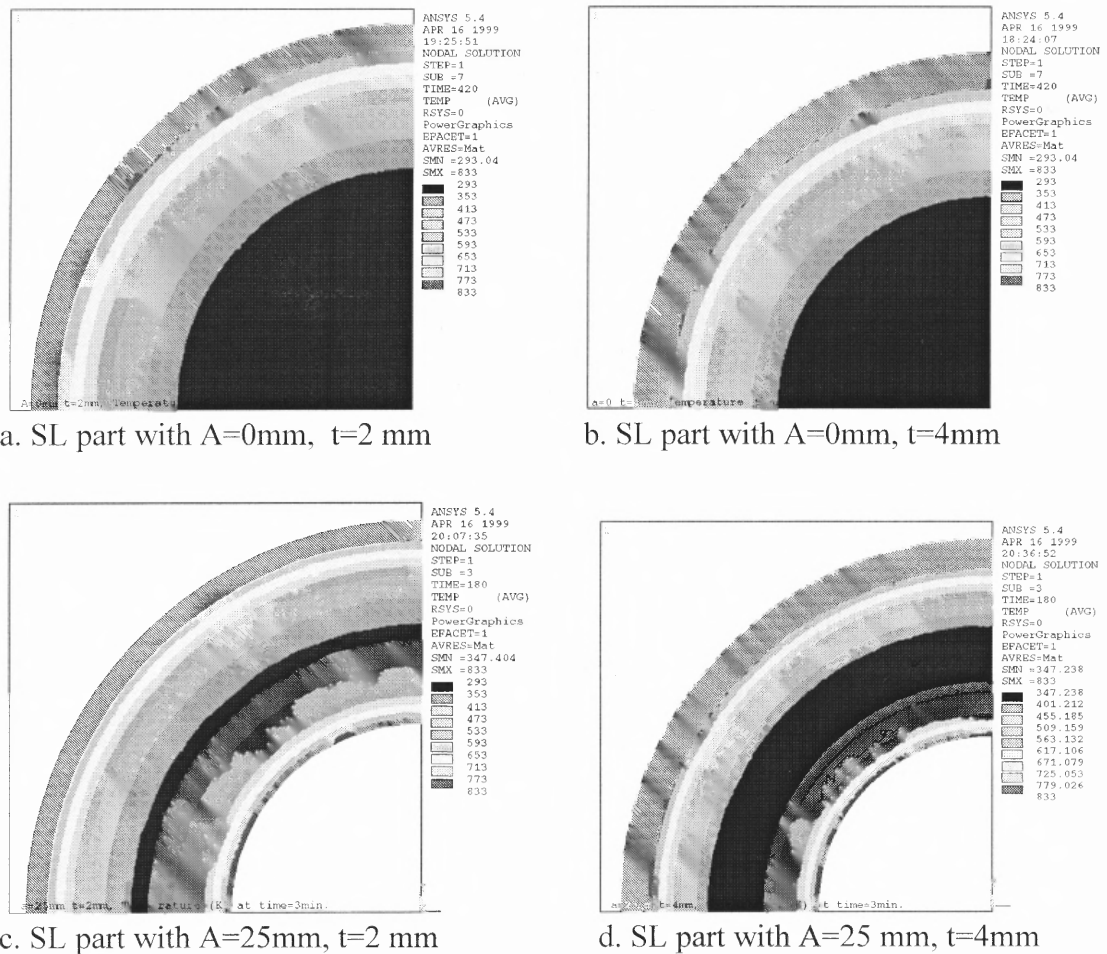
Oven temperature = 560 °C  
 R=50 mm, L=100mm  
 A and t are variables

**Figure 6.10** Two dimensional case: nickel electroformed SL cylinder

## 6.6 Simulation Results and Discussion

### 6.6.1 Thermal Stress Simulation for a Two-Dimensional Case

A nickel electroformed SL cylinder with outer radius of 50 mm and length of 100 mm, as shown in Fig 6.10 is used as a case to perform a two dimensional thermal stress analysis. The dimension A of the inner hole of the cylinder and the electroform thickness t are variables. The thermal stress is analyzed using the thermomechanical model. We assume that the oven is preheated to the burnout temperature (560 °C for SL 5170) and it is



**Figure 6.11** Temperature distribution for the two dimensional models with different SL parts and electroform thickness

constant during the burning process. Element type PLANE55 and element size 1mm is used to simulate the thermal stress resulted from the burnout of the SL cylinder.

Figure 6.11 shows the temperature distributions for different SL parts and electroforming thickness. For solid SL parts, heat can only be transferred from the outer surface to the inside of the bimaterial model. However, heat is transferred not only from the outer surface of the model but also from the surface of the inner hole for hollow SL parts. As a result, it takes 420 seconds for the model with solid SL parts to reach the temperature distribution under which the maximum first principal stress  $\sigma_1$  is reached inside the model and it takes 180 seconds for the model with hollowed SL parts to reach the maximum first principal stress. Figure 6.12a, 6.12b, 6.12c and 6.12d illustrate the first principal stress simulations with the temperature distributions as shown in Fig.6.11a, 6.11b, 6.11c and 6.11d, respectively. For solid SL parts, when electroform thickness increases from 2 mm to 4 mm, the maximum  $\sigma_1$  decreases from 144 MPa to 81.3 Mpa (see Fig.6.12a and Fig.6.12b. If the SL part is built with a inner hole of 25 mm radius, compared with solid SL part the maximum  $\sigma_1$  with 2 mm electroform thickness reduces from 144 MPa to 119 Mpa (see Fig.6.12a and Fig.6.12c), and that with 4 mm electroform thickness reduces from 81.3 MPa to 66.5 Mpa (see Fig.6.12b and Fig.6.12d). Fig.6.13 illustrates that with the same structure of SL part, the maximum thermal stress ( $\sigma_1$ - $\sigma_3$ ) decreases when the electroform thickness increases. The yield strength of the nickel electroform is also illustrated in Fig.6.13. The thermal stress above the yield strength results in permanent deformation for the nickel electroform. The thermal stress below the yield strength will not generate permanent deformation for the electroform. Inner hole can always decrease the thermal stress, and the larger the hole, the smaller the thermal

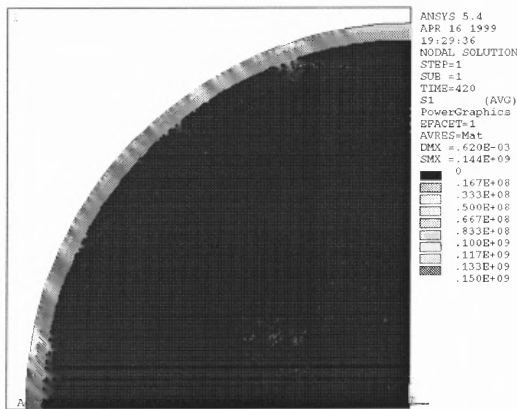
stress. This observation gives certain guidance for building RP parts for electroforming: The thermal stress induced by the burnout process can be reduced when a RP part is built with a uniform wall thickness so that the RP part is an inner hollow structure. The structure needs to be strong enough to resist the electroforming stress which is determined by the electroforming process parameters. In this case if the electroforming stress exerted on the electroformed nickel shell is 10 MPa, the deformation caused by the electroforming stress can be calculated and is listed in Table 6.10. From the table, we can see that for a specified electroforming thickness, solid SL part always has smaller electroforming deformation (ED). As the wall thickness decreases, the ED increases. Fig.6.14 shows that the maximum thermal stress is a function of burning time. At a certain time point, a specific model will reach its maximum thermal stress and at that point the model experiences maximum thermal deformation: when  $|\sigma_1 - \sigma_3| > \sigma_{yp}$ , it is a mixture of thermoplastic and thermoelastic deformation, and when  $|\sigma_1 - \sigma_3| < \sigma_{yp}$ , it is only thermoelastic deformation. Table 6.11 lists the build time and material costs for different SL parts. It can be seen that the inner hollow structure can save build time and materials.

**Table 6.10** Electroforming deformation (ED) for different sets of parameters A and t

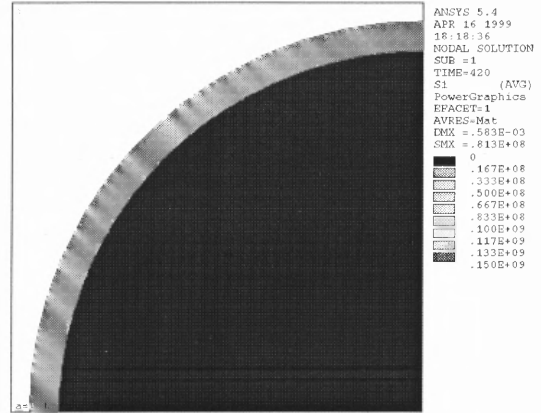
	t =1 mm	t =2 mm	t =3 mm	t =4 mm	t =5 mm	t =6 mm
A=0 mm	0.0024	0.0046	0.0067	0.0078	0.0109	0.0128
A=25 mm	0.0042	0.0085	0.0142	0.0187	0.0231	0.0275
A=35 mm	0.0096	0.0194	0.0282	0.0372	0.0461	0.0547

**Table 6.11** Comparison of build time and material cost for different SL parts

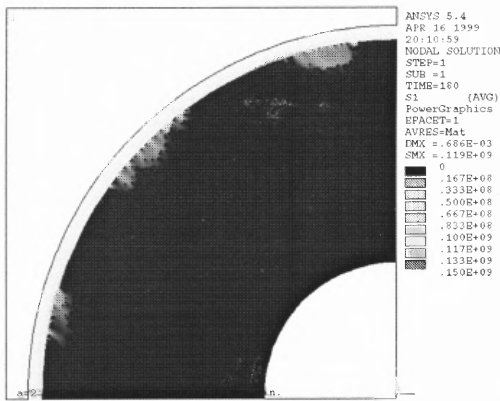
	Build Time (Hour)	SL 5170 Material Cost (USD)
Solid	35.27	161.63
A=25mm	26.46	121.25
A=35mm	17.98	82.43



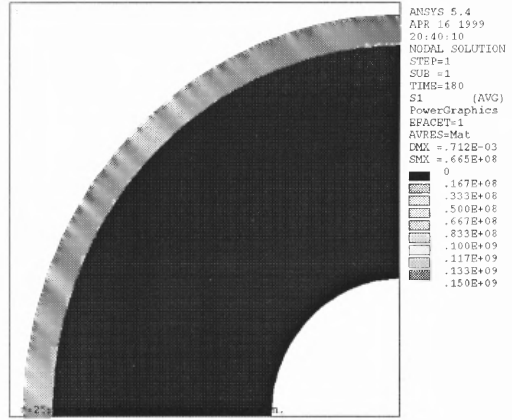
a. SL part with A=0mm, t=2 mm



b. SL part with A=0mm, t=4mm



c. SL part with A=25mm, t=2 mm



d. SL part with A=25 mm, t=4mm

**Figure 6.12** Two dimensional simulation of thermal stresses with different SL parts and electroform thickness

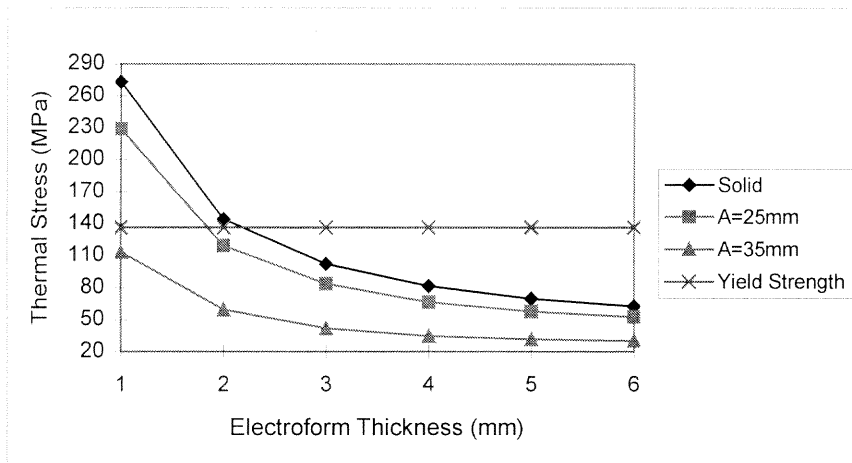


Figure 6.13 Maximum thermal stress vs. electroform thickness for burnout process

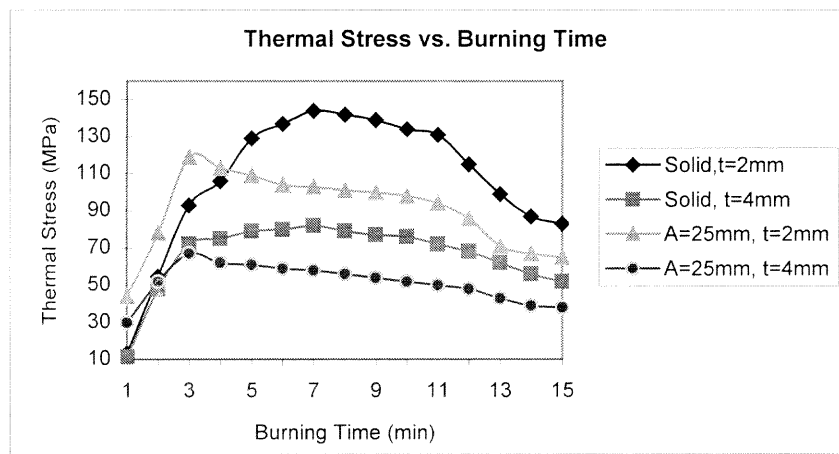
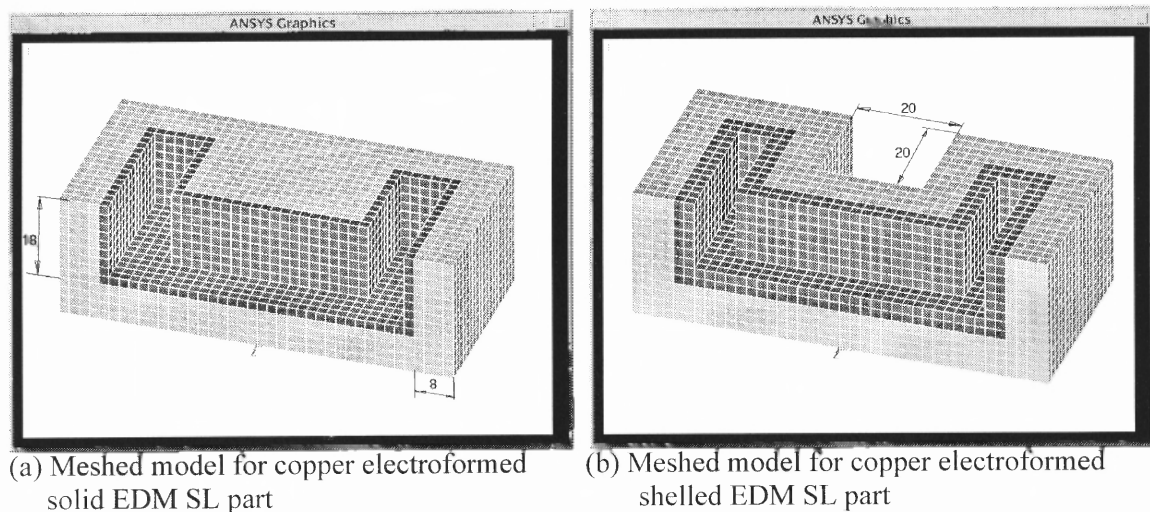


Figure 6.14 Maximum thermal stress vs. time during burnout process

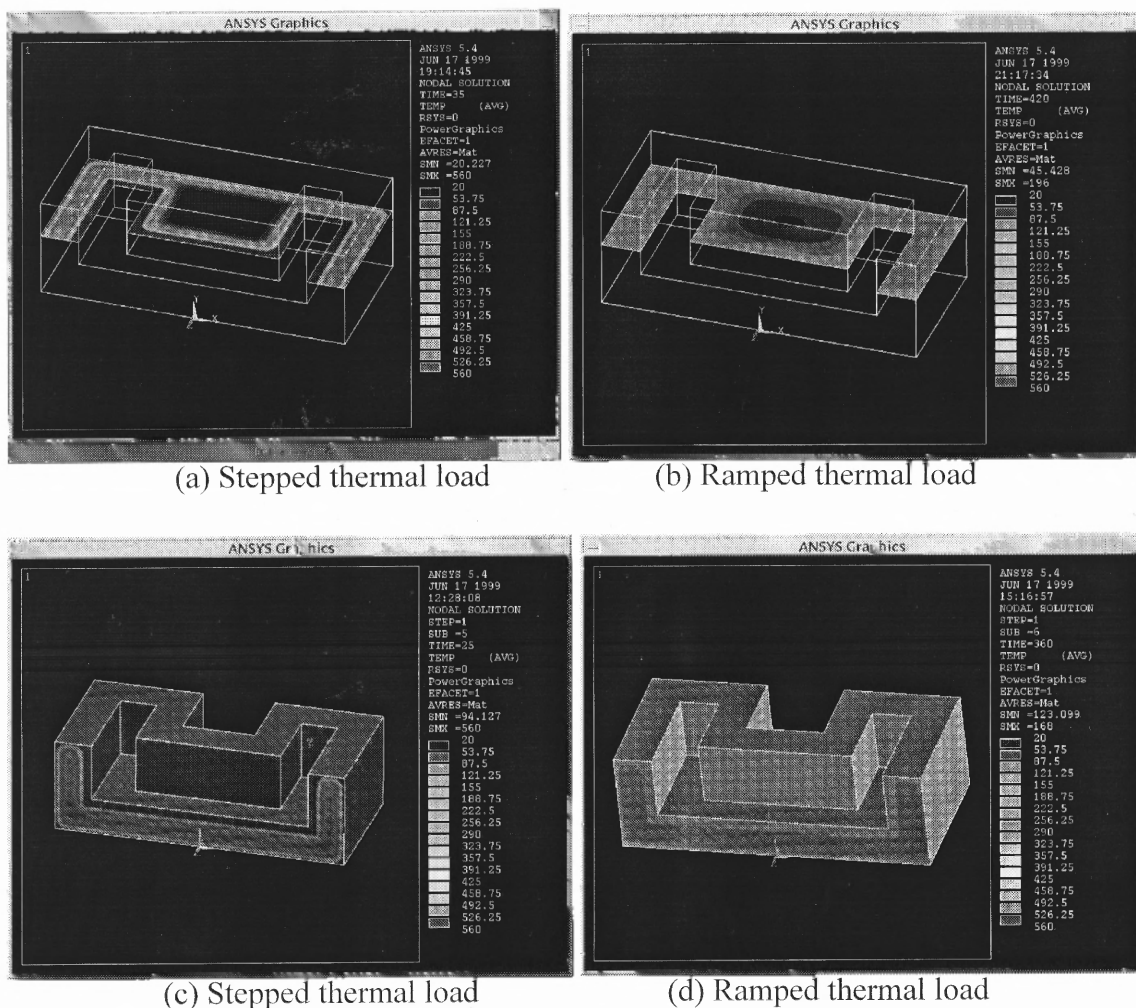


### 6.6.2 Thermal Stress Simulation for an EDM Electrode

The established thermomechanical model is applied to simulate the thermal stress induced during the burnout process for EDM electrodes. The samples are from the case study of Section 5.2.3 where practical EDM electrodes were made but the thermal stresses are simulated here. In order to compare the thermal stresses between different structures of the SFF parts, two kinds of SL parts are used in this analysis. One is the solid SL parts, as shown in Fig.6.15a and the second kind is the shelled SL parts as shown in Fig.6.15b. The dimensions for the working surfaces, i.e., the surfaces used for forming the EDM electrode, are same with the dimensions as the CAD model for the EDM electrode. The difference between the solid SL part and shelled SL part is that the shelled SL part is made by cutting a brick from the solid SL part so that the thickness of the shelled SL part is 8 mm.

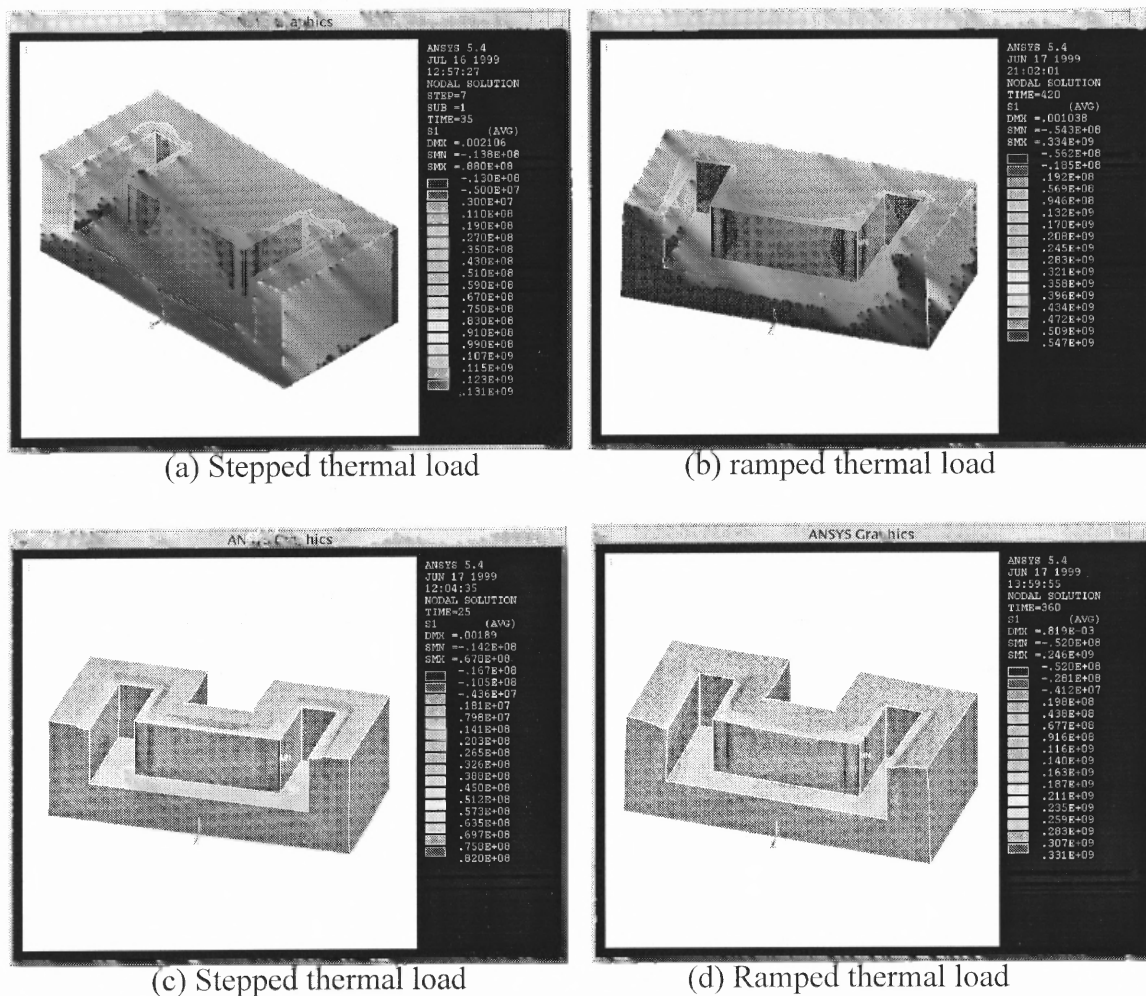


**Figure 6.15** Meshed models for EDM electrodes



**Figure 6.16** Heat transfer simulation for solid and shelled SL parts with 2 mm thick of copper electroform

The model is meshed using element size 2 mm for both thermal and structure elements. Element type SOLID70 is used for thermal element while element type SOLID42 is used for structure element. The meshes generated for the model of solid SL part with 2 mm thick of copper electroform and the model of shelled SL part with 4 mm thick of copper electroform are shown in Fig.6.15a and Fig.6.15b, respectively. Two scenarios of thermal loads (see Fig.6.6) are used for this sets of analysis. Solid and



**Figure 6.17** First Principal Thermal stress simulation for solid and shelled SL parts With 2 mm thick of copper electroform

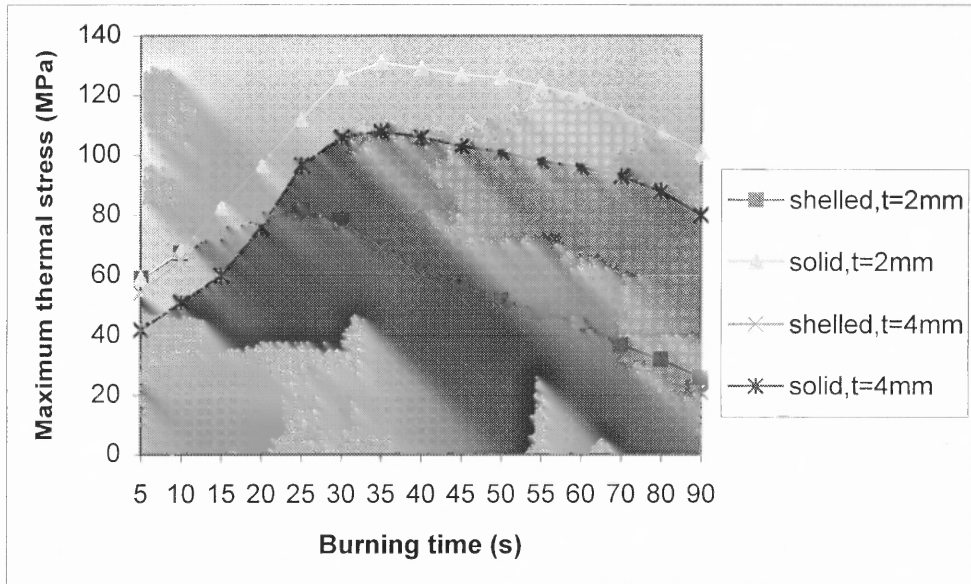
shelled SL parts are electroformed with 2 mm and 4 mm thick of copper, respectively, so that four analysis for each scenario of thermal load are performed.

Figure 6.16 illustrates heat transfer simulation results for solid and shelled SL parts with 2 mm thick of copper electroform under stepped and ramped thermal load. The figures show that the difference for stepped thermal load between maximum temperature and minimum temperature is much larger than the difference for ramped thermal load.

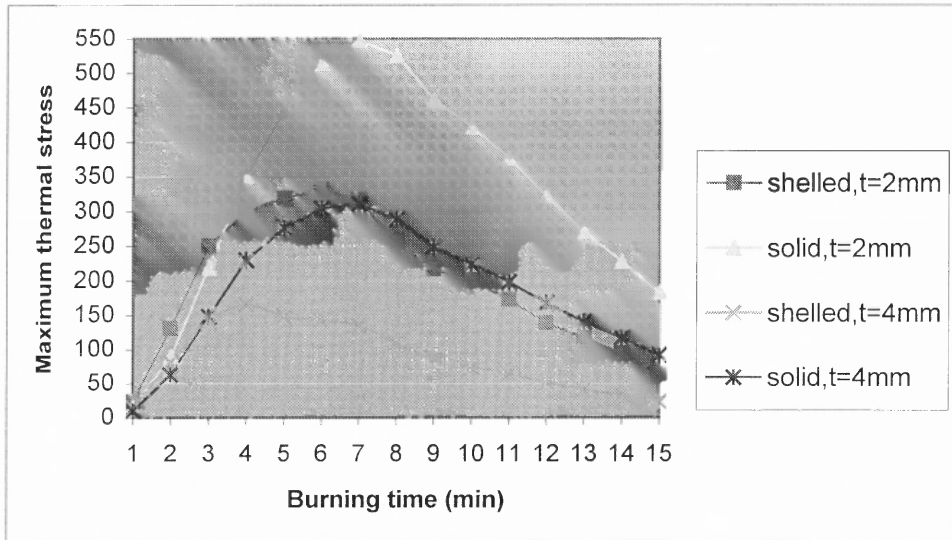
For solid SL parts, the maximum first principal stress within the model reaches its highest point at 35 seconds and 420 seconds for stepped thermal load and ramped thermal load, respectively. And, for shelled SL parts, the corresponding burning time for reaching the highest first principal thermal stresses are 25 seconds and 360 seconds for stepped thermal load and ramped thermal load, respectively. Thermal stresses induced by the corresponding temperature distribution shown in Fig.6.16 are shown in Fig.6.17. Under stepped thermal load and 2 mm thick of copper electroform, the maximum first principal stress reduces from 131 MPa occurring at 35 seconds for solid SL part (see Fig.6.17a) to 82 MPa that happens at 25 seconds for shelled SL part (see Fig.6.17c). In the case study performed in Section 5.2.3, the SL parts are burnout using stepped thermal load. It is noticed that the maximum stresses generated at the portion where dimensions I and J are measured and the largest deviation occurred (refer to Fig.5.2.a and Table 5.4). At these portions, the thermal stresses ( $\sigma_1 - \sigma_3$ ) for 2 mm thick of copper electroform are larger than the yield strength of the electroformed copper that is 110 MPa at the temperature of 560°C, while the thermal stresses for 4 mm thick of copper electroform are about the amount of the yield strength. This explains why dimensional deviation at these portions for 2 mm thick of copper electroform is 0.26% while that for 4 mm thick of copper electroform is 0.14%. However, the thermal stresses for other parts of the electroform are smaller than the yield strength of the copper electroform so the dimensional deviation at those parts are relatively smaller. Under ramped thermal load and 2 mm thick of copper electroform, the maximum first principal stress that happens at 420 seconds for solid SL part, reduces from 547 MPa (see Fig.6.17b) to 331 MPa that happens at 360 seconds for shelled SL part (see Fig.6.17d). For the ramped thermal load, the temperatures of the

furnace are 209 °C and 182 °C for burning time 420 seconds and 360 seconds, respectively. However, the lowest temperatures inside the two models are 45 °C and 123 °C, respectively. These figures demonstrate that the distribution of temperatures determinately affects the amount of thermal stresses. The thermal stresses generated due to ramped thermal load are much larger than that generated due to stepped thermal load.

The maximum thermal stress generated during the burnout process is also a function of time, i.e. it is actually a function of temperature distribution inside the model because the temperature distribution is a function of burning time. Figure 6.18 and Fig.6.19 show the maximum thermal stresses ( $\sigma_1 - \sigma_3$ ) changes over time for stepped and ramped thermal loads, respectively. The curve for maximum thermal stress over time is first gradually increases to a summit point and then the thermal stress gradually decreases. Different structures of SL parts generate different maximum thermal stresses, and SL parts with shelled structure can always reduce the thermal stress. The thinner the shell thickness, the smaller the thermal stress. This demonstrates that thermal stress induced by the burnout process can be reduced when an SL part is built with appropriate design of its structure. The shell structure needs to be strong enough to resist the electroforming stress, which is determined by electroforming process parameters. Assume that the electroforming stress exerted on the electroformed nickel shell is 1 MPa, the deformation caused by the electroforming stress would be 0.0018 mm and 0.0024 mm for solid and shelled SL masters, respectively. Table 6.12 lists the build time and material costs for solid and shelled SL parts. It shows that SL parts built with shelled structure can save build time and materials.



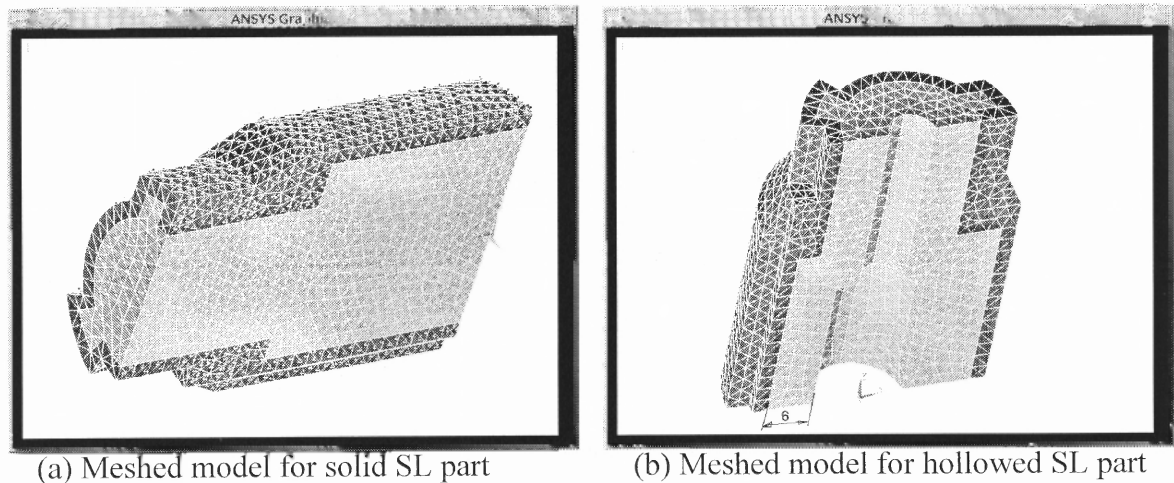
**Figure 6.18** Maximum thermal stresses vs. burning time under stepped thermal load for EDM electrodes



**Figure 6.19** Maximum thermal stresses vs. burning time under ramped thermal load for EDM electrodes

**Table 6.12** Comparison of build time and material cost for different SL parts

	Build Time (hour)	SL 5170 Material Cost
Solid	5.8	\$ 20.53
Shelled	4.6	\$ 17.48



**Figure 6.20** Meshed models for molds with 2 mm thick of nickel electroform

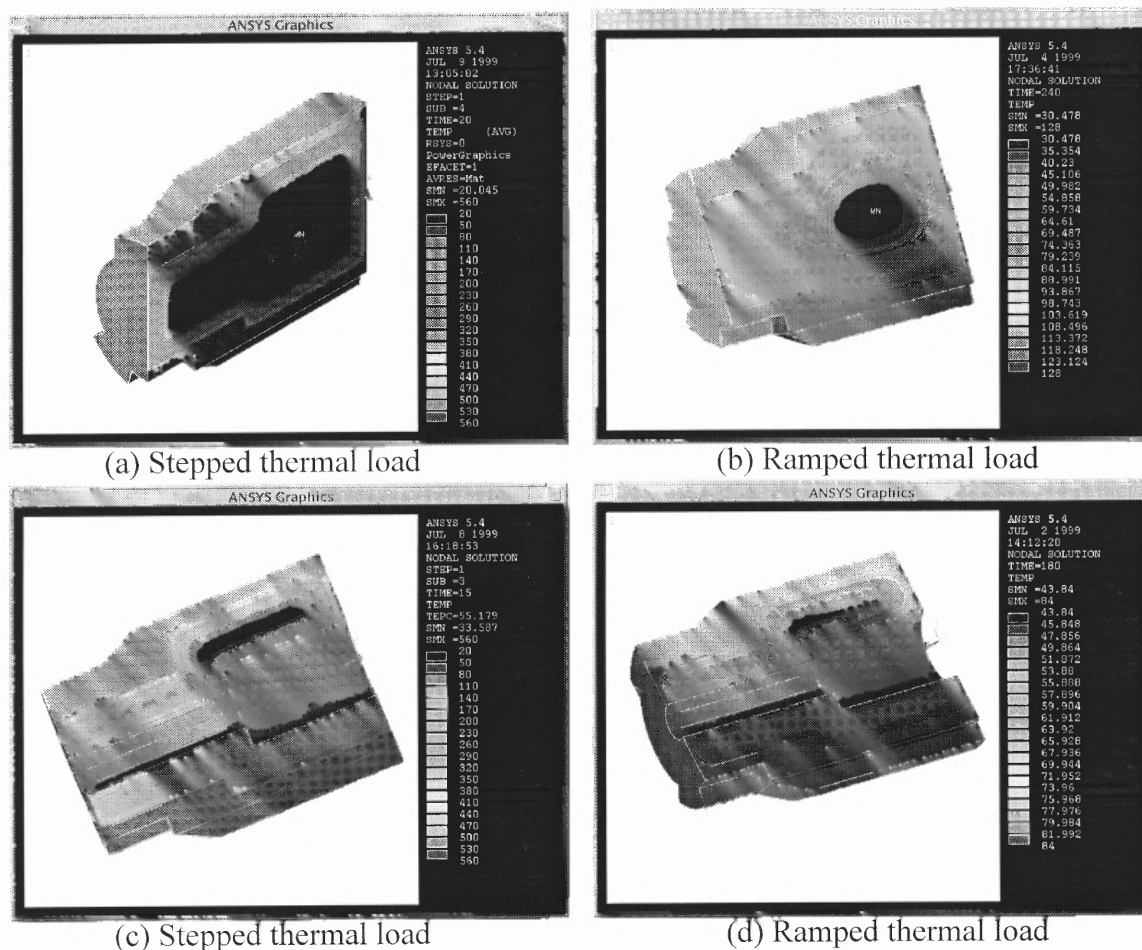
### 6.6.3 Thermal Stress Simulation for a Mold

The mold cavities generated using the mold tooling process are described in Section 5.3. These mold cavities are adopted for performing the thermal stress analysis. The dimensions for the working surface are same with the dimensions of the CAD model for building the SL parts. Solid and hollowed SL parts and two scenarios of thermal load, namely stepped and ramped thermal load, are used to perform the analysis. The wall thickness for hollowed SL part is about 6 mm. Total of eight analysis, four analysis for stepped thermal load and four for ramped thermal load, are performed.

Although element type SOLID70-SOLID45, a regular brick element for thermal-structural analysis, can produce very accurate results, but they are difficult to mesh solid with irregular geometries. The geometry of the nickel electroformed SL part for mold is too complex to be meshed by SOLID70 element, so element type SOLID87, a 3-D 10-node tetrahedral thermal solid, is used to mesh the bimaterial model to generate thermal element. Its corresponding structural element type, SOLID92, is used as the structural

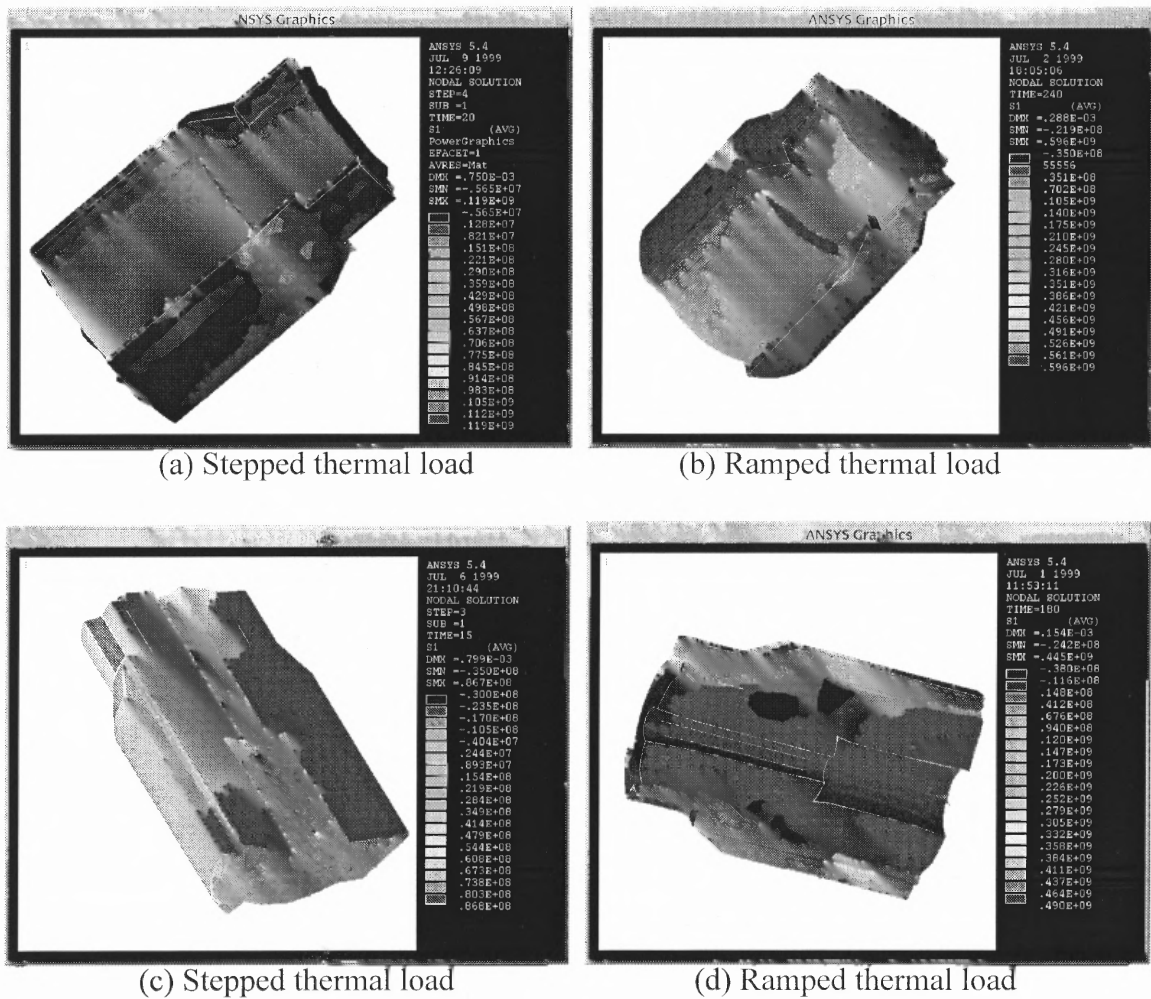
element. The element size is 2 mm. Meshes generated for solid SL part and hollowed SL part with 2 mm thick of nickel electroform are shown in Fig.6.20a and Fig.6.20b, respectively.

Figure 6.21 shows the heat transfer simulation for solid and hollowed SL parts with 2 mm thick of nickel electroform when the bimaterial model is burnt. Under stepped thermal load, it takes 20 seconds for the model with solid SL part to reach the temperature distribution, with maximum temperature of 560°C and minimum temperature



**Figure 6.21** Heat transfer simulation for solid and hollowed SL part with 2 mm thick of nickel electroform for mold tooling





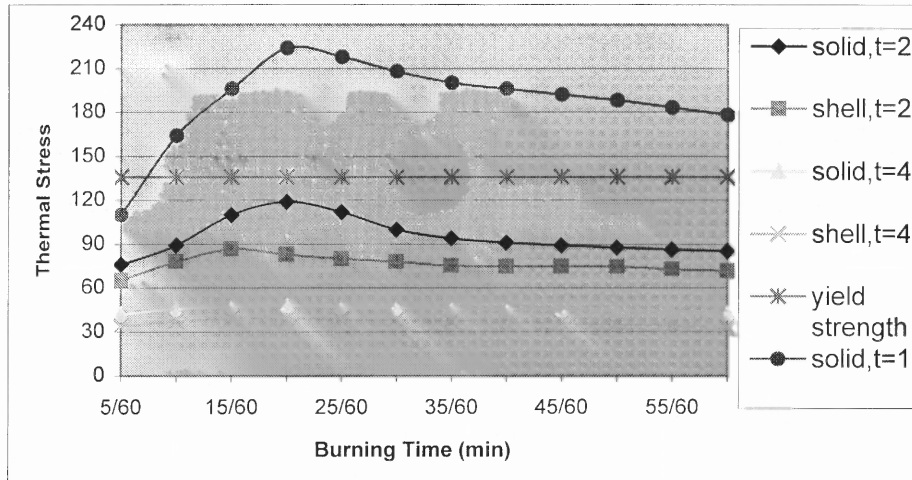
**Figure 6.22** First principal stress simulation for solid and hollowed SL parts with 2 mm thick of nickel electroform

of 20 °C, that generates maximum thermal stress and it takes 15 seconds for model with hollowed SL part to reach the temperature distribution, with maximum temperature of 560 °C and minimum temperature of 34 °C, that generates maximum thermal stress during the burnout process. Under ramped thermal load, it takes 240 seconds for the model with solid SL part to reach the temperature distribution, with maximum temperature of 128 °C and minimum temperature of 30 °C, that generates maximum

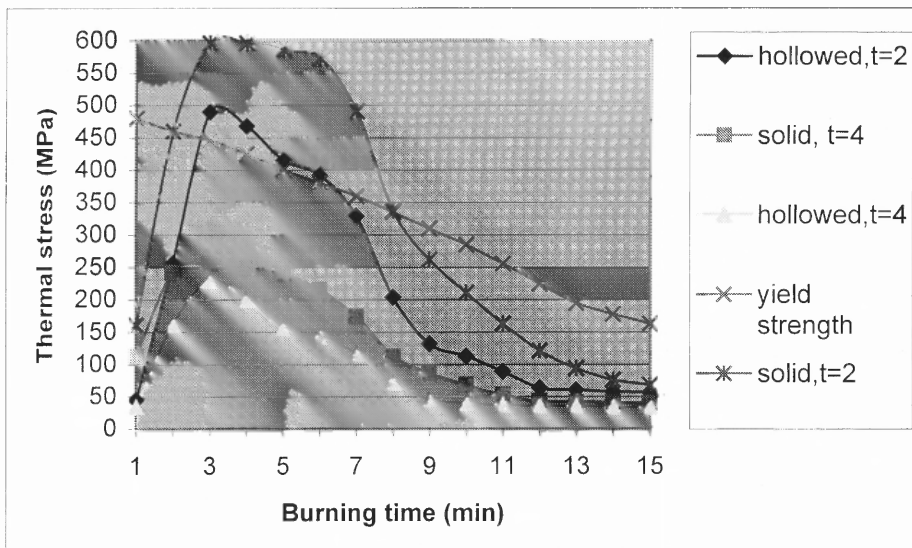
thermal stress and it takes 180 seconds for model with hollowed SL part to reach the temperature distribution, with maximum temperature of 84 °C and minimum temperature of 44 °C, that generates maximum thermal stress during the burnout process. First principal stresses induced by the corresponding temperature distributions shown in Fig.6.21 are shown in Fig.6.22. Under stepped thermal load, the maximum first principal stress reduces from 119 MPa that takes place at 20 seconds for solid SL part (see Fig.6.22a) to 86.7 MPa that takes place at 15 seconds for hollowed SL part (see Fig.6.22c). Under ramped thermal load, the maximum first principal stress reduces from 596 MPa that takes place at 240 seconds for solid SL part (see Fig.6.22b) to 445 MPa that takes place at 180 seconds for hollowed SL part (see Fig.6.22d). These figures demonstrate that built-in hollow structure inside the SL part can dramatically reduce the maximum thermal stress when the electroformed part is burnt. Also the temperature distribution is critical for determining the amount of the thermal stress. Ramped thermal load always generates much larger thermal stress than stepped thermal load.

Figure 6.23 and Fig.6.24 show that the maximum thermal stresses generated for the nickel electroform are a function of burning time for stepped thermal load and ramped thermal load, respectively. The model with hollowed SL part always generates smaller thermal stress compared with the model with solid SL part. This demonstrates that thermal stress induced during the burnout process can be reduced by design an appropriate hollow structure inside the SFF part. The hollowed SFF part needs to be strong enough to resist the deformation resulted from the electroforming stress that is normally generated during the deposition of nickel onto the SFF part. Assume that the electroforming stress exerted on the SL part was 5MPa, the deformation caused by the

stress would be 0.0008 mm and 0.0021 mm for solid and hollowed SL parts, respectively. Inner hollow structure not only can reduce thermal stress, it can also save material and build time.



**Figure 6.23** Thermal stress generated on nickel electroform vs. burning time for stepped thermal load for mold



**Figure 6.24** Thermal stress generated on nickel electroform vs. burning time for ramped thermal load for mold

#### 6.6.4 Discussion of Non-uniform Electroform Thickness

In the previous analysis, the electroform is uniformly distributed over the surface of the RP pattern. However, it is very difficult to produce a uniform electroform over the RP pattern due to the non-uniformity in the distribution of the current density between the anode and the cathode (workpiece) [Spiro, 1968; Yang and Leu, 1999b]. The areas of the RP pattern which are closer to the anode have higher current density so more metal is plated onto these protruding areas of the master than onto the recesses. The faster deposition in these areas consequently increases the current density and thus makes the deposition rate in these areas higher and higher, and likewise the deposition rate in the recess areas lower and lower. The uneven distribution of current density results in uneven distribution of the electroform.

Practically, when we say that 2 mm thick of electroform means that the minimum thickness of the electroform is 2 mm. This is also true for other electroforming thickness. The minimum thickness is termed nominal thickness. The average thickness of the electroform is always larger than the nominal thickness if no conformal anode is used for electroforming process. The nominal thickness is used in our analysis and supposed to be uniform throughout the model. If the metal shell was modeled in its real thickness distribution, the metal shell would be non-uniform with the minimum thickness being equal to the nominal thickness. Due to the fact that some areas of the electroform would have larger thickness than that used in our analysis, the thermal stresses obtained in the previous analysis should be larger than the stresses obtained using non-uniform electroform for the real situation. This means that the thermal stresses obtained using uniform nominal thickness are reliable and at the safe side for failure evaluation.

Conforming the shape of the anode to the shape of the workpiece to be electroformed can provide a uniform distribution of current density, thus the metal can be deposited onto the workpiece more uniformly. However, making of a conformal anode by machining is expensive and time consuming. Yang and Leu [1999b] proposed a method for making conformal anode by electroless plating of an RP part that has the inverse shape of the workpiece to be electroformed. The anode can be generated by the CAD system using the geometrical data of the RP pattern. The conforming anode enables the distribution of metal in the electroform more uniform (and thus resulting in smaller variation in the electroform thickness).

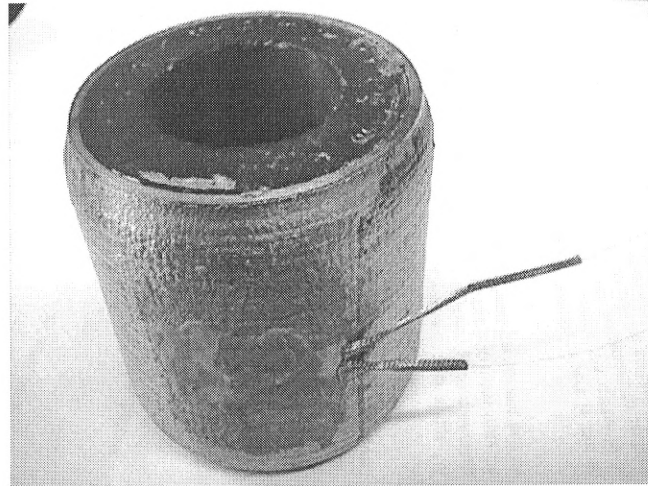
## 6.7 Experimental Verification

### 6.7.1 Sample Preparation

In order to verify that the thermomechanical model and the ANSYS based finite element analysis reflect the real situation for burnout process, an experiment has been performed



**Figure 6.25** Strain gage on a nickel electroform with solid SL part



**Figure 6.26** Strain gage on a nickel electroform with hollow SL part

using strain gage based thermal stress measurement approach. The SL parts used for thermal stress experiment are cylinders. The dimension, cost for SL parts and electroforming are listed in Table 6.13.

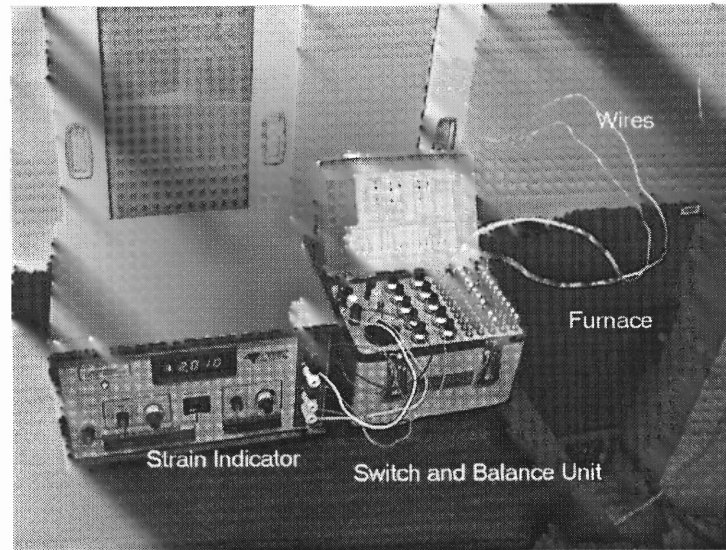
The strain gage is mounted on the outer surface of the electroformed nickel shell. The position for bounding strain gage is accurately matched with the position where the analytical thermal stress is queried so that the measured stress can be comparable with the stress obtained by the analysis. The strain gage is mounted at the center position along the circumferential direction of the cylinder. Figure 6.25 and Fig.6.26 illustrate that the strain gages are attached to the 4 mm thick nickel shell with solid and hollowed SL patterns, respectively.

**Table 6.13** Samples for experimental verification

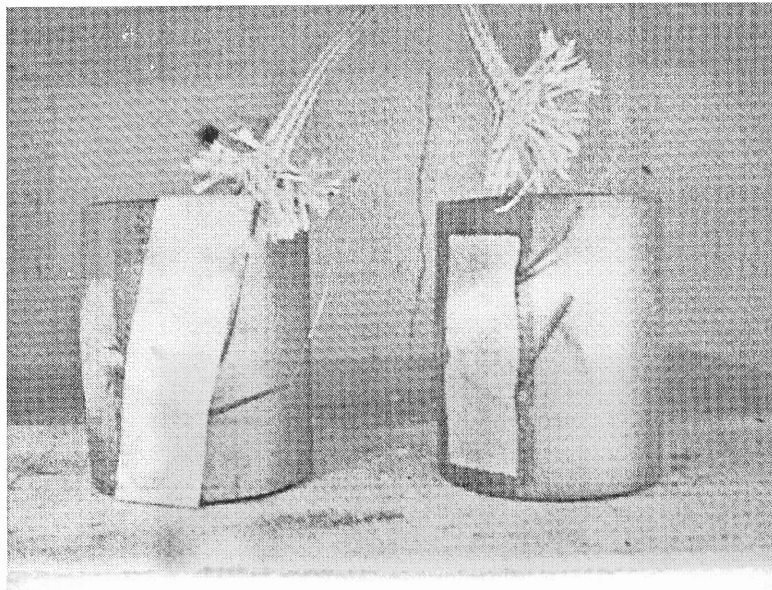
Electroform thickness	Φ50X60 solid cylinder		Φ50X60 cylinder with Φ30 hole	
	SL part cost	Electroforming cost	SL part cost	Electroforming cost
1 mm	\$265 each	\$194	\$ 214 each	\$244
2 mm	\$265 each	\$203	\$ 214 each	\$254
4 mm	\$265 each	\$212	\$ 214 each	\$262

### 6.7.2 Experiment Environment

The thermal stress induced during the burnout of the SL master is measured using strain gage instrument. The measuring environment (see Fig.6.27) consists of programmable furnace with a small hole on top, strain indicator, switch and balance unit, strain gage and wires. The hole at the top of the furnace is used to pass the wires through out of the furnace. Fig.6.28 illustrates that two wire samples are put into the furnace with lead wires pass through the top hole. The furnace is a programmable, fully automatic electrical furnace with wide range of controllable temperatures. The strain gage can stand temperature from room to 600 °C. Because it is very difficult to wire up the sample under high temperature, namely 560°C, only the ramped thermal load is tested.

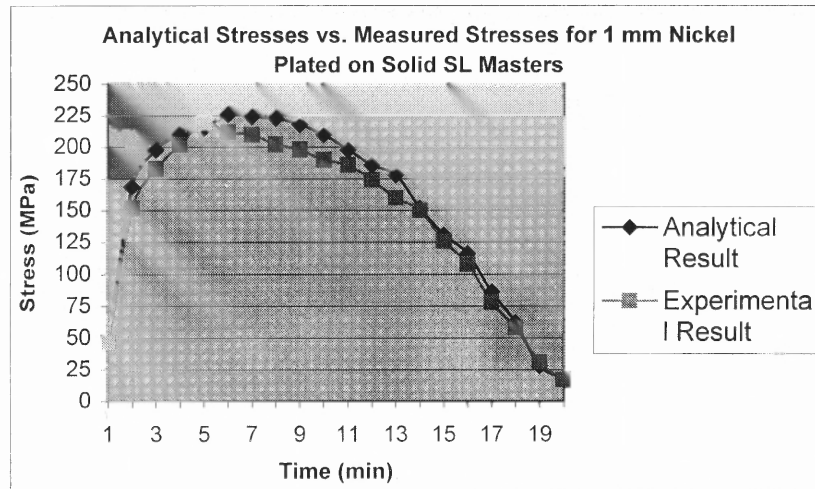


**Figure 6.27** Thermal Stress measuring Environment

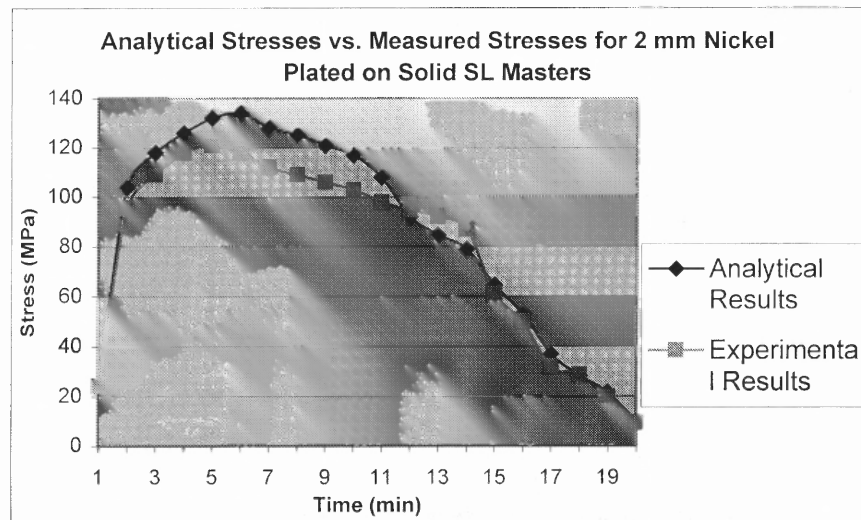


**Figure 6.28** Wired samples in the furnace





**Figure 6.29** Analytical first principal stress vs. measured first principal stress for 1 mm nickel plated on solid SL part

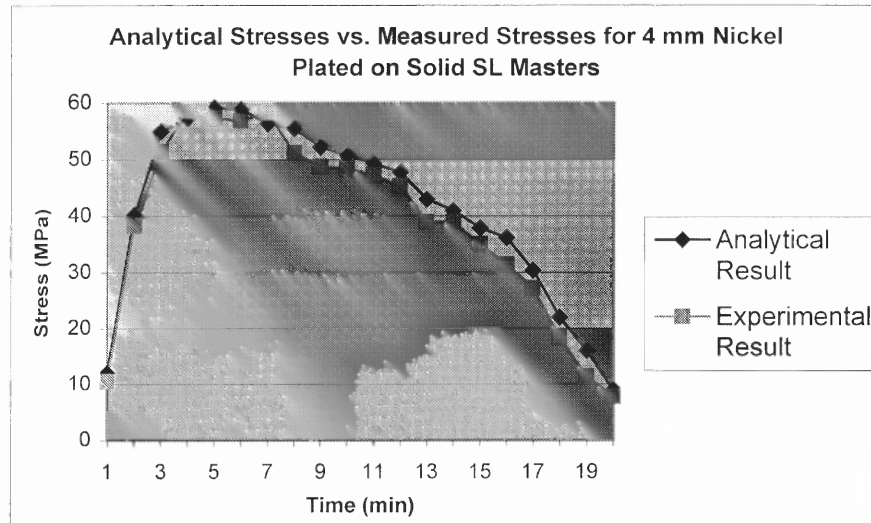


**Figure 6.30** Analytical first principal stress vs. measured first principal stress for 2 mm nickel plated on solid SL part

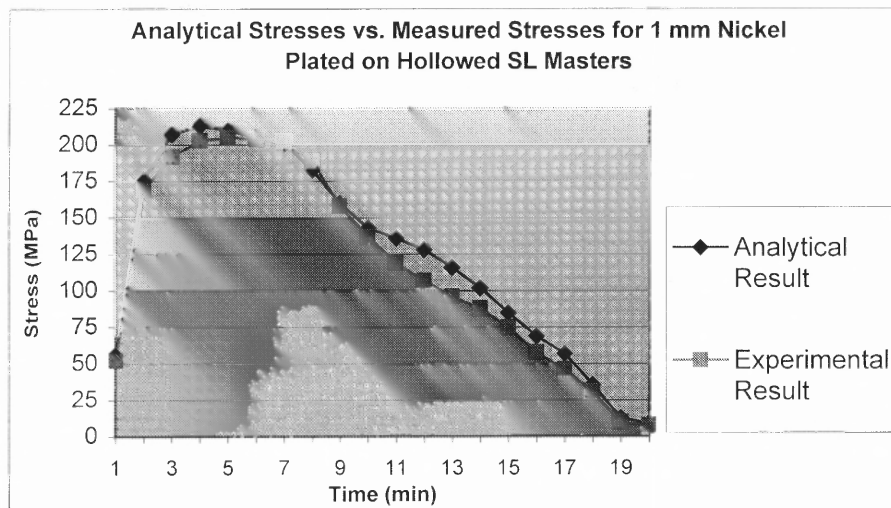
### 6.7.3 Experimental Results

The experimental results are illustrated in Fig.6.29 to Fig.6.34. The results show a closer trend with the prediction of the finite element analysis, which demonstrate that the

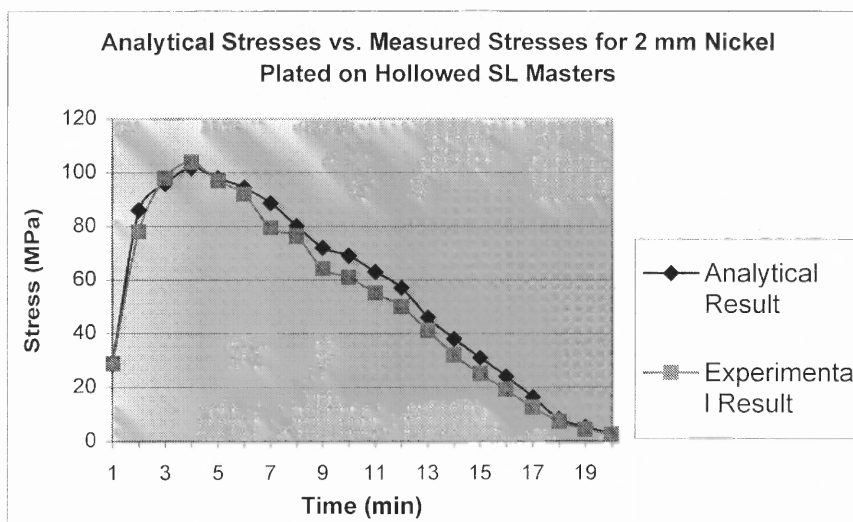
established thermomechanical model and finite element based numerical simulation can be used to predict the thermal stress resulted from the burnout of the SL part.



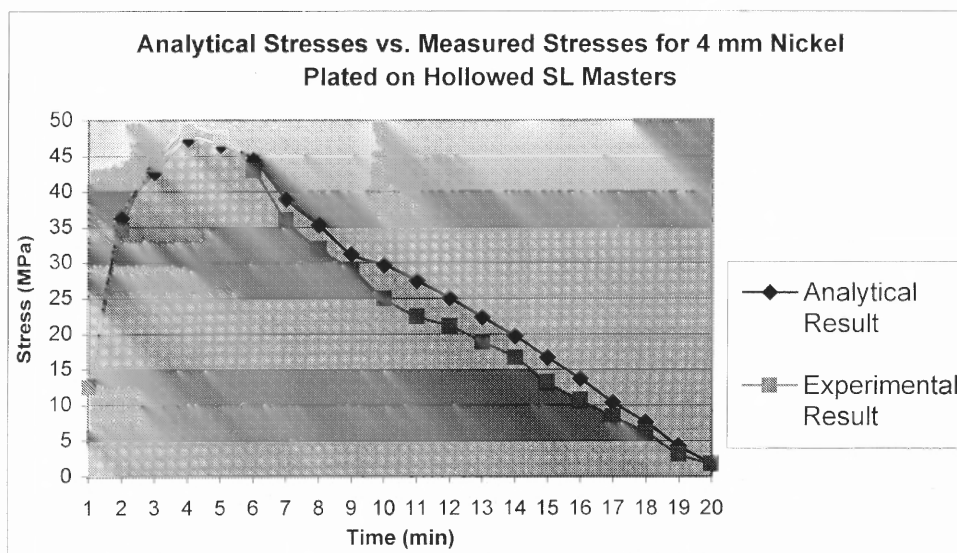
**Figure 6.31** Analytical thermal stress vs. measured thermal stress for 4 mm nickel plated on solid SL master



**Figure 6.32** Analytical thermal stress vs. measured thermal stress for 1 mm nickel plated on hollowed SL master



**Figure 6.33** Analytical thermal stress vs. measured thermal stress for 2 mm nickel plated on hollowed SL master



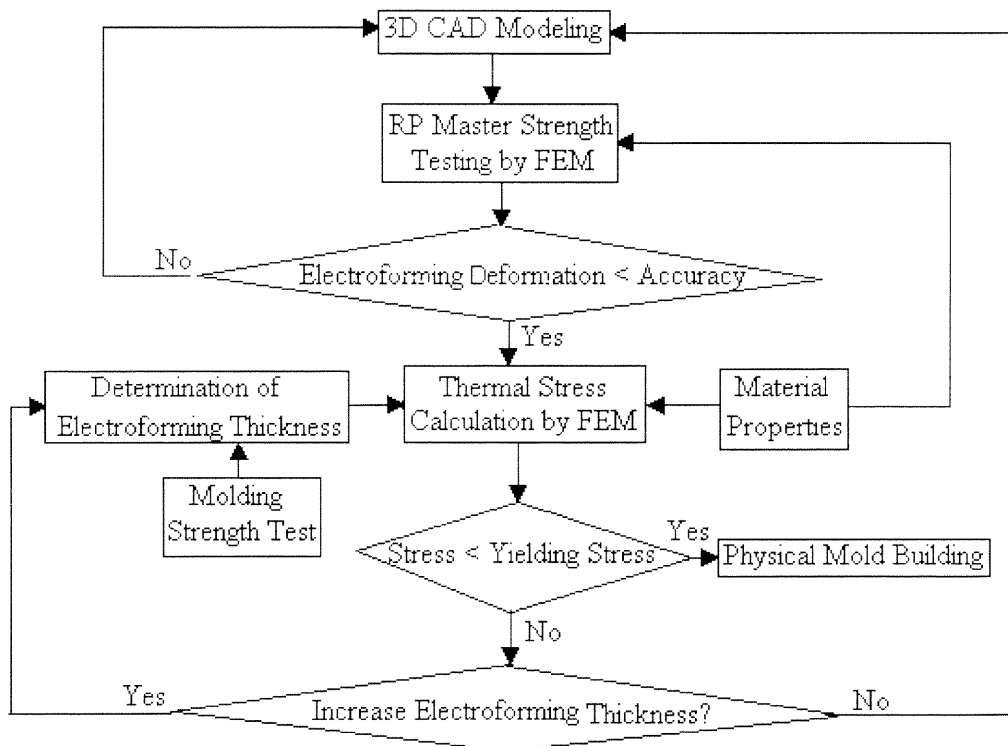
**Figure 6.34** Analytical thermal stress vs. measured thermal stress for 4 mm nickel plated on hollowed SL master

## 6.8 Process Implementation

The presented rapid electroforming tooling process involves two main stages. One is the accuracy analysis stage that determines the structure of the SFF parts and the electroform

thickness, and the second is the physical tooling process that uses the determined part structure and electroform thickness to build the physical tool. The structure of SFF part is determined by two criteria. The first criterion is that the SFF part needs to be strong enough to resist the deformation induced by the electroforming stress during the electroforming process. The second criterion is that the thermal stress induced during the burnout process is smaller than the yield strength of the electroformed metal. This criterion also determines the electroform thickness. So during the analysis stage of the tooling process, the structure of the SFF and the electroform thickness need to be determined for physical tooling.

The determination of the SFF part structure is performed as described in this section. The geometry of a hollowed SFF part with a predetermined wall thickness is constructed inside the ANSYS software. The wall thickness of the SFF part is a parameter. The initial value of the wall thickness is estimated according to the geometry of the SFF part, typically 5mm to 20 mm. The geometry is then used to perform finite element analysis (FEA). The electroforming stress, material properties and boundary conditions for the FEA model are defined for the analysis software to perform the calculation of the deformation caused by the electroforming stress. If the deformation is larger than the accuracy requirement of the tool to be fabricated, the wall thickness is increased to perform the analysis again until the deformation is smaller than the accuracy requirement. After the desired wall thickness of the RP master is determined, the next step is to analyze the thermal stress induced during the burnout process.



**Figure 6.35** Implementation model for determining the SFF part structure and electroforming thickness.

The surface of the determined SFF part are covered with a layer of electroformed metal to provide geometry for thermal stress analysis. The electroform thickness is a parameter in this analysis. The initial electroform thickness is determined by the tool requirement. The strength of the mold is critical for resisting mold deformation during the molding process, and the duration of the mold. The minimum electroform thickness is given by experience, normally 1 to 2 mm. After the geometry has been created, the thermal stress is analyzed using the method described in this Chapter. If the thermal stress is larger than the yield strength of the electroformed metal, the electroform thickness needs to be increased and do the analysis again till the thermal stress is smaller than the yield strength.

Figure 6.35 summarizes the implementation steps for determining the wall thickness of the RP master and the electroforming thickness by finite element methods.

### **6.9 Closure**

Finite element based thermomechanical modeling and analysis are presented in this chapter for predicting the thermal stress generated during the burnout process that removes the SFF part from the electroform. The model is implemented in ANSYS, a commercial FEA software package. Two and three dimensional thermal stress analysis are performed and these analysis are related and matched with the case studies performed in Chapter 5. Different structures of the SFF part and electroform thickness generate different amount of thermal stresses. The thicker the electroform, the smaller the thermal stress for a same SFF part structure. Built-in hollow structure can always reduce thermal stress. It is also found that for an FEA model with same SFF part and same electroform thickness, ramped thermal load generates much larger thermal stress than stepped thermal load does. Experimental verifications demonstrate that the results obtained from FEA-based thermomechanical and analysis model accurately match the results measured from the experiment. Thus the model can be used to predict the thermal stress induced during the burnout process. The established thermomechanical model and FEA based numerical simulation provide a method to determine the geometry of the SFF part and the electroform thickness for minimizing the manufacturing time and cost while satisfying the tooling accuracy requirement.

## CHAPTER 7

### CONCLUSION AND FUTURE WORK

This chapter summarizes the results of this research and major contributions. The future research issues are also discussed.

#### 7.1 Major Contributions

This dissertation presents two rapid tooling processes that combine solid freeform fabrication with electrodeposition to make metal tools such as dies, molds and EDM electrodes. The first is the electroplating tooling used for making of EDM electrodes, while the second is the electroforming tooling for making dies, molds, and EDM electrodes. Feasibility studies, process development and understanding, FEM based process modeling and numerical simulation, as well as experimental verification were performed in this study. This research has led to the following major contributions:

1. An experimental study using electroplated stereolithography models as electrodes for electrical discharge machining (EDM) has been performed. The experimental results indicate that under roughing, semi-roughing and finishing EDM machining, a copper-plated SL-generated model works as well as a regular copper electrode until the thickness of the copper layer becomes the depth of the largest crater burned on the copper layer by the electrical discharge. The performance charts of these EDM electrodes versus regular EDM electrodes are generated. The plating with thick copper layer can prevent burning of the plating; however, the thicker the copper layer

plated on the surface of the master, the less uniform the copper distributed on the entire surface of the electrode, especially if the electrode consists of cavities, sharp corners and complex surfaces. This results in the loss of accuracy of the EDM electrode.

2. A novel rapid electroforming tooling (RET) process has been developed. RET consists of the steps of SFF part generation, metalization, electroforming, separation of SFF part from electroform, and backing the electroform. Although it involves more steps than electroplating tooling, it does not have the uniform electroplating requirement for electroplating tooling. RET can generate tools that conventional machining can not or has difficulty to produce.
3. Case studies of mold and EDM tooling indicate that SFF combined with electroforming technologies for generation of metal molds and EDM electrodes is viable. The accuracy and surface finish are much better than other rapid metal tooling processes, such as 3D Keltool, SLS, 3DP, etc.
4. It is found that material properties, geometry, and process parameters are important factors that affect the tooling accuracy. Thermal stresses induced during the burnout process that removes the SFF part from the electroform are one of major sources for inaccuracy. Another major resource for inaccuracy is the deformation due to the solidification of the molten metal during the backfilling process.
5. Thermomechanical modeling and FEM-based numerical simulation for the burnout process have been performed. The simulation results are used to determine if the electroform undergoes permanent deformation based on the maximum shearing stress theory. The model is used to simulate the thermal stresses resulted from burning of



the electroformed EDM electrodes and mold cavities, and it is found that the portions where the largest dimensional deviation occurred during the burnout process for tooling case studies are the portions where the simulated thermal stresses are larger than or equal to the yield strength of the electroformed metal.

6. The thermal stress is largely reduced when an SFF part is designed as a shelled structure, or when the electroform thickness is increased. The wall thickness of the shelled SFF part is determined by two criteria. The wall thickness must be small enough to guarantee that the thermal stresses are smaller than the yield strength of the electroformed metal at a specified electroform thickness. On the other hand, the wall thickness must also be thick enough to resist the electroforming stress during the electroforming process. The electroform thickness is strongly related to tooling time, cost and tool strength. The implementation model for determining SFF part structure and electroform thickness is presented.
7. It is also found that the thermal stresses are determined by the thermal load during the burnout process. A stepped thermal load for the pattern burnout generates smaller thermal stresses than a ramped thermal load.
8. Thermal stress measurements with strain gages demonstrate that the results obtained from the experiment accurately match the results obtained from the FEA-based thermomechanical analysis model. Thus the model can be used to predict the thermal stresses induced during the burnout process.
9. The established thermomechanical model and FEA based numerical simulation provide an effective method to determine the geometry of the SFF part and the

electroform thickness for minimizing the manufacturing time and cost while satisfying the tooling accuracy requirement.

## 7.2 Future Research Issues

The proposed future research issues and tasks are:

1. The thermomechanical modeling and analysis for the backing process needs to be studied in the future. The melting temperatures of backing metals used in this dissertation study are 103°C and 138.5°C for EDM electrodes and molds, respectively. These temperatures are so low that little thermal deformation is generated During the backing process. However, a harder metal with higher melting temperature, such as aluminum, is better for a high-strength mold. When a high melting metal is used for backing, larger thermal stresses will be generated. Modeling and control of the thermal stresses induced from backing need to be studied.
2. The electrodeposition condition and environment are very complicated and careful control of the electroforming process is extremely necessary. The metal deposition control aspects include adjusting the composition of the plating solutions, monitoring impurity levels, controlling PH value, temperature and current density, measuring thickness in-situation, adjusting current distribution to obtain uniform thick deposit, monitoring and controlling stress continuously by automatically tuning process parameters and adding stress reducing agents, adjusting the concentration of organic additives to control the electrochemical characteristics of individual metal layers. These controlling issues require multi-parameter logic control by means of a

computer. The improvement on the electroforming process is likely to lead to genuine improvement in the quality of electrodeposited metal coatings.

## APPENDIX A

### DISCUSSION OF BOUNDARY CONDITIONS FOR THE THERMOMECHANICAL MODEL

When an electroformed bi-material object is put inside an oven to be heated up, two kinds of boundary conditions can be specified. The first one is that the temperature of the hot air is the same as the temperature at the exterior surface of the object being burned, i.e.

$$T(p,t) = f(p,t) \quad (\text{B.1})$$

where the point  $p$  is on the surface of the metal shell, and  $f(p, t)$  is the oven temperature function.

The second one takes the convection effect into account. In this case, the boundary condition is expressed as:

$$-k \frac{\partial T}{\partial n} \Big|_s = h(T_s - T_o) \quad (\text{B.2})$$

where,  $k$  is the thermal conductivity of the air;  $h$  is the film convection coefficient, which is determined by the geometry, material properties and the boundary temperatures;  $T_s$  is the temperature of exterior surface of the object;  $T_o$  is the temperature of the hot air;  $n$  is the normal of the convection surface.

The exact value of the film convection coefficient is extremely difficult to evaluate [Kreith and Bohn, 1986]. It is obtained by analytical calculation and experimental correlation for various shapes. In our case, the heat transfer between the boundary of the hot air and the exterior surface of the object is natural convection. If the ramped thermal load and the boundary condition of (B.1) are applied, the temperatures

over the exterior surface of the object are almost the same with the temperature of the hot air surrounding the object during the heating up process. However, if the stepped thermal load and the boundary condition of (B.2) are applied, there exists small difference between the temperature close to the exterior surface of the object and the temperature of the hot air during the initial few minutes. After several minutes, the difference between these temperatures becomes negligible. This can be seen from the thermal stress analysis results as shown in Table B.1. This analysis uses the model presented in Fig.6.10 in Section 6.6.1. All the material properties are from Section 6.1. The film convection coefficient is evaluated at the temperature of  $(20+560)/2$  °C. The value for the cylinder geometry is  $32 \text{ W/m}^2.k$ . It can be concluded that the thermal stresses generated using the two different kinds of boundary conditions are almost the same. This is especially true for the largest thermal stress that is the most important stress of concern.

**Table B.1** Comparison of first principal stresses between B.1 and B.2 boundary conditions for the model of Fig.6.10 in Section 6.6.1

Burning time (Second)	Solid, t=2mm		A=25mm, t=2mm	
	B.1	B.2	B.1	B.2
10	1.3	0.8	1.6	1.2
20	2.6	2.2	4.8	4.2
30	5.2	4.9	10.7	9.8
40	8.1	7.8	20.9	20.5
50	10.8	10.6	32.2	31.9
60	13.2	13.0	43.6	43.4
70	18.7	18.5	50.0	49.7
80	25.8	25.7	54.5	54.3
90	33.4	33.3	60.2	60.1

**Table B.1** (Continued)

110	41.0	40.9	66.6	66.5
120	48.5	48.4	77.5	77.6
130	54.6	54.5	84.8	84.8

## REFERENCES

1. Arthur, A., J. R. Carol, P. M. Dickens and R. C. Cobb, "Rapid EDM electrodes using stereolithography models -- combining pin matrix and electroplating techniques." *2nd national conference on developments in rapid prototyping and tooling*, UK, 1996.
2. Ashley, S., "From CAD Art to Rapid Metal Tools", *Mechanical Engineering*, Vol. 119, No.3, March 1997, PP 82-87.
3. Aubin, R.F., Chapter 11 "Tooling Applications" of *JTEC/WTEC Panel Report on Rapid Prototyping in Europe and Japan*. March 1997.
4. Altan, T., B.W. Lilly, J.P. Kruth, W. Konig, H.K. Tonshoff, C.A. van Luttervelt, A.B. Khairy, "Advanced Techniques for Dies and Mold Manufacturing", *Annals of the CIRP*, Vol. 42/2, 1993
5. Beaman, J. J., J.W. Barlow, D.L. Bourell, R.H. Crawford, H.L. Marcus, and K. P. McAlea, *Solid Freeform Fabrication: A New Direction in Manufacturing*, Kluwer Academic Publishers, Norwell, MA 02061, USA, pp. 25-49, 1997.
6. Boley, B. A. and H. W. Jerome, *Theory of Thermal Stresses*, John Wiley & Sons, New York, 1960.
7. Bourell, D.L., R.H. Crawford, H.L. Marcus, J.J. Beaman, J.W. Barlow, 1994, "Selective Laser Sintering of Metals", *Journal of Manufacturing Science and Engineering ASME*, Vol. 68/2, PP:519-527.
8. Chartoff, R. P., J. S. Ullett, and J. W. Schultz, "New High Temperature SLA Resin for Rapid Plastic Tooling", *Proceedings of the North American Stereolithography Users Group Conference*, San Antonio, Texas, March 1998.
9. Charmilles Technologies Inc., *Roboform 100, 200, 400 Operator's Manual*. Geneva/Switzerland, 1990.
10. Conley, J.G. and H.L. Marcus, "Rapid Prototyping and Solid Freeform Fabrication". *Journal of Manufacturing Science and Engineering*, November 1997, Vol. 119, PP 811-816.
11. Dai, C., G. Qi, et al., "High Quality, Fully Dense Ceramic Components Manufactured Using Fused Deposition of Ceramics (FDC)". *Proceedings of Solid Freeform fabrication Symposium*, Austin, Texas, August 1997.
12. Dawson, K., "The Effect of Rapid Tooling on the Final Product Properties", *Proceedings of the North American Stereolithography Users Group Conference*, San Antonio, Texas, March 1998.

**REFERENCES**  
**(Continued)**

13. Decelles, P., "Direct AIM Prototype Tooling", *Proceedings of the North American Stereolithography Users Group Conference*, San Antonio, Texas, March 1998.
14. Degarmo, E.P., J.T. Black and R.A. Kohser. *Materials and Processes in Manufacturing*, Sixth edition, Macmillan Publishing Company, New York, 1984.
15. Dibari, G. A., *Nickel electroforming*, Inco Limited, Inc. New Jersey.1991.
16. Dibari, G. A., "Nickle electroplating Applications & Trends", *Plating and Surface Finishing*, Vol. 83, Oct. 1996.
17. Dickens, P., "Research and Development of QuickCast 2.0", *Proceedings of the North American Stereolithography Users Group Conference*, San Antonio, Texas, March 1998.
18. Duffy, J. I., *Electroless and Other Non- electrolytic Plating Techniques*, Noyes Data Corporation, New Jersey, 1980.
19. Jacobs, P. F., "The effects of Shrinkage Variation on Rapid Tooling Accuracy", *Proceedings of 1998 North American Stereolithography Users Group Annual Conference & Meeting*, San Antonio, Texas, March 1998.
20. Jacobs, P. F., "Recent Advances in Rapid Tooling from Stereolithography", *Proceedings of the seventh International Conference on Rapid Prototyping*, Allan Lightman, et al. (eds), March 1997, San Francisco. PP:338-354.
21. Jacobs, P.F., *Stereolithography and Other RP&M Technologies, from Rapid Prototyping to Rapid Tooling*, SME/RPA, ASME Press, 1996.
22. Karapatis, N.P., J.S.Griethuysen, and R.Glardon, "Direct Rapid Tooling: a Review of Current Research," *Rapid Prototyping Journal*, Vol. 4, No 2: 77-89, 1998.
23. Kochan D., *Solid Freeform Manufacturing*, Elsevier Science Publishers, Amsterdam, The Netherlands, 1993.
24. Killander, L. A. and G. Sohlenius, " Future Direct Manufacturing of Metal Parts with Free-Form Fabrication", *Annals of the CIRP* Vol.44/1/1995, PP 451-454.
25. Kreith, F. and M.S. Bohn, *Principles of Heat Transfer*, Harper & Row Publishers, Inc, New York, 1986.



## REFERENCES (Continued)

26. Kruth, J. -P., M. C. Leu, N. Nakagawa, "Progress in Additive Manufacturing and Rapid Prototyping," *Annals of the CIRP*, 47/2, 1998.
27. Kumar, V., and D. Dutta, "Solid Model Creation for Materially Graded Objects", *Proceedings of Solid Freeform Fabrication Symposium*, Austin, TX, USA, 1997, pp: 613-620.
28. Leu, Ming C., B. Yang, W. L. Yao, "A Feasibility Study of EDM Tooling Using Metalized Stereolithography Models". *North American Manufacturing Research Conference, NAMRC XXVI*, May 19-22, 1998, Atlanta, USA.
29. Leu, M.C. and W. Zhang, "Research and Development of Rapid Prototyping and Tooling in United States", *Proceedings of First International Conference on Rapid Prototyping and Manufacturing*, August 1998, Beijing, China.
30. Li, Q., Y. Wu, J. Wu and W. You, "Process Study on Accurate Mold Making Using Ni-Co Electroforming". *Dies and Molds Industry*, 1992, No.2, pp: 35-43.
31. Lu, Y., "Accurate Injection Mold Fabrication Using Electrolyte Methods". *Dies and Molds Industry*, 1991, No. 4, pp:61-63
32. Luo, Y., M. C. Leu, Z. Ji, and R. J. Caudill, "Lifecycle Assessment of Solid Freeform Fabrication Processes," *Proceedings of 6th International Seminar on Life Cycle Engineering*, Kingston, Canada, 1999a, pp350-360.
33. Luo, Y., M. C. Leu, and Z. Ji, "Assessment of Environmental Performance of Rapid Prototyping and Rapid Tooling Processes", *Proceedings of Solid Freeform Fabrication Symposium*, Aug. 1999b, Austin, Texas.
34. McAlea, K., P. Forderhase, U. Hejmadi and C. Nelson, "Materials and Applications for the SLS Process", *Proceedings of the Seventh International Conference on Rapid prototyping*, 1997, San Francisco, CA.
35. Muller, T.J., "Model to Predict Tolerances in Parts Molded in Pattern Based Alternative Tooling." *Proceedings of Rapid Prototyping & Manufacturing 98 Conference*, May 19-21 1998, Dearborn, MI, SME, pp:287-294.
36. Noguchi, H. and T. Nakagawa, "High Precision Sintered Hard Tooling by Metal Powder Casting", *Proceedings of Solid Freeform Fabrication Symposium*, Aug. 1997, Austin, Texas.
37. Poco Graphite, Inc., *EDM Technical Manual*, Decatur, Texas, 1994.

**REFERENCES**  
**(Continued)**

38. Raetz, T., "3D Keltool", *Proceedings of the North American Stereolithography Users Group Conference*, San Antonio, March 1998, Austin, Texas.
39. Rajurkar, K.P., and S.M. Pandit, "Formation and ejection of EDM debris," *Transactions of the ASME, Journal of Engineering for Industry*, Vol. 108,1986.
40. Rangarajan, S., G. Qi, A. Bandyopadhyay, C. Dai, J.W. Han, P. Bhargava, S. Wu, A. Safari, S.C. Danforth, "The Role of Materials Processing Variables in the FDC Process", *Proceedings of Solid Freeform fabrication Symposium*, Austin, Texas, August 1997.
41. Rees, H., *Mold Engineering*, Hanser, New York, 1995.
42. Ryall, C., "Rapid EDM electrodes: linking rapid prototyping to high volume production," *Proceedings of 1<sup>st</sup> National Conference on Rapid Prototyping and Tooling Research*, Nov. 1995, Buckinghamshire College (Brunel University), UK.
43. Sachs, E., M.Cima, J.Cornie, "Three-Dimensional printing: Rapid Tooling and Prototyping Directly from a CAD Model," *Annals of the CIRP*, 1990, vol. 39/1, pp:201-204.
44. Sachs, E., S.Allen, H.Guo, J.Banos, and M.Cima, "Progress on Tooling by 3D Printing; Conformal Cooling, Dimensional Control, Surface Finish and Hardness", *Proceedings of Solid Freeform Fabrication Symposium*, 1997, Austin, TX, USA, pp:115-123.
45. Safranek, W.H., "Physical and Mechanical Properties of Electroformed Copper", *Proceedings of Symposium on Electroforming – Applications, Uses, and Properties of Electroformed Metals*, Feb., 1962, Dallas, Texas.
46. Safranek, W.H., *The Properties of Electrodeposited Metals and Alloys*, 2<sup>nd</sup> edition, published by American Electroplaters and Surface Finishers Society, Orlando, Florida, 1986.
47. Sample, C.H. and B.B.Knapp, "Physical and Mechanical Properties of Electroformed Nickel at Elevated and Subzero Temperatures", *Proceedings of Symposium on Electroforming – Applications, Uses, and Properties of Electroformed Metals*, Feb.1962, Dallas, Texas.
48. Shanahan, J.E., "CNC Milling of Graphite electrodes", *Proceedings of LeBlond-Makino Symposium on Die & Mold Manufacturing*, June 1993, Cincinnati, Ohio.

**REFERENCES**  
**(Continued)**

49. Sheng, P., D. Bennet and S.Thurwachter, "Environmental-Based System Planning for Machining," *CIRP Annals*, Vol. 47/1, 1998.
50. Spiro, P., *Electroforming*, Robert Draper LTD. Teddington, UK. 1968.
51. Stein, B., "A Practical Guide to Understanding, Measuring and Controlling Stress in Electroformed Metals", *Proceedings of the AESF Electroforming Symposium*, March, 1996, Las Vegas, NV, USA.
52. Stephenson Jr., W.B., "Development and Utilization of a High Strength Alloy for Electroforming", *Plating*, Vol. 53, 1966.
53. Ugural, A.C. and S.K. Fenster, *Advanced Strength and Applied Elasticity*, Prentice Hall, Inc., New Jersey, 1995.
54. Wang, Wen Z., "Plastic Injection Mold Making Using Electroforming and Used Plastic Parts". *Dies and Molds Industry*, 1990, vol. 8, pp:45-47.
55. Wang, W.M., K.P. Rajurkar and K. Akamatsu, "Digital gap monitor and adaptive integral control for auto-jumping in EDM," *Transactions of the ASME, Journal of Engineering for Industry*, Vol. 117, May 1995.
56. Wang, W.M., K.P. Rajurkar and M.S. Ahmed. "Improvement in EDM tool wear ratio and material removal rate with modified R.F. control unit". *Transactions of NAMRI/SME*, 1990.
57. Weck M., and J.M. Dehmer. "Analysis and adaptive control of EDM sinking process using the ignition delay time and fall time as parameter". *Annals of the CIRP*, Vol.41/1, 1992.
58. Yang, B., M.C. Leu and W. Zhang, "Rapid Tooling Through Rapid Fabrication of EDM Electrodes", *1998 3DSNASUG*, March 1998, San Antonio, Texas,.
59. Yang, B., M. C. Leu, "EDM Tooling by Electrodeposition of Rapid Prototyping Masters," *The International Journal of Agile Manufacturing*, Vol.1, 2000.
60. Yang, B., M.C. Leu, "Integration of Rapid Prototyping and Electroforming for Tooling Application," *Annals of the CIRP*, Vol.48/1, 1999a.
61. Yang B., M. C. Leu, "Rapid Production of Engineering Tools and Hollow Bodies by Integration of Electroforming and Solid freeform Fabrication." *Filed with the United States Patent and Trademark Office*, 1999b.

**REFERENCES**  
**(Continued)**

62. Yao, W. L., H. Wong, M.C. Leu, and D. H. Sebastian, "An Analytic Study of Investment Casting with Webbed Epoxy Patterns", *ASME 1996 Winter Annual Conference and Rapid Response Manufacturing (RRM) Symposium*, Nov., 1996, Atlanta, GA.
63. Zhu, L. Z., X. L. Liu and D. Zhu, "Electroforming of EDM Electrode for molding of Sprocket Gears". *Dies and Molds Industry*, No. 2:45-50, 1992.
64. Zhou, J. G., Z. He, "Rapid Pattern Based Power Sintering Technique and Related Shrinkage Control." *Materials and Design*, Vol. 19, 1998, pp:241-248.
65. Zsysys Inc., "An Innovative, Integrated, UV Cured System for Rapid Tooling". Torrance, 1998, CA, USA,